DASA-1275

HUGHES

RESEARCH LABORATORIES

RESEARCH STUDY OF SURFACE BARRIER DETECTORS*

Final Report
Contract No. DA-49-146-XZ-016

31 December 1960 through 28 February 1962

NOX

*This is the Final Report for Mod. No. 2, covering a study to determine the feasibility of utilizing p-n junction phosphorous diffused detectors to map the radiation field of a pulsed reactor or a linear accelerator.

DASA-1275

HUGHES RESEARCH LABORATORIES
Malibu, California

a division of hughes aircraft company

RESEARCH STUDY OF SURFACE BARRIER DETECTORS*

Final Report
Contract No. DA-49-146-XZ-016

31 December 1960 through 28 February 1962

*This is the Final Report for Mod. No. 2, covering a study to determine the feasibility of utilizing p-n junction phosphorous diffused detectors to map the radiation field of a pulsed reactor or a linear accelerator.

This research is supported by the Defense Atomic Support Agency. Requests for copies of this report should be submitted to ASTIA, Arlington Hall Station, Arlington 12, Virginia.

TABLE OF CONTENTS

LIST OF ILLUSTRATIONS

I. INTRODUCTION

This report describes work performed by the Radiation Physics Department of the Hughes Research Laboratories under Defense Atomic Support Agency Contract DA-49-146-XZ-016. The purpose of the study was to determine the feasibility of utilizing p-n junction phosphorous-diffused detectors to map the radiation field of a pulsed reactor and a linear accelerator.

The detectors produced large signals in these radiation fields which were easily observed without any amplification. The characteristics of the p-n junction detectors, i.e., compactness, linearity with energy deposited, and rapid response, were demonstrated. The operation of the units agreed well with theoretical predictions.

Radiation from the reactor flux had a damaging effect on the detector characteristics. These were examined before and after the irradiations at temperatures ranging from 77 to 325°K. An understanding of the changes was obtained from consideration of basic semiconductor properties. The possibility of a gamma-ray neutron dosimeter combining the transient and permanent effects of the reactor flux will be discussed on the basis of the experimental data.

No permanent effects were observed from the gamma-ray field of the linear accelerator at dosages up to 10^5 r.

The fabrication of very thin detectors for dE/dx determinations using charged particles and for rapid response to a LINAC beam is examined. Methods for optimizing detectors in various applications by increasing the sensitive area through the use of series and parallel combinations was considered theoretically and verified experimentally.

The p-n junction detectors used in this study were made by diffusing phosphorous into boron-doped silicon wafers of various resistivities. These units were developed for use as charged-particle detectors. Their construction and characteristics in this application are discussed in an earlier DASA report, covering work done in 1960.

II. DETECTION OF HIGH-INTENSITY PULSED RADIATION (THEORETICAL)

The interaction of a mixed radiation field with a silicon crystal lattice produces two general types of reactions which may be classified as either ionization or permanent effects.

A. Ionization Effects

Ionization produces hole-electron pairs which act as carriers for electric current. These pairs are observed during the radiation pulse and persist after it for an average time τ called the "carrier lifetime." The carrier lifetime is defined as the average time interval between the generation and recombination of minority carriers in a homogeneous semiconductor. Ion pair formation may be induced by any of the following processes:

1. Gamma Rays Interactions – Three processes are mainly responsible for the absorption of gamma rays. These are (1) photoelectric absorption, (2) Compton scattering of x and gamma rays by orbital electrons and the consequent absorption of the secondary electrons, and (3) production of electron positron pairs as a result of the interaction between gamma rays and the electric fields of the nuclei. The gamma rays utilized had energies in the region in which the Compton effect was dominant (see Fig. 1).[1] Thus the Compton recoil electrons were mainly responsible for the observed generation of hole-electron pairs in silicon. The energy of the recoil electrons is dissipated in part by the production of these carriers. The average energy for the production of hole-electron pairs in silicon[2] is 3.5 ev.

2. Recoil Ionization – The incident neutrons are scattered by the silicon nuclei and produce recoil nuclei which contribute to the ionization. This is an elastic scattering interaction, and the highly energetic fast neutrons produce the most energetic recoils. Thus the fast neutrons are the main contributors to this process.

3. Nuclear Reactions – The interaction of neutrons with silicon atoms produces secondary radiation by means of thermal neutron capture and a high-energy (n,p) reaction. The thermal neutron absorption cross section in silicon is 0.09 barns. The major fraction of thermal absorptions occurs in the lower mass isotopes Si^{28} and Si^{29}, and in each case the resulting isotope formed is the next heavier stable isotope of silicon. The gamma ray emitted in each case contributes to the ionization. The small fraction of neutrons captured in Si^{30} results in the formation of Si^{31}, which decays with a half life of 2.6 hours to stable P^{31}. The beta emission from this decay process, plus beta radiation emitted from interactions with materials surrounding the silicon also produces ionization.

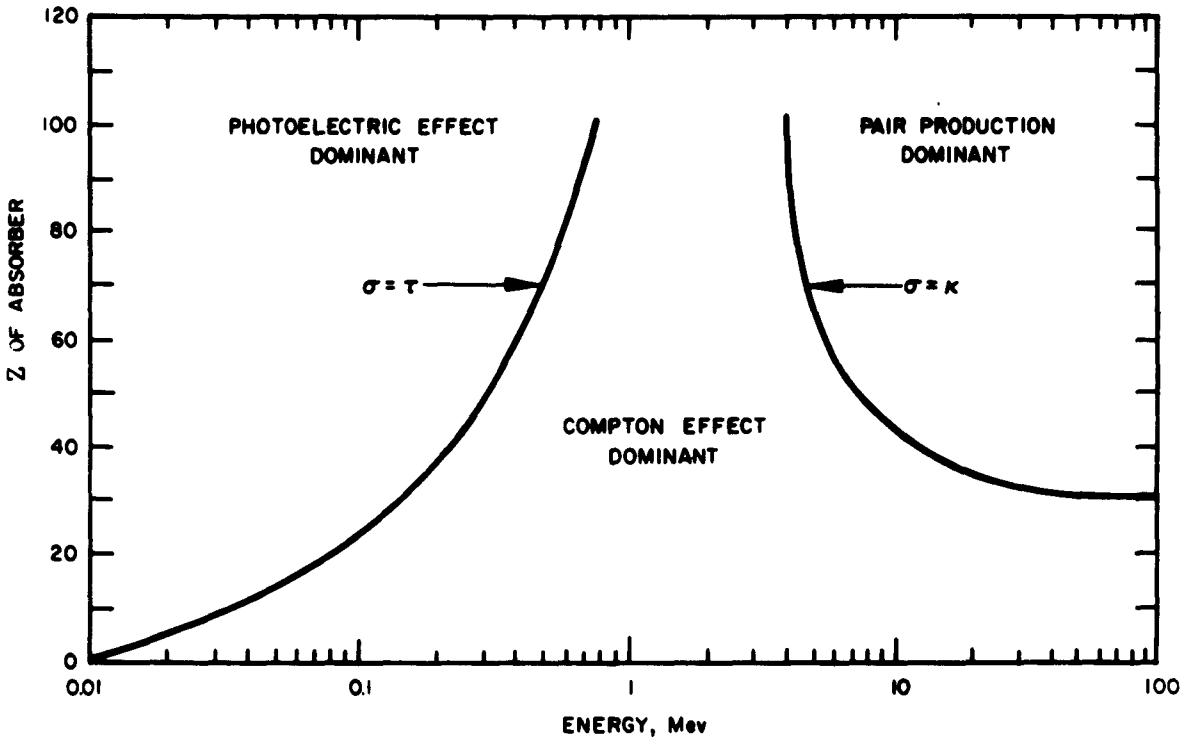

Fig. 1. Relative cross sections for the three principal photon interactions in matter.

The significant fast neutron reaction is $Si^{28}(n,p)Al^{28}$, which has a threshold of 4.5 Mev. The resulting proton energy is $E_p = E_n - 4.5$ Mev, where E_n is the incident neutron energy. The reaction cross section increases from zero at threshold to 0.3 to 0.4 barns in the neutron energy range of 6.5 to 8 Mev. The Al^{28} decays with a half life of 2.30 minutes to Si^{28}. The beta and gamma emission from this decay and the proton from the original reaction will generate additional carriers.

It will be shown that gamma ray absorption is the principal factor in the generation of holes and electrons in the radiation field of a pulsed reactor. This ionization produces an increase in current of a reverse biased p-n junction. Such photoconduction is caused by the carriers generated by the radiation traversing the electric field of the junction. The photocurrent has two components:

a. There is a current resulting from minority carriers which are created outside the field, diffuse to the field region, and are then swept across the junction by the field. This current arises from carriers generated within a diffusion length on either side of the field region.[3] Fig. 2 shows the geometrical configuration of the field regions. The carriers require an average time $\tau_{n,p}$ to diffuse to the junction; the diffusion current per unit area is

$$I = ge\left[L_p\left(1 - e^{-t/\tau_p}\right) + L_n\left(i - e^{-t/\tau_n}\right)\right], \qquad (1)$$

where

$L_p \equiv$ diffusion length of holes in the n region

$L_n \equiv$ diffusion length of electrons in the p region

$\tau_{n,p} \equiv$ lifetime of electrons and holes, respectively

$D_{n,p} \equiv$ diffusion constant for holes in n material and electrons in p material, respectively

$g \equiv$ generation rate (e-h pairs/cm^3/sec) assumed uniform throughout material

$e \equiv$ electronic charge

$L_p \equiv \sqrt{D_{p,n}\tau_{p,n}}$.

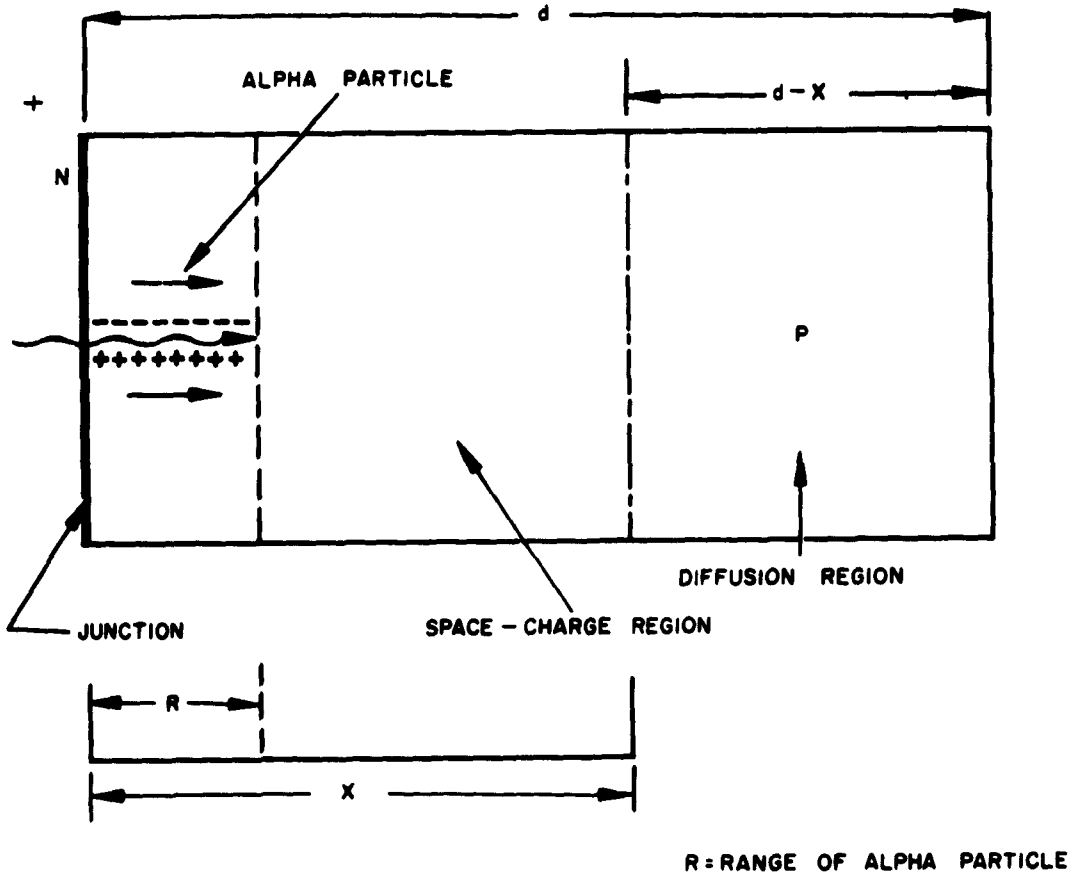

Fig. 2. Schematic drawing of spatial and geometrical configuration of the p-n junction radiation detector.

b. The second component of the current is a result of carriers generated within the space-charge region (also referred to as field or depletion region). The width of this region from the junction into the n- and p-type material, respectively, is $X_{n,p}$. The magnitude of $X_{n,p}$ is given approximately by[4]

$$X_{n,p} = \left(\frac{\epsilon V_{n,p}}{2\pi e N_{n,p}} \right)^{1/2} , \tag{2}$$

where

$V_{n,p}$ ≡ potential across the depletion region in the n and p areas, respectively

ϵ ≡ dielectric constant of the silicon

$N_{n,p}$ ≡ concentration of ionized impurities centers in the n and p regions, respectively.

The electric field is given by

$$E_{n,p} = - \frac{N_{n,p} e X}{\epsilon} . \tag{3}$$

The carriers will transverse the field region in an average time

$$T_R = \frac{E}{\mu N e} ,$$

where μ is the carrier mobility $cm^2/volt/sec$. The total current, considering the time for the diffusion component to traverse the field region, is given by

$$\frac{I}{cm^2} = ge\left[X_n\left(1-e^{-t/T_{Rn}}\right)\eta_n + X_p\left(1-e^{-t/T_{Rp}}\right)\eta_p + L_n\left(1-e^{-t/\tau_n + T_{Rp}}\right) + L_p\left(1-e^{-t/\tau_p + T_{Rn}}\right)\right] \quad , \tag{4}$$

where $\eta_{n,p}$ is the collection efficiency in depletion region. It is to be noted here that as the resistivity of material increases, the width of depletion region increases:

$$\rho = \frac{1}{Ne\mu} \qquad X_p \propto (\rho)^{1/2} \quad .$$

The detectors that were employed in this work were shallow diffused n-p junctions. The n region was highly doped and thus had very low resistivity; the p region had high resistivity, 6000 ohm-cm. The junction was less than 1 micron below the surface. Thus there was practically no diffusion component from the n region, and the depletion region component was negligible:

$$L_p >> L_n \qquad X_p >> X_n \quad .$$

The lifetime τ in normal detectors is several orders of magitude greater than the transit time T_R. Thus the current for shallow diffused p-n junctions becomes

$$\frac{I}{cm^2} = ge\left[\eta_p X_p\left(1-e^{t/T_{Rp}}\right) + L_n\left(1-e^{-t/\tau_n}\right)\right] \quad , \tag{5}$$

where $\eta_p X_p\left(1-e^{-t/T_{Rp}}\right)$ is the depletion region contribution and $L_n\left(1-e^{-t/\tau_n}\right)$ is the diffusion region contribution.

B. Permanent Effects

Permanent effects in the silicon persist after the diode is removed from the radiation field. They result from defects formed in the crystal lattice, and include vacancies, interstitials, thermal spikes, defect clusters, and replacement or transmuted atoms. The principal effects with which we are concerned are (1) increased resistivity due to carrier removal, (2) decrease in lifetime due to introduction of recombination centers, and (3) decreased mobility due to scattering of carriers from defects. The effects which reduce the photocurrent response to successive irradiations are: (1) The decrease in lifetime, which causes a decrease in diffusion length $L = \sqrt{D\tau}$; thus the diffusion component of the photocurrent is reduced. (2) The collection efficiency of the depletion region component will decrease when the lifetime degrades to the order of magnitude of the transit time T_R. The transit time can be expected to increase as a result of a decrease in mobility. This decrease is caused by recombination of the electrons and holes within the space-charge region. After successive irradiations, the diffusion component will decrease first since it is sensitive to any change in lifetime. The field region component is only affected as $\tau \rightarrow T_R$.

The defects causing these permanent effects are produced when a bombarding particle displaces a silicon atom. The threshold energy for a lattice displacement as determined by Klontz[5] is 30 ev. The heavier and the more energetic the incident particle, the greater is the transfer of energy to the recoiling nucleus. Thus, it is to be expected that for the same bombardment rates, fast neutrons, as compared with Compton electrons from gamma rays and thermal neutrons, will produce the most lattice displacements and will be responsible for permanent damage effects.

III. DETECTION OF ELECTROMAGNETIC RADIATION (EXPERIMENTAL RESULTS)

A. Response to Steady-State Sources

In exploring the detector's response to a mixed radiation field, the initial step was to determine the response of a p-n junction to pure gamma-ray pulses, such as that obtained from the bremsstrahlung output of a linear electron accelerator. First, however, we examined the output from the following steady-state radiation sources in order to eliminate the complications resulting from high-intensity pulsed beams.

1. X Rays (100-kvp) — A 3-mm aluminum filter was used in this machine, giving an HVL of approximately 3mm Al.

2. Silicon-Filtered Light — The diodes were irradiated under white light passed through a 0.025-inch-thick silicon filter. This thickness is equal to the average width of detector used; thus, the softer nonpenetrating wavelengths were filtered out and only the more penetrating radiation was transmitted, which assured a uniform generation rate of carriers throughout the silicon.

Several detectors were exposed to the above sources of ionizing radiation to determine the increase in reverse current over "dark" current, i.e., photocurrent, and to examine the voltage dependence of the photocurrent and its variation with dose. Measurements were made using the circuit shown in Fig. 3.

The value of R_L was varied between 10^6 and 10^7 ohms. The x-ray dose rate was 1.67 r/sec. To monitor the relative ionization in air of the machine output as the beam current was varied, we used an extrapolation type ionization chamber designed and built at Hughes. The intensity of the silicon-filtered light was not measured.

The measurements indicated that the photocurrent response was of the same order of magnitude as the normal dark current and was the limiting factor in detecting ionizing radiation. However, by use of a potentiometer the lower limit may be extended. The photocurrent, which is the excess reverse current due to radiation, is plotted in Fig. 4 for both x rays and silicon-filtered light as a function of the square root of bias voltage. The width of the depletion region as a function of applied potential was determined by measuring the junction capacity using a bridge circuit. The width of the depletion region was proportional to the square root of the applied potential as predicted by theory.

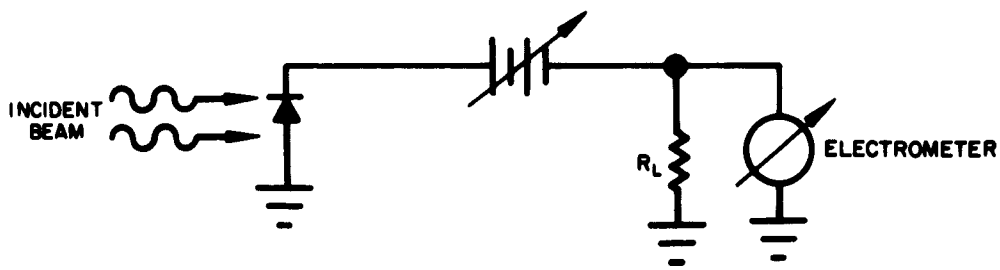

Fig. 3. Circuit used for measurement of photocurrents induced by the action of ionizing radiations on p-n junction radiation detectors.

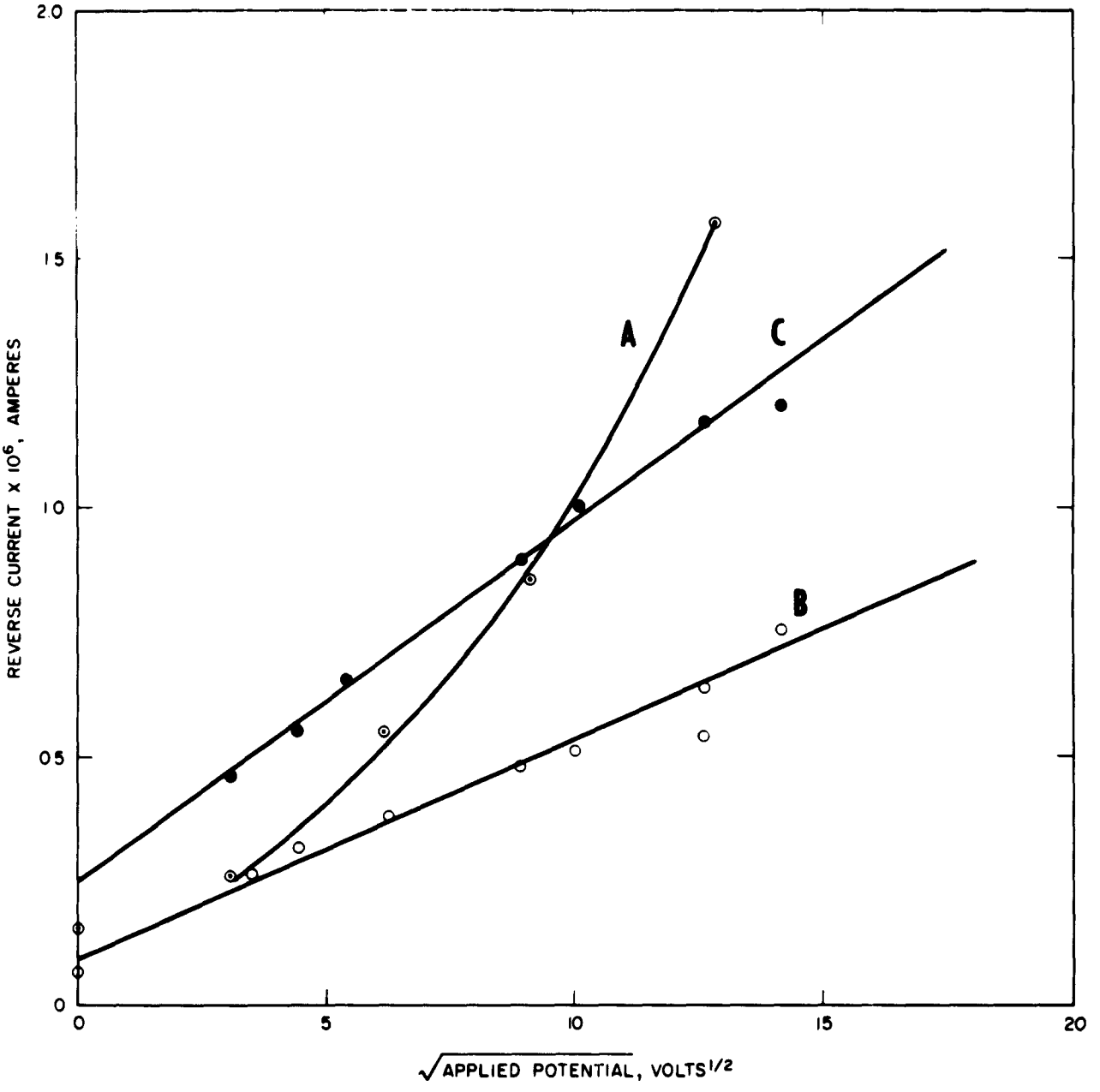

Fig. 4. Reverse photocurrent as a function of applied potential across a p-n junction. Curve A shows the normal dark current: Curve B, the increase in the dark current when the detector was irradiated with silicon-filtered light; and, Curve C, the change in dark current when the detector was irradiated with an x-ray beam. It will be noted that the change in dark current which was a result of either light or x rays is directly proportional to the width of the depletion region.

It will be noted that the depletion region component of the photocurrent varies linearly with depletion region width. The intercept at zero bias represents the diffusion component, while the voltage-dependent portion represents the depletion-region component. The absolute sensitivity was found to be 7.8×10^{-9} amps/cm^2/micron/r/sec. We see by the larger intercept and greater slope of the diode photocurrent response that the x-ray irradiation produced a greater hole-electron pair generation than silicon-filtered light.

The response of a very thin (0.012-inch thick) detector to the silicon-filtered light is shown in Fig. 5. The photocurrent reaches a peak as the depletion region approaches within a diffusion length of the back of the unit and then seems to decrease slightly. The photocurrent response at constant bias was directly proportional to x-ray intensity. This is shown in Fig. 6.

To illustrate the feasibility of obtaining high-resolution mapping of the radiation field, a plot of the photocurrent at different positions in the cross section of the beam was obtained. The experimental data are shown in Fig. 7. Greater resolution is easily obtainable. The data were taken using a 5- by 5-mm detector; however, units with sensitive areas down to 1 mm in diameter have been operated successfully.

B. Response to Pulsed Gamma Rays – Linear Accelerator

Following the experiments with steady-state sources, detectors were exposed to a pulsed gamma-ray source. The machine produced an 8-Mev beam, with an 8-μsec pulse width. The beam current was 50 ma, and it was operated at a repetition rate of 10 pps. A 1/8-inch-thick lead target was used to generate a bremsstrahlung spectrum and a 1/2-inch lucite shield was used to absorb electrons which might otherwise contribute to the detector response. The experimental setup is shown in Fig. 8.

The electron beam was monitored by observing the voltage across a 100-ohm resistor connected from the lead target to ground. This voltage was observed as one trace of a dual-beam oscilloscope, while the detector response was shown as the second. In this manner the two could be directly compared. Since the response to this very intense source was so great, no amplification of the detector response was necessary. The circuitry used is shown in Fig. 9.

Figs. 10 and 11 show the response of a 5- x 5-mm, 100-ohm-cm unit to the linac pulses as a function of applied bias. The dose rate was 2.5×10^7 r/sec. Fig. 12 shows the response of the same detector during a period of erratic machine operation. It is clear from these responses that

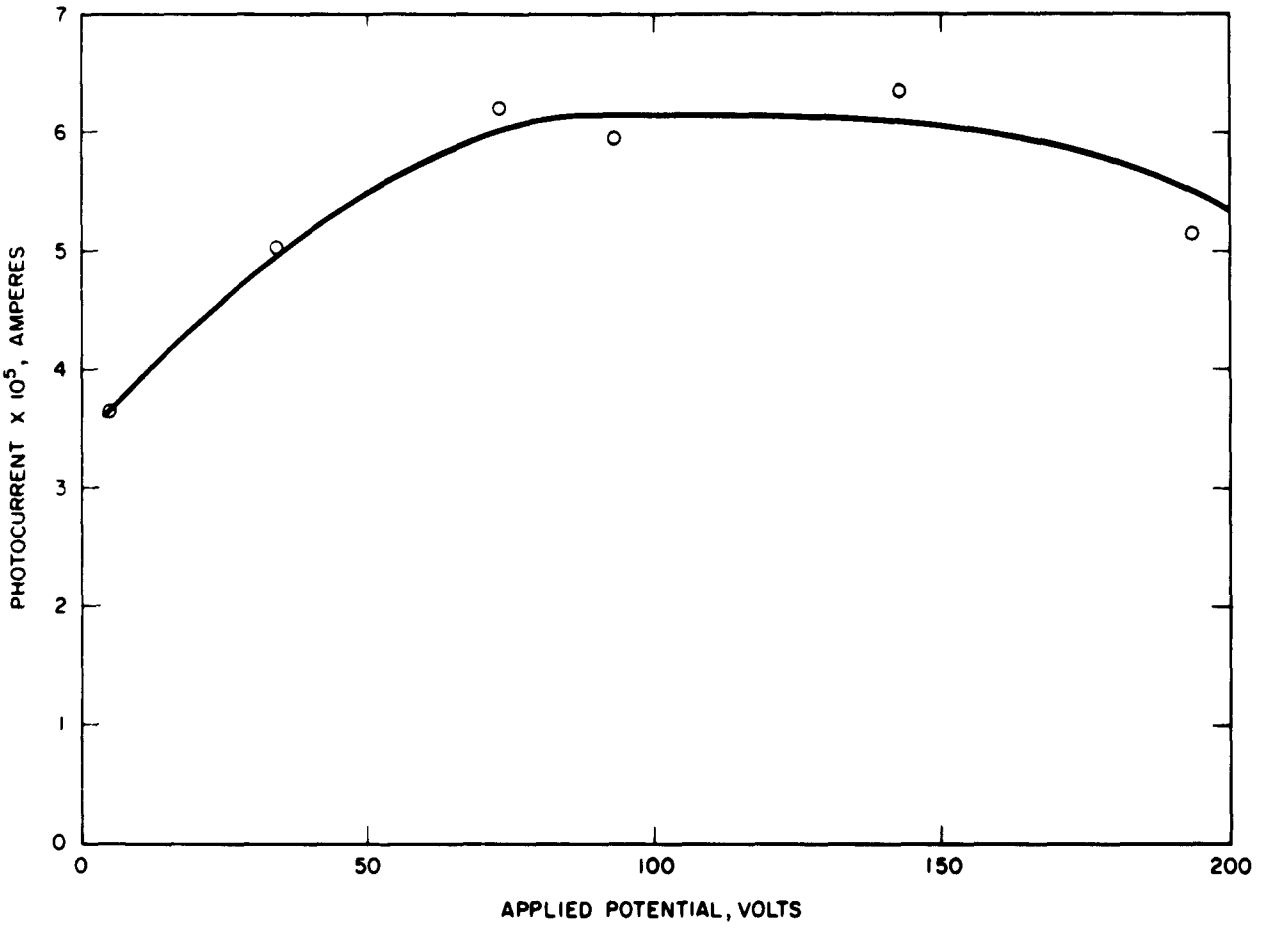

Fig. 5. Photocurrent due to silicon-filtered light in very thin (0.012-inch thick) detector to silicon-filtered light as a function of applied potential. This illustrates the effect of depletion region width on the change in photocurrent obtained.

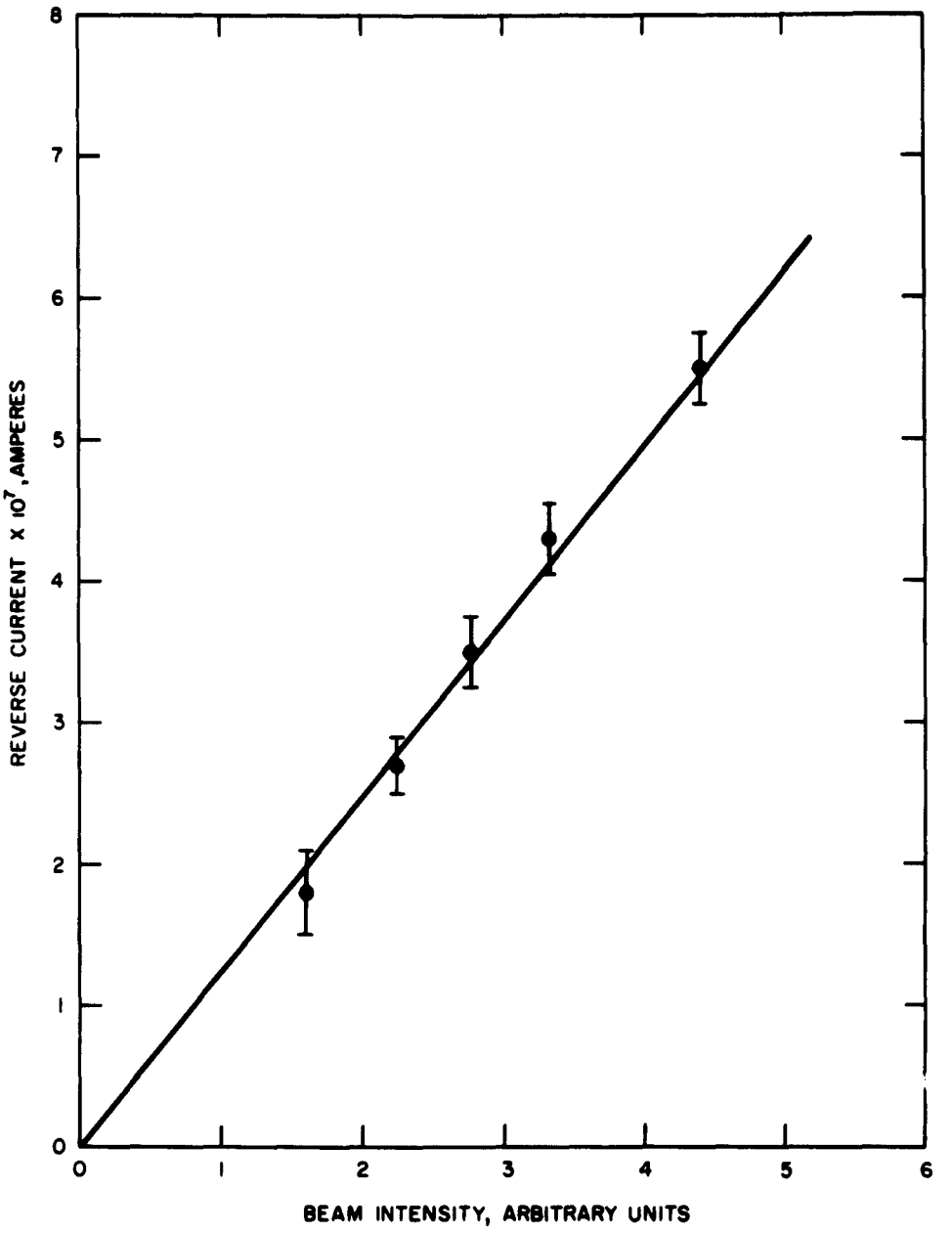

Fig. 6. Reverse current obtained as x-ray intensity is varied is shown to be a linear function for a p-n junction detector when depletion region width is held constant.

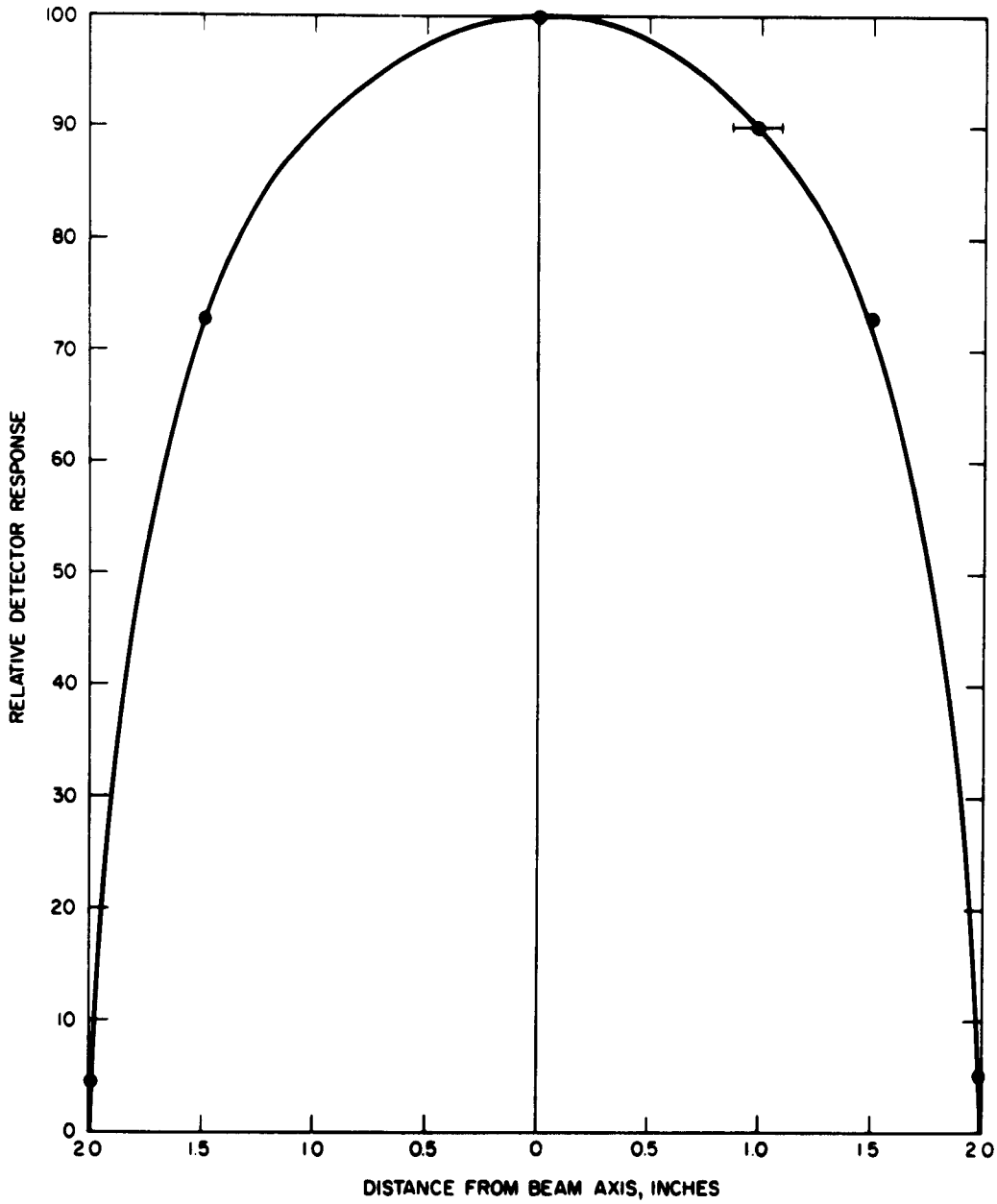

Fig. 7. The feasibility of using p-n junction radiation detectors for plotting beam profiles is illustrated by these data showing relative detector response as a function of distance from the axes of an x-ray beam.

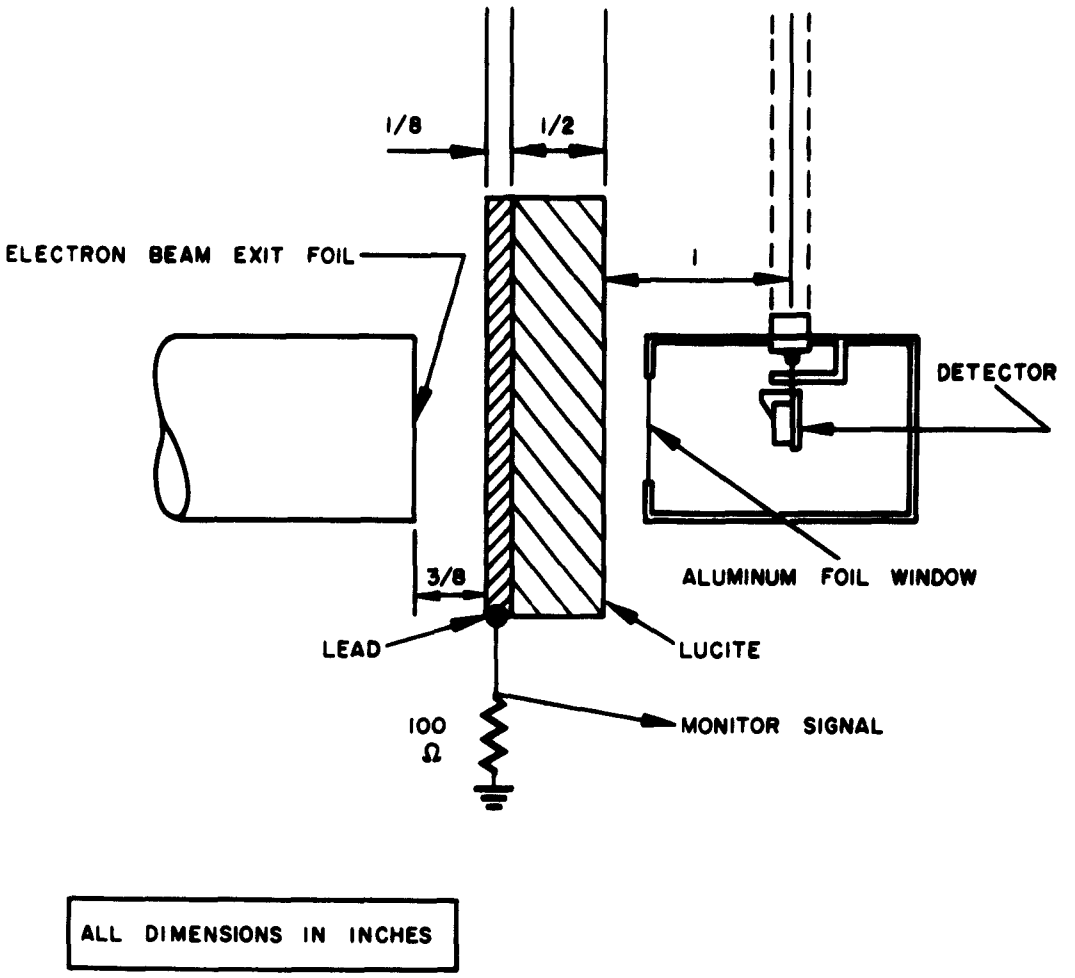

Fig. 8. Experimental arrangement used for performing experiments with p-n junction detectors in a pulsed linear accelerator beam.

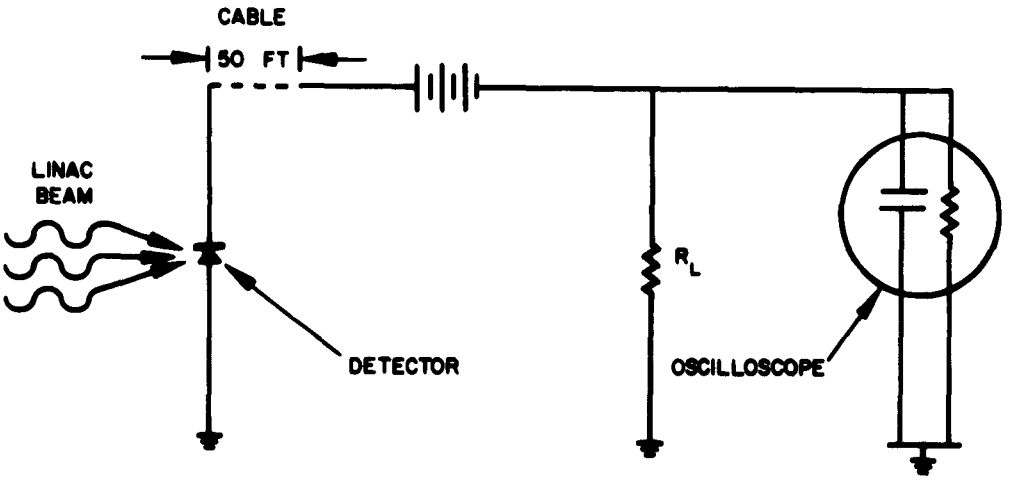

Fig. 9. Circuitry used for display of detector response when irradiated by high-intensity linear accelerator x-ray beams.

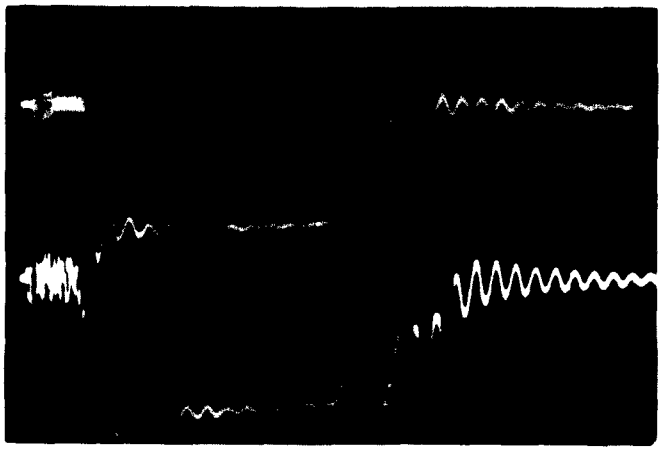

(a)

(b)

(c)

Fig. 10. Response of a 100-ohm-cm p-n junction radiation detector to the high-intensity x-ray pulses of a linear accelerator. Operating characteristics in each case were: (a) when no potential is applied to the detector, oscilloscope sensitivity = 0.2 volt/cm; (b) 10 volts applied bias, oscilloscope sensitivity = 5 volts/cm; (c) 20 volts applied bias, oscilloscope sensitivity = 5 volts/cm; (d) 40 volts applied bias, oscilloscope sensitivity = 10 volts/cm; (e) 100 volts applied bias, oscilloscope sensitivity = 10 volts/cm. Exposure dose rate = 2.5×10^7 r/sec.

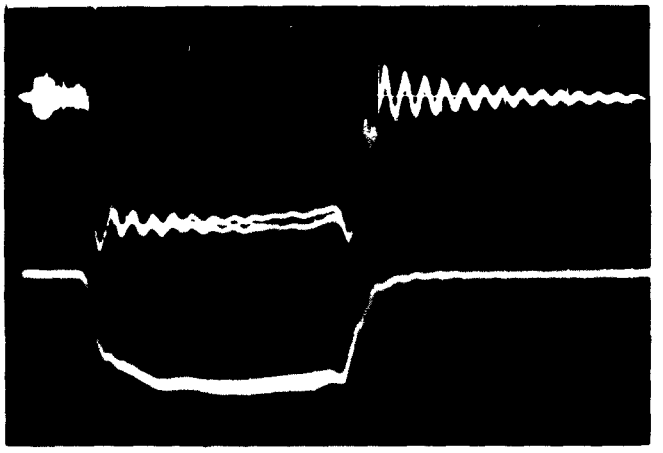

(d)

(e)

Fig. 10. (continued)

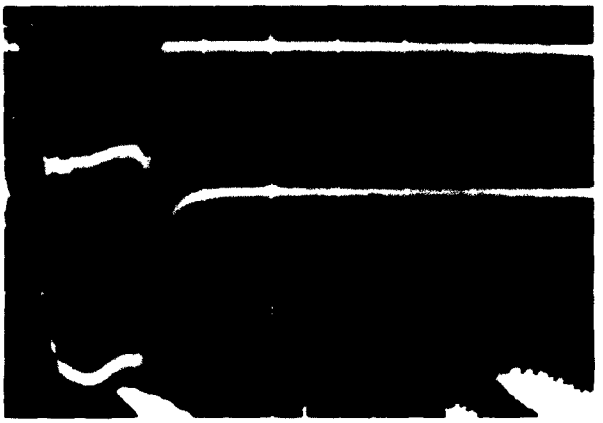

(a)

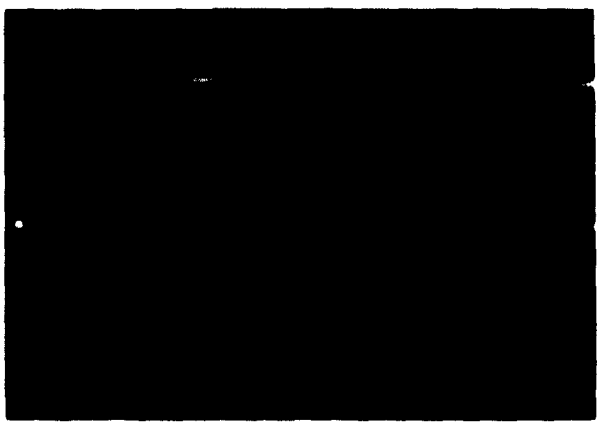

(b)

(c)

Fig. 11. These oscilloscope photographs illustrate the response of a second detector to the same pulses. This detector was operated with a small load resistance (356 ohms) and a low impedance battery supply. The operating characteristic in each case were (a) applied bias = 1.5 volts, oscilloscope sensitivity 0.01 volt/cm; (b) applied bias = 10 volts, oscilloscope sensitivity = 0.02 volt/cm; (c) applied bias = 90 volts, oscilloscope sensitivity 0.02 volt/cm. Dose rate = 2.5×10^7 r/sec. Oscilloscope sweep speed = 5 μsec/cm.

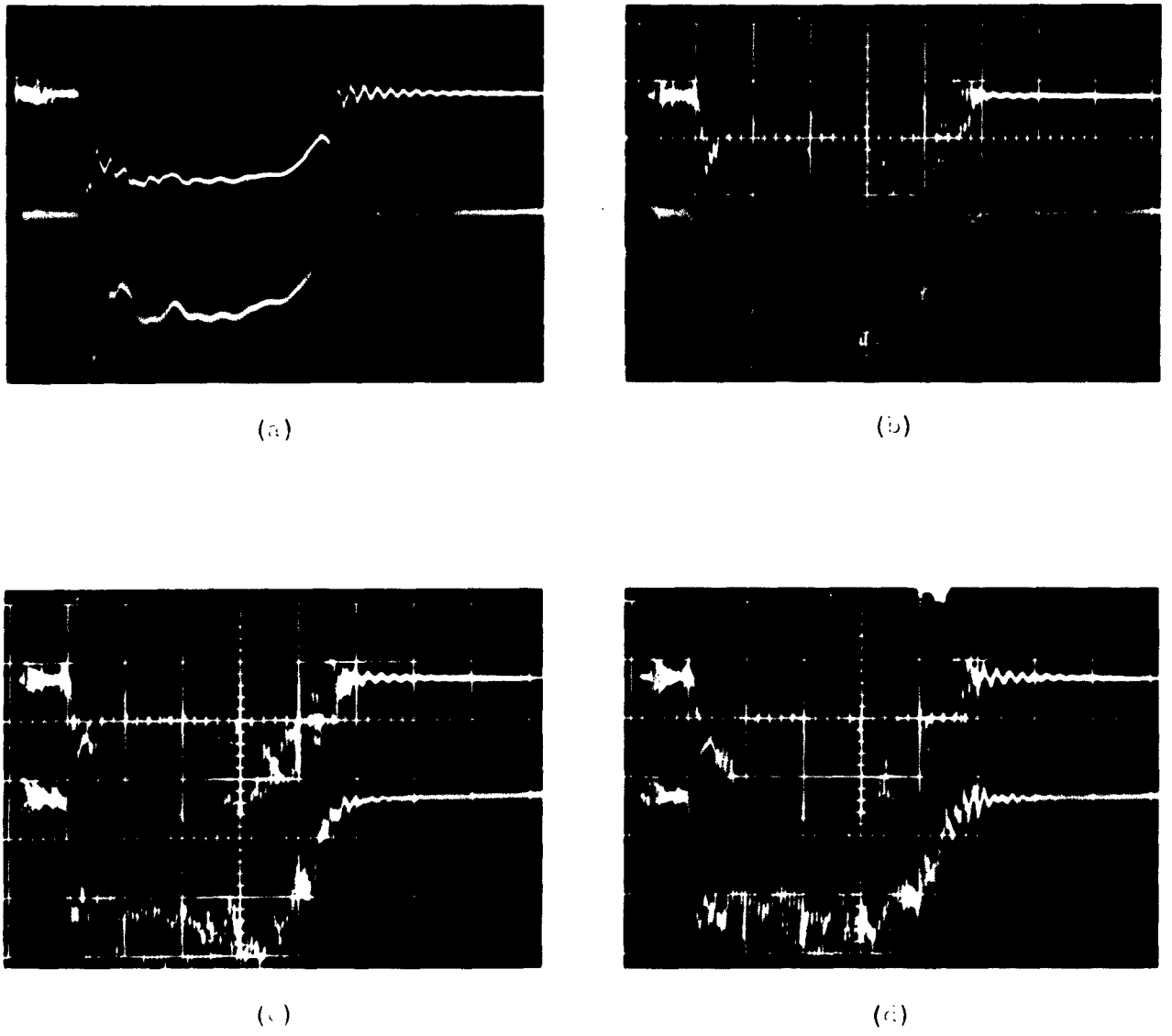

Fig. 12. The very fast response of these detectors to changes in the x-ray beam is shown by the oscilloscope photographs above. In these photographs, the upper trace represents the response of the oscilloscope to the electron beam monitor, while the lower trace represents the response of the p-n junction detector to the gamma rays produced by the x-ray tube.

1. The detector signal as demonstrated by the bremsstrahlung spectra follows the pulse shape of the electron beam.

2. Signal height increased with increasing bias voltage. The voltage dependence of the signal was a result of the increase of the depletion region component with applied voltage. The signal has two components: a diffusion and a depletion region component. The response as a function of time is expected to obey the relationship of (5).

The diffusion component limits the time response of the units, since its rise time is governed by the lifetime of the minority carriers. The fast rise demonstrated in Figs. 10, 11, and 12 indicates that the lifetime is less than 0.5 μsec. The lifetime of the minority carriers may be estimated by determining their diffusion length.

A plot of signal versus bias voltage for the detector used in these experiments is given in Fig. 13. The experimental data show that

1. The signal height is a linear function of the applied potential and is proportional to the depletion region width.

2. The intercept at zero-bias corresponds to the diffusion component. It is seen that at an applied voltage of approximately 40 volts, the depletion region component is equal in magnitude to the diffusion region component. The width of the depletion region at this potential is 10 microns. The diffusion length of minority carrier electrons in the p region is therefore[6] also 10 microns. This is consistent with the consideration determined above that the lifetime of minority carriers τ_n should be less than 0.5 μsec to produce the fast-rising signal response obtained.

3. The sensitivity of this unit is therefore 2.43×10^{-8} amps/cm^2/micron/r/sec.

The dosimetry was accomplished using DuPont film dosimeters. The dose per pulse at 3-5/8 inch from the lucite shield was found to be 7 r. Thus, for an 8-μsec pulse, the dose rate would be 8.75×10^5 r/sec.

A thin detector having a total thickness of 0.016 inch was also used. This unit could be operated at a potential which extended the depletion to the back of the detector. Its response as a function of applied potential is shown in Fig. 14. When the depletion region approaches within a diffusion length of the back, a plateau is obtained.

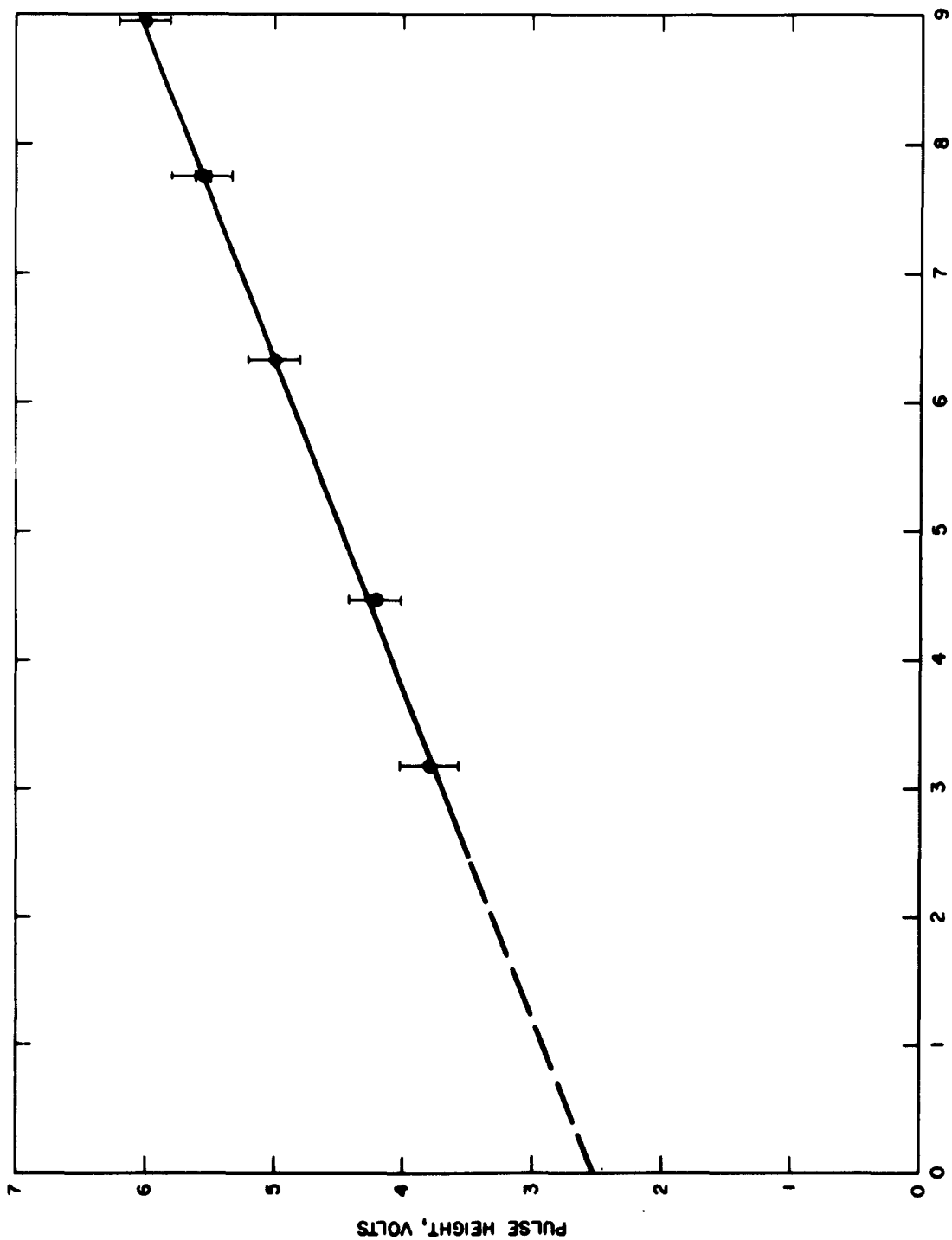

Fig. 13. Detector pulse height as a function of depletion region width.

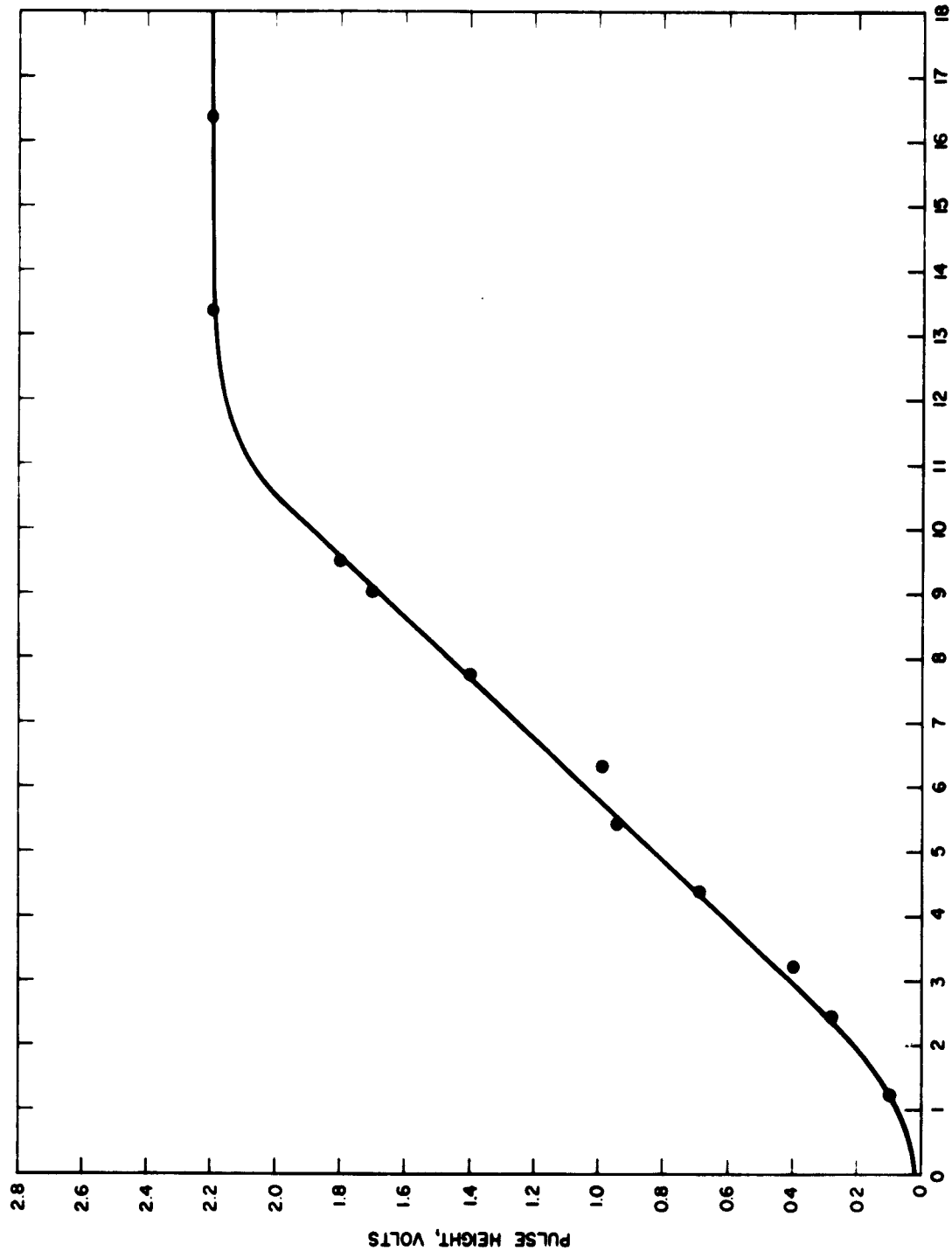

Fig. 14. Pulse height as a function of depletion region width showing that constant detector response is obtained when the depletion region extends through the complete volume of the unit.

The response of a high-resistivity 6000-ohm-cm unit is shown in Fig. 15. Here the response is very much a function of load resistance. As the load resistor is lowered, the decay of the signal across it becomes very rapid so that it no longer marks the decay of the signal across the diode. The diode decay is observed clearly in Fig. 15(c) where a 5-ohm load resistor was used.

Since the depletion width is shown to be significant for the high-resistivity units, the signal must clearly have two components. The depletion component rise and decay is a very rapid function of T_R. The diffusion component decays much more slowly with its time constant equal to the lifetime τ.

The response of a very-low-resistivity (ρ = 10 ohm/cm) detector in which the diffusion component dominates is seen in Fig. 16. The signal is seen to rise and decay slowly and its time constant is completely governed by the minority carrier lifetime, which is 10 μsec. The signal is independent of applied voltage since the depletion region thickness is much smaller than diffusion length.

The cross section and profile of this beam were plotted using a 100-ohm/cm diode having a low lifetime and therefore a fast time response. The sensitive area of this detector was 5 x 5 mm. The results are shown in Figs. 17 and 18. Greater resolutions are easily obtainable by using detectors of smaller sensitive areas. There were no radiation damage effects observed during these irradiations, nor were signals observed when the diode alone was removed from the beam, leaving cables, etc., in place.

It should be pointed out that high-quality units are not a requirement for this work. The photocurrents are of the order of 0.1 ampere, making normal reverse currents and detector noise insignificant. An optimum detector for this work should therefore have the following characteristics: (1) high resistivity, (2) small diffusion region, and (3) operation at a high reverse bias. These characteristics would make it possible to use the entire sensitive volume of the detector, thereby removing all voltage dependence. In addition, the slow-rising diffusion component would be eliminated and the time response improved.

It would be of interest to continue this work with very fast pulses such as the 10^{-8} second wide pulses now obtainable. The reproducibility of absolute sensitivities from unit to unit should be investigated further. The technique of measuring diffusion length for the high-resistivity material described in this section is unique and may warrant further consideration. Its advantage over conventional methods[7] of measuring L_n is that the generation rate need not be known, since the diffusion length is determined by comparing it with the depletion region thickness, which is determined by capacitance measurements.

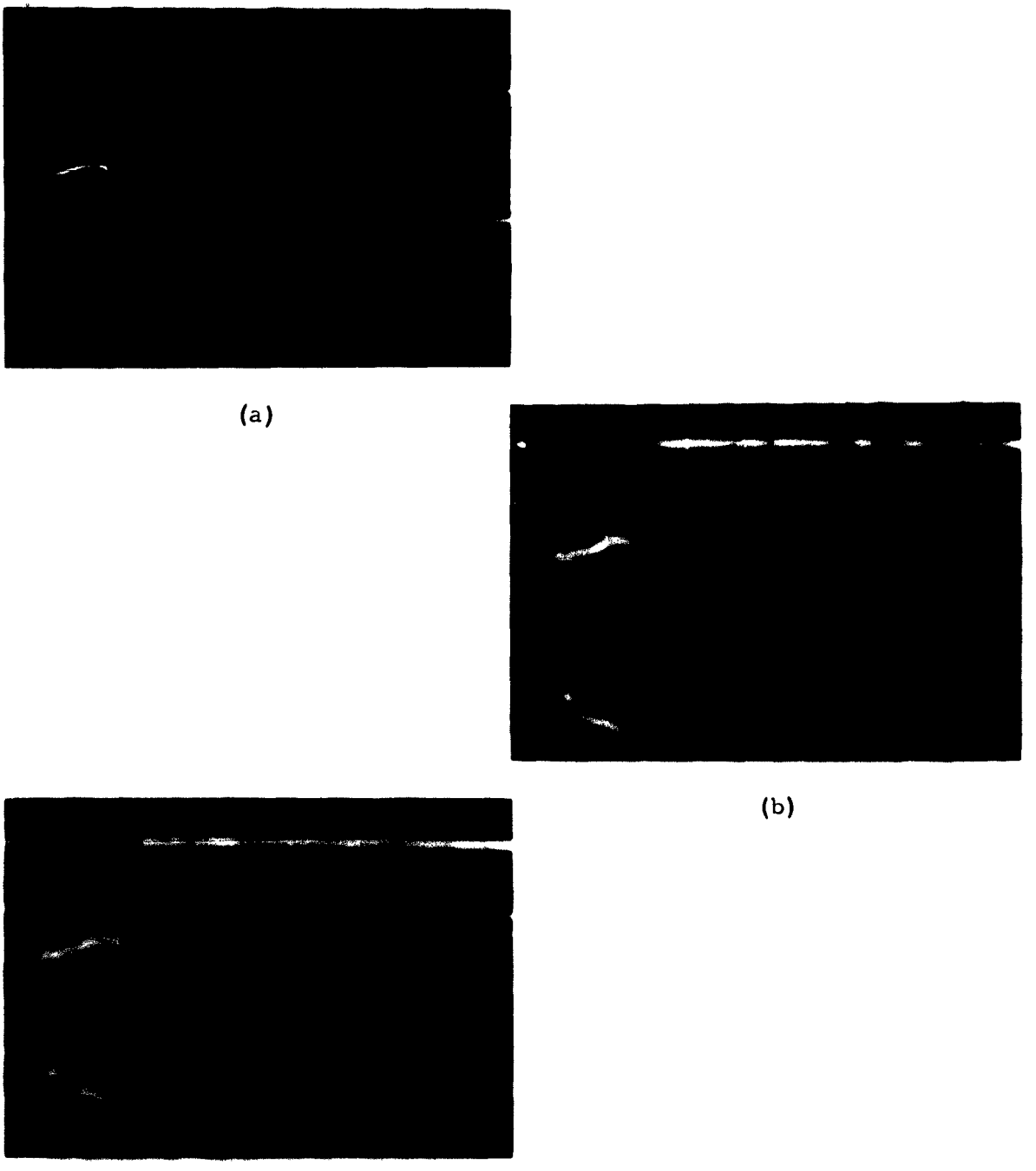

(a)

(b)

(c)

Fig. 15. Response of a high-resistivity (6000 ohm-cm) p-n junction radiation detector to the high-intensity pulses of a linear accelerator. Curves shown utilized a load resistance of (a) 2000 ohms; (b) 75 ohms; (c) 5 ohms.

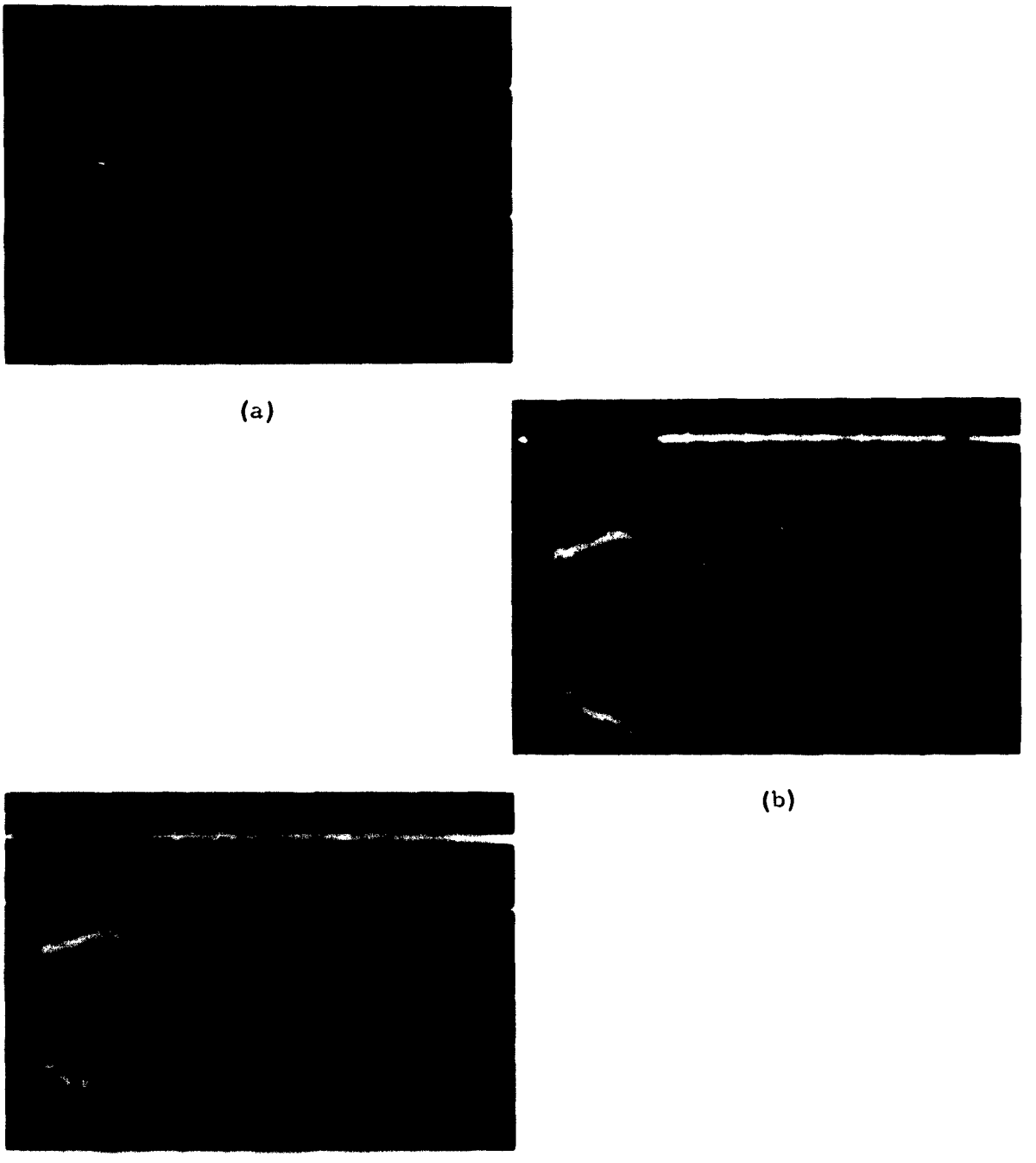

(a)

(b)

(c)

Fig. 15. Response of a high-resistivity (6000 ohm-cm) p-n junction radiation detector to the high-intensity pulses of a linear accelerator. Curves shown utilized a load resistance of (a) 2000 ohms; (b) 75 ohms; (c) 5 ohms.

(a)

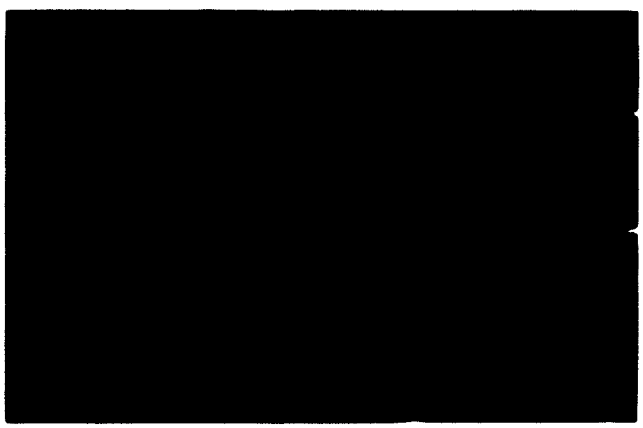

(b)

Fig. 16. Response of a low-resistivity (10 ohm-cm) p-n junction detector to high-intensity linear accelerator pulses. Load resistances used were (a) 10 ohms; (b) 25 ohms.

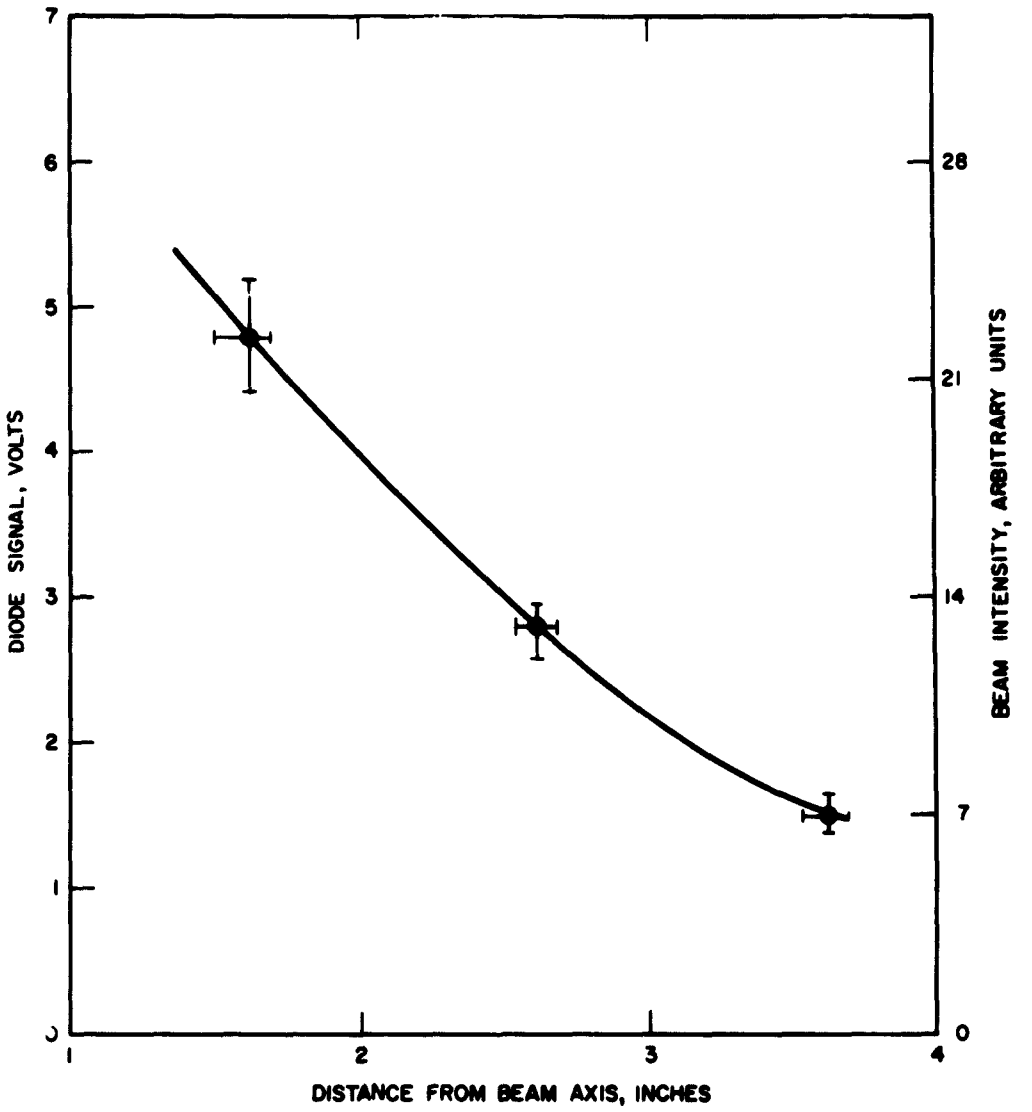

Fig. 17. Beam intensity as a function of distance from the beam axes plotted in a vertical direction. A 5- x 5-mm p-n junction detector was used in the linear accelerator gamma-ray beam.

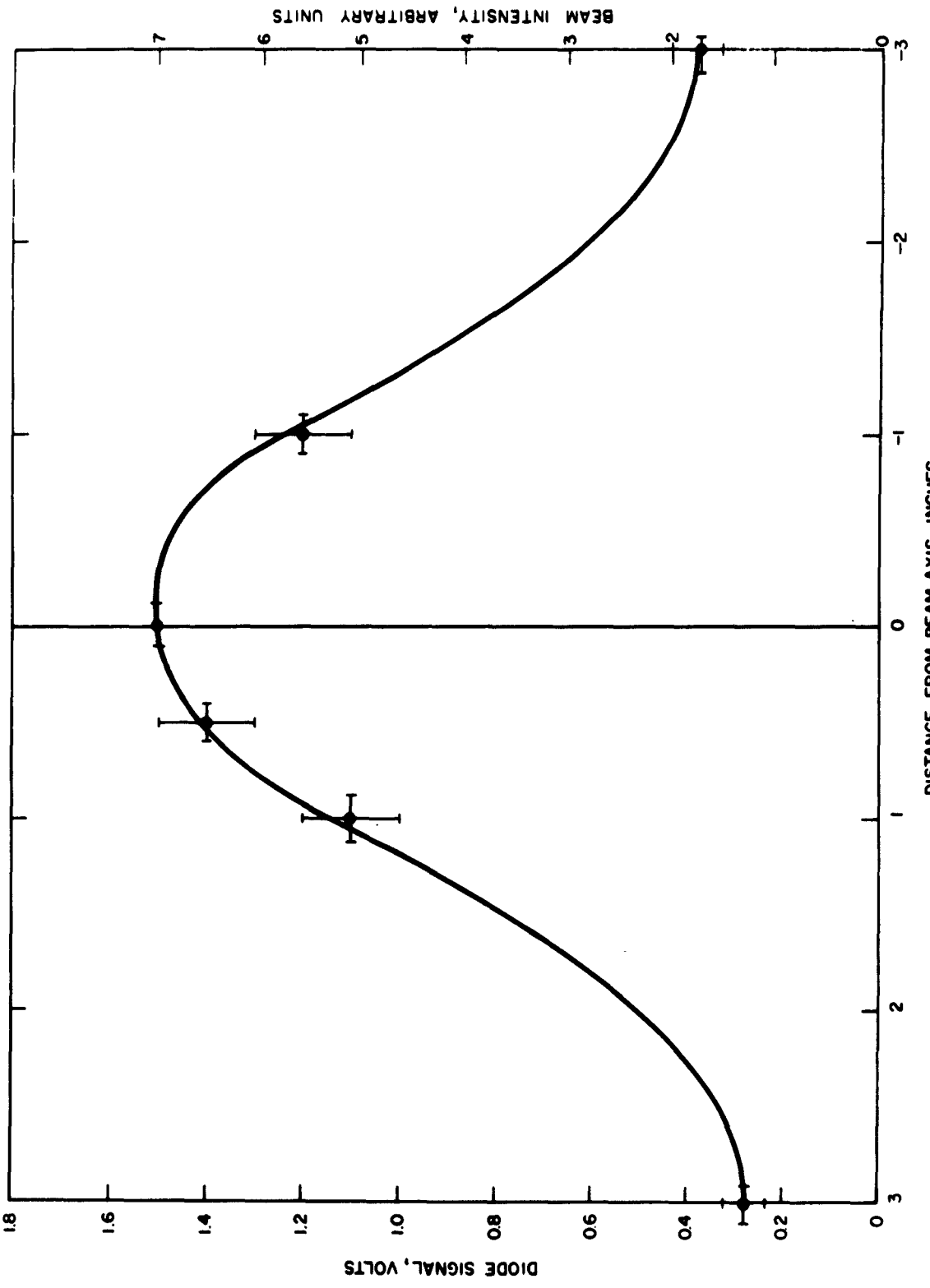

Fig. 18. Beam intensity versus distance from the beam axes plotted in a horizontal direction using a 5- x 5-mm p-n junction detector in the linear accelerator gamma-ray beam.

C. Permanent Effects

Several experiments were performed to determine whether any permanent effects were produced by gamma radiation which would affect the response characteristics of p-n junction detectors. The flux and integrated dose were chosen to simulate those levels used for dosimetry of pulsed reactors or linear accelerators.

Two detectors were irradiated using the gamma-ray bremsstrahlung produced by a linear accelerator having a maximum flux of 1.4×10^5 r/sec which produced total dosage levels of 1.25×10^4 r and 1.50×10^5 r, in the detectors. No change was observed in any detector characteristics, such as pulse height response to charged particles, rise time, forward and reverse current, junction capacitance, and photocurrent response to silicon-filtered light.

The irradiation geometry is shown in Fig. 19. A 0.025-inch platinum target was used to produce the bremsstrahlung spectra. A magnet was used to deflect electrons from the transmitted beam, thus providing a photon beam which was relatively free of electrons. The energy of the electron was 20 Mev, producing an average photon energy of 7 Mev.

The pulse width was 5 μsec, and the machine was run at a repetition rate of 60 pps. The dosimetry here is uncertain by about ± 25 percent since an ionization chamber whose recombination rate was unknown was used. These experiments have clearly shown that for photons of this energy there is no observable effect on silicon p-n junction detector characteristics at the dose rates and levels utilized. Since these are the dose levels usually found in conjunction with pulsed reactors, we can expect that the gamma-ray contribution from the reactor irradiations on the diodes did not produce permanent effects. The radiation damage observed in the reactor-irradiated diodes thus must have resulted solely from the associated neutron flux.

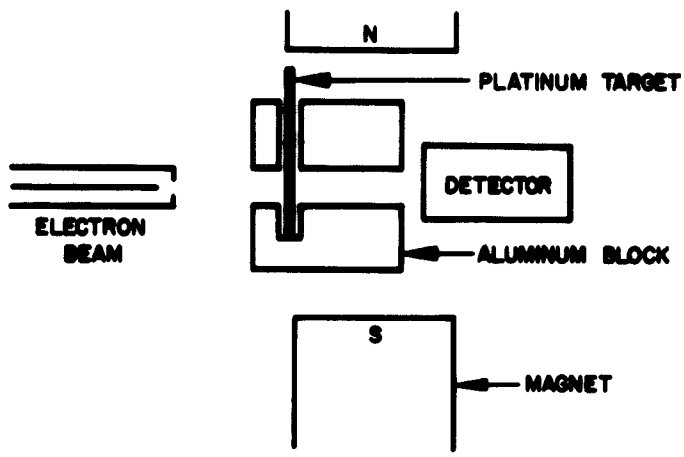

Fig. 19. Geometry used for the radiation of p-n junction detectors in an electron accelerator beam.

IV. DETECTION OF A REACTOR FIELD (EXPERIMENTAL RESULTS)

A. Response to Pulsed Reactor Fields

1. The Triga Reactor – The experimental runs were made at the Triga Mark I Reactor of General Atomic at La Jolla, Calif. A general view of the reactor is shown in Fig. 20. Additional details are shown by the cutaways in Fig. 21. The most convenient method of irradiation would be to use the specimen tube leading to a rotary specimen rack in the reflector or the pneumatic transfer tube leading to the core of the reactor. Unfortunately, these were not suitable for this experiment since the reflector tends to accentuate the thermal flux, and the pneumatic tube does not allow electrical leads to be brought out from our detector.

We therefore chose to replace a fuel element in the D-ring of the core using a water tight tube which led to a position directly above the water shielding. A normal fuel element assembly is shown in Fig. 22. The replacement tube contained half of a fuel element, replacing the lower half of the original one. Above this was the detector followed by a plastic tube. The tube diameter was such that the cable was able to pass between it and the housing. This resulted in maximizing the fast-to-thermal neutron flux ratio. The experimental arrangement is shown in Fig. 23.

Both steady-state and pulsed modes of reactor operation were used. The steady-state runs were made at power levels of about 10^{-3} to 1 Mw. The pulses were at integrated powers of about 16 Mw-sec. Operating in both modes gives a better understanding of the relation between dosimetry and power levels. While it was a very simple matter to vary a steady-state power, it was extremely difficult to vary the pulsed mode without changing detector position. Because of the asymmetry produced by the disturbance of the fuel elements, an uncertainty in neutron spectra was introduced.

This change in the relative positions of the sample and control rod positions tended to have its maximum effect on the thermal flux. In the pulsed mode the control rod was completely withdrawn during the pulse of radiation, thereby again producing a different neutron spectrum.

2. Dosimetry – The dosimetry here involved only the neutron flux. Gamma-ray measurements inside the reactor are difficult, and it was not considered feasible to attempt these because of the limited scope of this contract.

Fig. 20. Cutaway view illustrating the geometry of the reactor which was used for radiations of the p-n junction detectors. This is a TRIGA Mark II reactor.

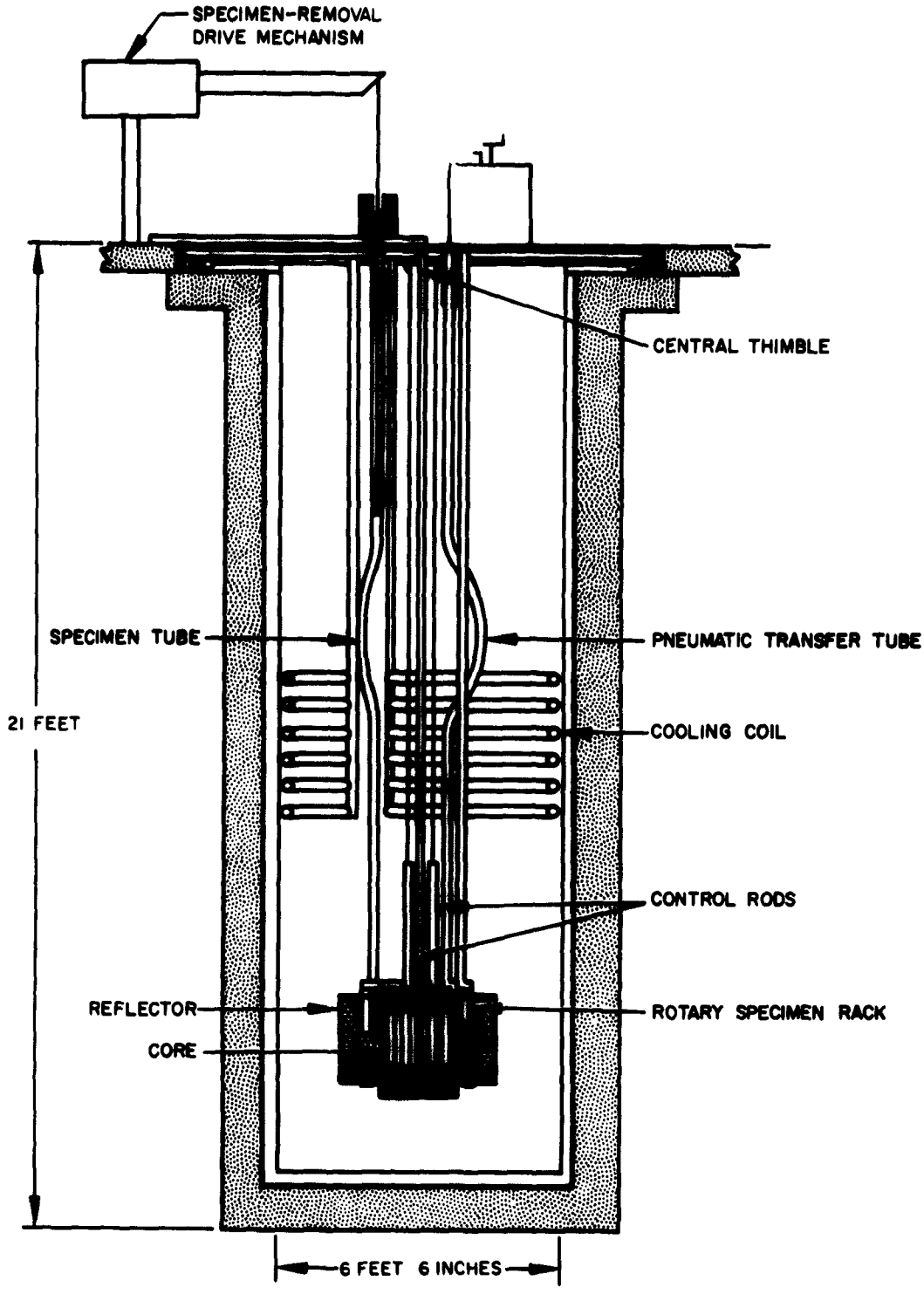

Fig. 21. Cross section showing elevation view of the TRIGA reactor.

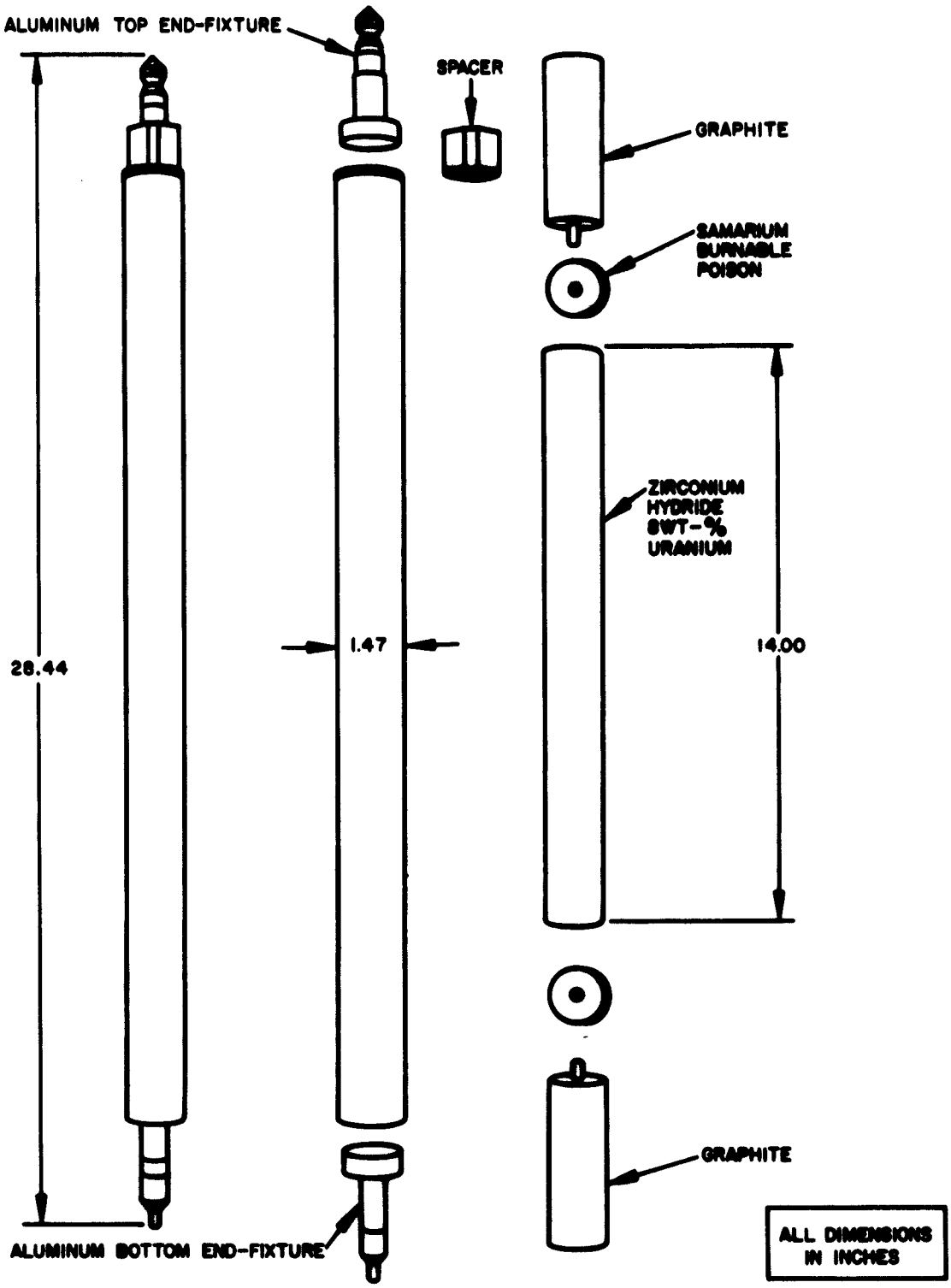

Fig. 22. TRIGA fuel element.

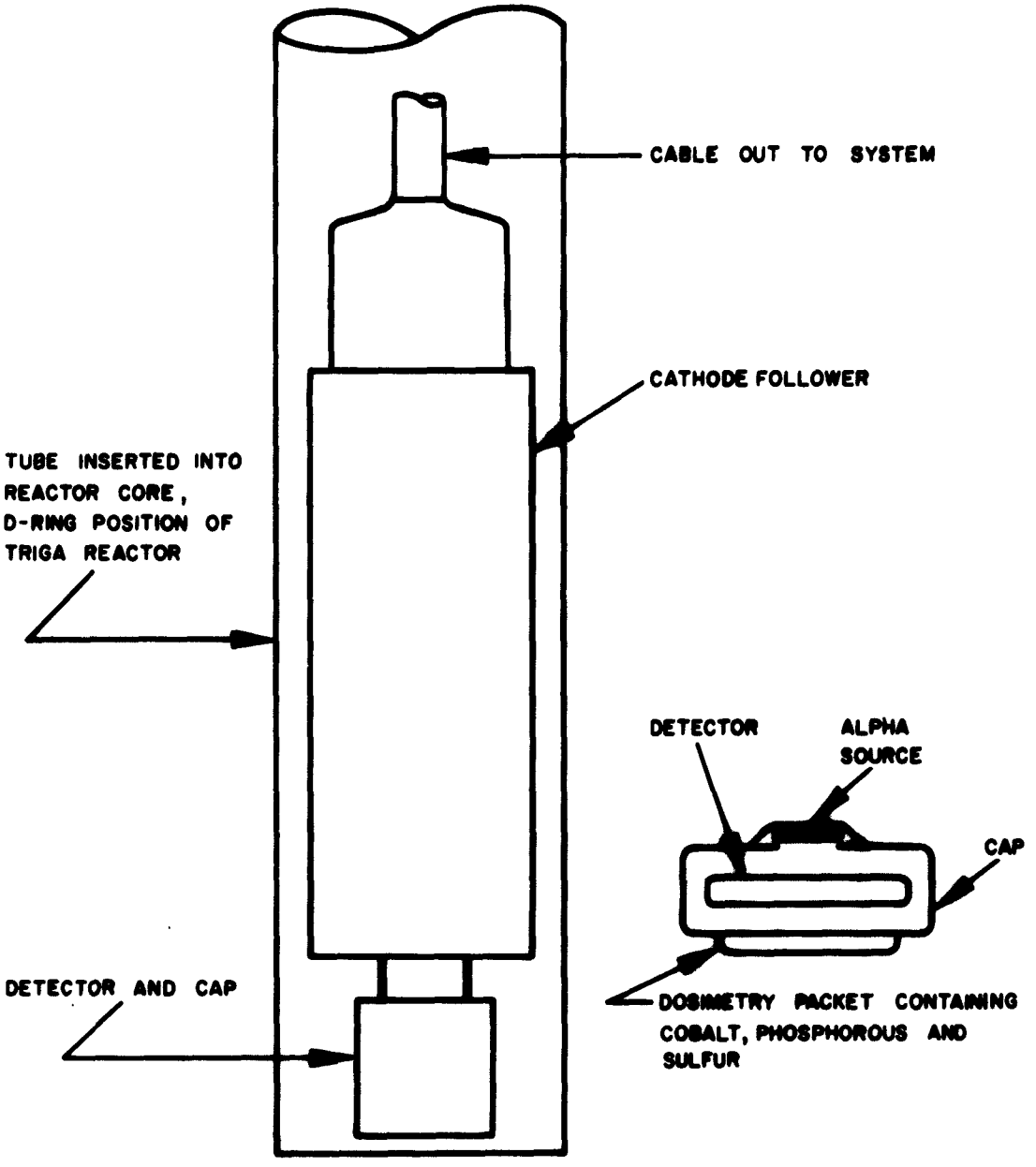

Fig. 23. Cross section of dummy fuel element section containing dosimetry packet, p-n junction detector, and cathode follower.

The neutron flux measurements were made by foil activation. Foils used were Co^{59}, S^{32}, and U^{238}.

The cobalt reaction was induced in wires about 0.030 inch in diameter and of very high purity. The wires were thick enough that the epithermal resonance was of negligible importance and the epithermal contribution was therefore only a function of "1/v" and easily calculated. The induced activity was measured using a scintillation counter. The activities due to impurities had been allowed to decay prior to assay. Absolute activity was obtained by comparison with an N.B.S. standard. The cross section for this reaction[8] was taken to be 37 barns.

The method of Hurst, et al.,[9] was used for the S^{32} (n,p) and U^{238} fission reaction with certain modifications. This method compares the cross section for fast neutron reactions with those for thermal reactions, which lead to the same radioactive products. In the original method the thermal reactions were induced by the use of a thermal column, which is a reactor facility with a negligible epithermal flux. In our measurements we calibrated foils using the thermal flux present at the point where the fast flux was utilized. This involved a considerable epithermal contribution to the U^{235} fission reaction, which was corrected for by a method discussed in the Appendix. The measured fluxes are given in Table I. The theoretical values shown were supplied by Gordon West of General Atomic and were computed using a group-type analysis of the neutron spectrum. The value given for the number of neutrons having energies greater than 2.9 Mev was interpolated by computing the numbers which should be found with energies above 3.7 and 1.4 Mev.

TABLE I

Flux/Power $\left(\frac{\text{Neutrons/cm}^2}{10^7 \text{ watts}}\right)$

Power Level kw	Neutrons/cm^2/10^7 watts					
	Thermal		1.3 Mev		2.9 Mev	
	Exp.	Theor.	Exp.	Theor.	Exp.	Theor.
0.65	1.69	↕		↕	0.39	↕
6.5	1.77				0.39	
65	1.51					
650	2.24					
Pulsed (800 Mw peak)	2.5	1.01	0.88	0.96	0.35	0.29

It is interesting to note that all the thermal flux values, independent of the mode of operation, are significantly greater than theoretical predictions, while in the case of the fast flux the theory gives accurate values. This illustrates the fact that the thermal flux is the most unreliable of all reactor parameters as a measure of power because the sensitivity to environmental conditions is so great. This is particularly true when control rods are varied, since the number of thermal neutrons in close proximity to a control rod changes rapidly with control rod position in the reactor.

B. Detection of Pulsed Reactor Radiation

Most investigations of the mixed neutron-gamma ray field in a reactor have involved the comparison of hydrogenous and nonhydrogenous detection systems. The basis for this approach is that a fast neutron will give up (on the average) half of its energy in an elastic encounter with a hydrogen nucleus but a much smaller fraction of its energy in encounters with heavier nuclei, such as carbon or oxygen. This is strikingly illustrated when energy loss is calculated on the basis of mass. On the other hand, gamma-ray interactions involving the Compton effect are proportional to the number of electrons per gram, and therefore the energy loss does not vary much from hydrogenous to nonhydrogenous materials.

In addition to the necessity of using two separate materials, the former techniques have involved time-consuming calorimetric measurements. By directly measuring the heat evolved, one obtains a parameter of direct physical interest, the energy absorbed per gram of irradiated material. Further analysis may produce values of the energy absorbed by both atoms, one hydrogen, and one representative of the other atoms of interest. This approach is applicable to problems of radiation chemistry and health physics, where the energy absorbed is the parameter of interest.

Although the calorimetric approach is a form of absolute dosimetry, it is a slow, tedious measurement. The p-n junction detector may be more suitable for this application, although it seems to have its greatest applicability as a relative monitor, to be calibrated by other means such as calorimetry.

The two most important categories of interactions are hole-electron generation due to ionization and lattice-defect production through elastic collisions. The latter effectively interferes with hole-electron collection. Defect production with gamma rays, although possible, has a cross section which is negligible compared with that for defect production by neutrons. Since the gamma rays produced in a reactor are associated with fission processes, the average energy is approximately 1 Mev. In this range ionization is primarily produced by the Compton effect.

Ionization by neutrons is an indirect process in which energetic recoils lose orbital electrons, these, in turn, causing ionization. The relevant energy ranges are difficult to pinpoint exactly because charge pickup by heavy ions has been studied only in isolated instances. An order-of-magnitude rule is that the ion will be neutralized when traveling at a velocity corresponding to an energy of 1 ev. For silicon this corresponds to a 52-kev recoil, which is produced on the average by a 720-kev neutron. Within the accuracy of this approximation, most of the energy transfer due to elastic neutron interactions with the silicon will produce ionization, since the neutron energy spectra decreases sufficiently rapidly with energy.

It is therefore indeterminate as to whether the ionization produced in silicon comes mainly from the gamma rays or from the neutrons. It has been found in several reactors that gamma ray interactions are predominant for medium-weight elements. The argument that follows in support of this statement may be made quite general, although in this case it is made only for silicon. For each thermal neutron in the fission spectrum, on the order of 8 Mev of prompt gamma rays are found. The neutron flux with energies higher than thermal is on the order of the thermal flux and by West's[10] calculation is no greater than ten times the thermal flux. If we consider a fast neutron having an energy of 100 kev, then we must compare the input ion produced with that of 8-Mev gamma rays having an average energy of 1 Mev. A 1-Mev gamma ray will deposit roughly 3 percent of its energy/gram/cm^2, or 3×10^4 ev. The neutron will deposit about $(N\sigma Z/A) \times 10^4$ ev, or about 3.1×10^2 ev/gram/cm^2. Since gamma-ray ionization is 100 times larger, other factors in the approximation become negligible.

Other neutron interactions may be considered by comparing them with the recoil problem. If they are comparable to this problem, then they are negligible, as compared with gamma rays. If they are as much as ten times greater, then they must be considered. The $Si^{28}(n,p)$ interaction is striking because the recoil photon energy (on the order of 1 Mev) is 70 times the energy of a silicon recoil due to a 100-kev neutron interaction. This factor is then reduced because the relevant cross sections are five to ten times smaller, and flux is approximately 20 times less. A similar argument will exclude the Si^{29} (n,p) reactions, the $Si^{30}(n,\gamma)$ Si^{31} interaction, and its subsequent beta rays. The latter interaction is particularly ineffective since Si^{30} is a 3-percent isotope. In effect, then, all possible interactions due to neutrons produced in the Triga reactor which might produce ionization in the detectors are negligible compared with gamma-ray interactions.

Several p-n junction detectors were inserted into a hole in the D-ring of the reactor. The circuitry used is shown in Fig. 24. Since the Triga pulses last approximately 10 msec, this arrangement was more than adequate to eliminate the possibility of any long time constants affecting the shape of the resultant pulse as seen by the recording galvanometer or the oscilloscope.

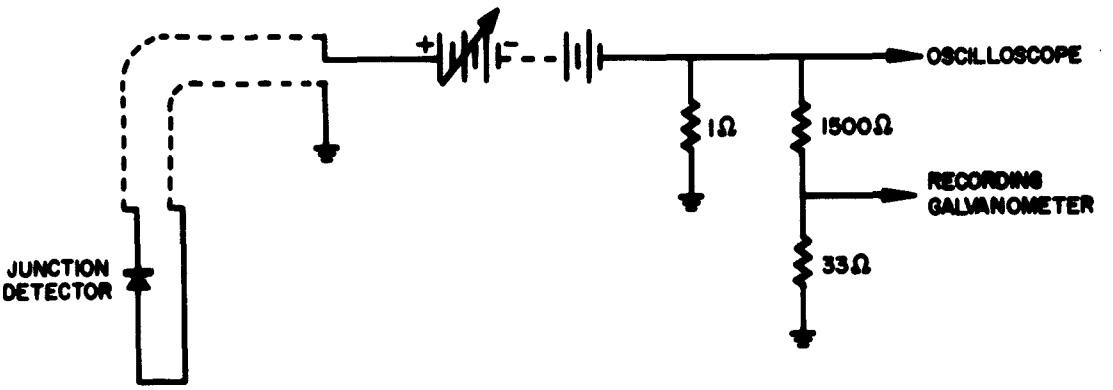

Fig. 24. Circuit diagram for evaluation of detector response to high-intensity neutron bursts associated with a pulsed reactor.

A typical reactor pulse is shown in Fig. 25. The reactor was operated at about 800 Mw peak power. The detector pulse was compared with the pulse from an ionization chamber normally used for monitoring the reactor. Although there are some differences between the pulses, there is a close similarity. The ionization chamber was located several feet from the actual reactor core, whereas the detector was in the middle of the core; this difference in geometry may account for the discrepancies. Also the chamber was sensitive to neutrons, whereas the detector is relatively insensitive to neutrons of all energies. It is thus possible that the peaking of the detector pulse at times earlier than that recorded from the ionization chamber was a result of the time required for the thermal neutrons to reach the ionization chamber. These are shown by both the oscilloscope and recorder traces in Figs. 26 and 27.

One difference between pulses is a slight asymmetry introduced into the detector pulse and not present in the chamber pulse. This appears to be accentuated by repeated pulsing and could be caused by an accumulation charge due to circuit parameters. An even greater difference is illustrated by the increased pulse width. These effects are difficult to analyze. A third interesting effect is on the pulse amplitude, which shows a decrease with repeated pulsing of the reactor.

Fig. 28 shows the results of repeated pulsing on two detectors. The applied bias was alternately changed from 10.5 to 60 volts following successive reactor pulses. In one case the detector was exposed behind a cadmium filter which effectively removed the thermal flux. Assuming the initial sensitivities were equal, the cadmium cover increased the response by a factor of 1.6 ± 0.2, probably because of the (n, γ) reaction in cadmium, which converts each thermal neutron into at least one gamma ray.

It also appears that the response at 10.5 volts saturates at a peak value of about 0.20 ma/Mw-cm^2. If we assume that the portion of the response curve which represents zero damage varies as $V^{1/2}$, then the saturated response found at 60-volts bias at the peak of the pulse is 0.48 ma/Mw-cm^2. In both cases, by subtracting values at saturation and replotting this value as a function of the number of pulses, we obtain the results shown in Fig. 29. These show that detector response is approximately an exponential function of the number of pulses.

It is clear that while the amplitude of the pulse is dependent on gamma-ray intensity, the progressive decrease in response is caused by radiation damage. This damage is due to the neutron interactions. If we assume the two-region model for the detector as previously described, then the infrared portion of the response depends only on the interactions occurring within the depletion region where carriers are rapidly swept out.

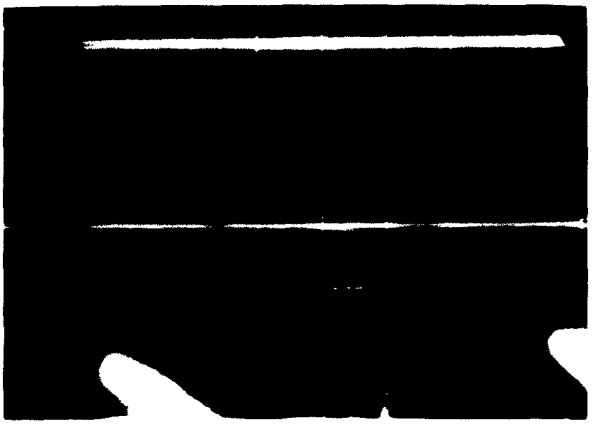

(a)

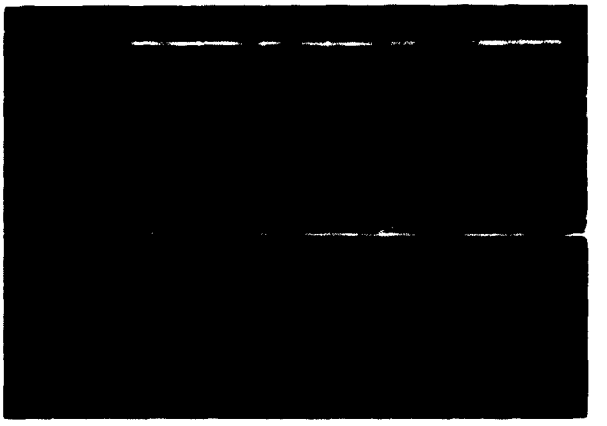

(b)

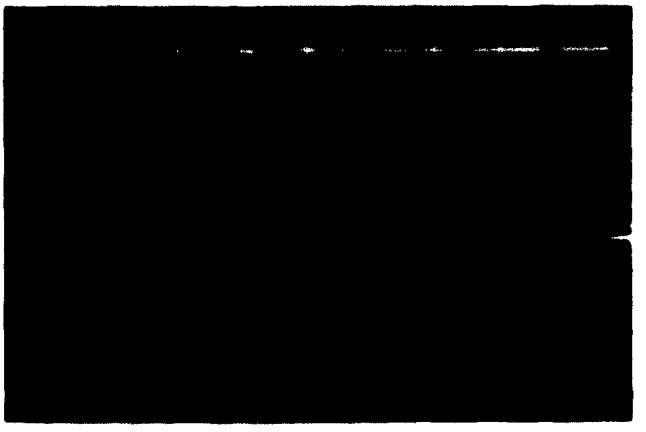

(c)

Fig. 25. Response of p-n junction radiation detectors to a pulsed reactor beam. The upper trace corresponds to the ionization intensity as a function of time as recorded by an ionization chamber, while the lower trace in each case represents the response of the p-n junction detector. The load resistance in each case was 1 ohm, and the upper trace sensitivity was 2 volts/cm. A sweep time of 10 μsec/cm was used. The junction potential was 10 volts. The lower trace sensitivity in (a) and (b) = 0.01 volt/cm, while that in (c) = 0.05 volt/cm.

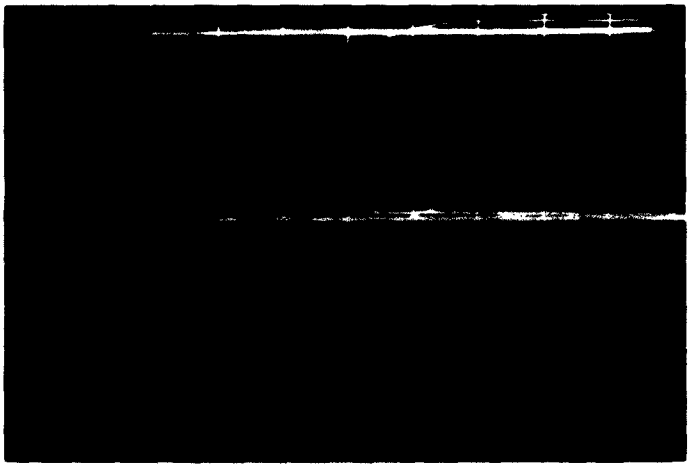

(a)

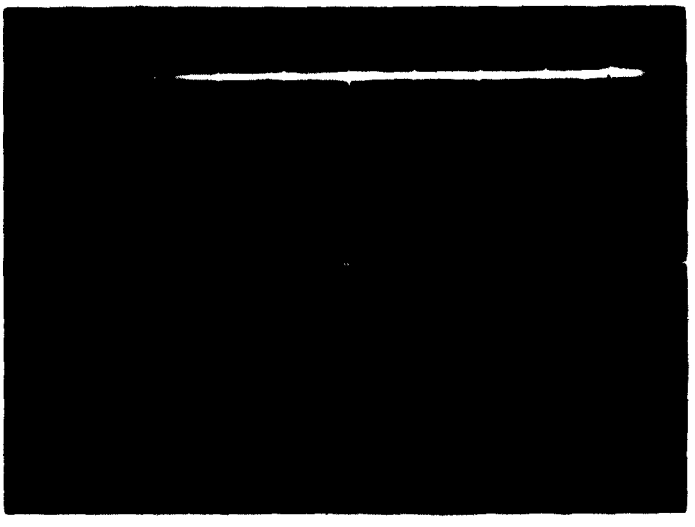

(b)

Fig. 26. Detector response to high-intensity fast neutron pulses. The upper trace was recorded at 0.02 volt/cm oscilloscope sensitivity and represents the ionization as a function of time in a monitor ionization chamber. The p-n junction detector was operated at 60 volts bias. Curve A was recorded with an oscilloscope sensitivity of 0.1 volt/cm, and Curve B at 0.05 volt/cm.

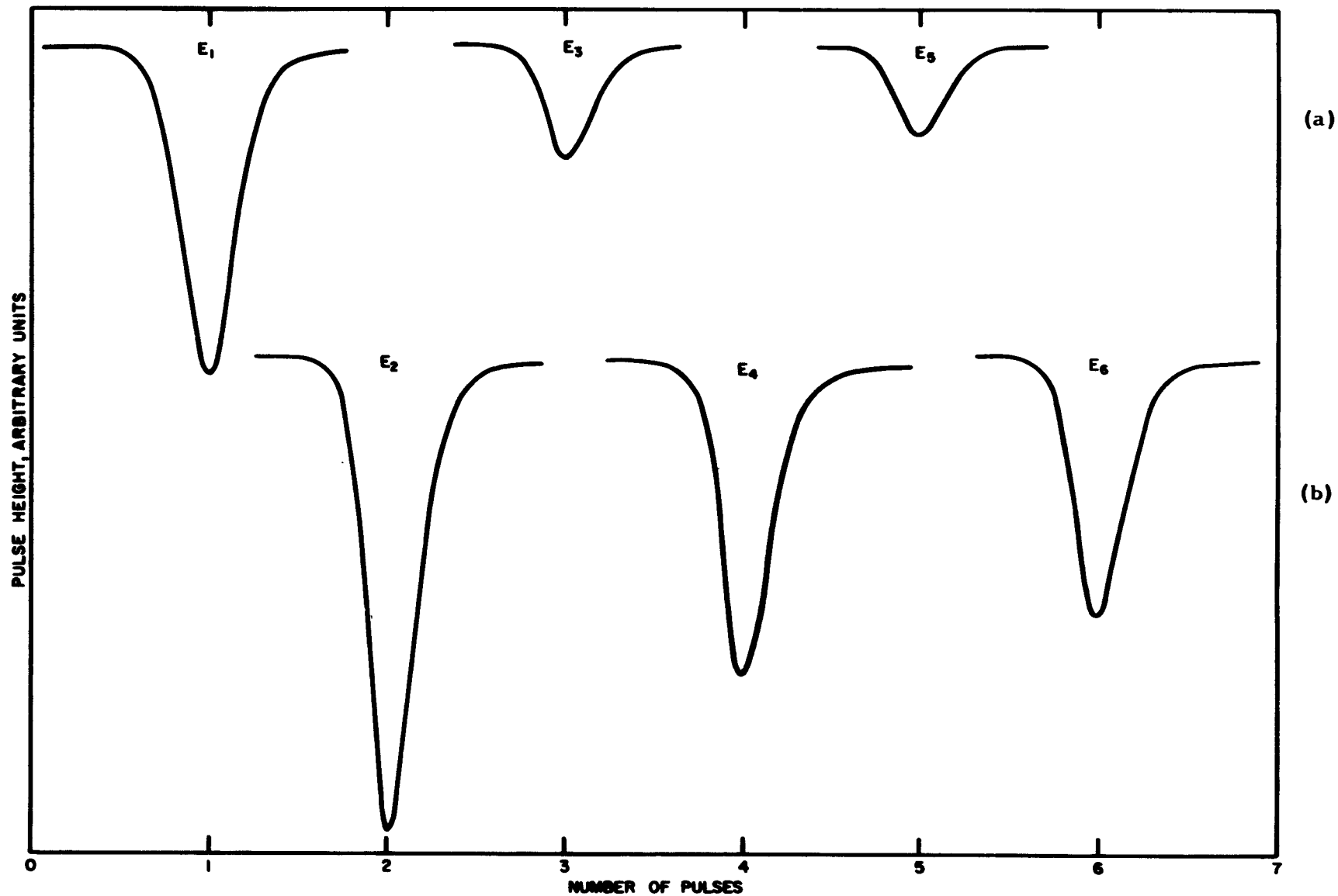

Fig. 27. Recorder traces of the response of a p-n junction detector to a high-intensity, pulsed neutron source showing the effects of radiation damage caused by successive neutron pulses. The three traces shown in (a) were recorded using a detector bias of 10.5 volts, while those shown in (b) were recorded using a bias potential of 60 volts.

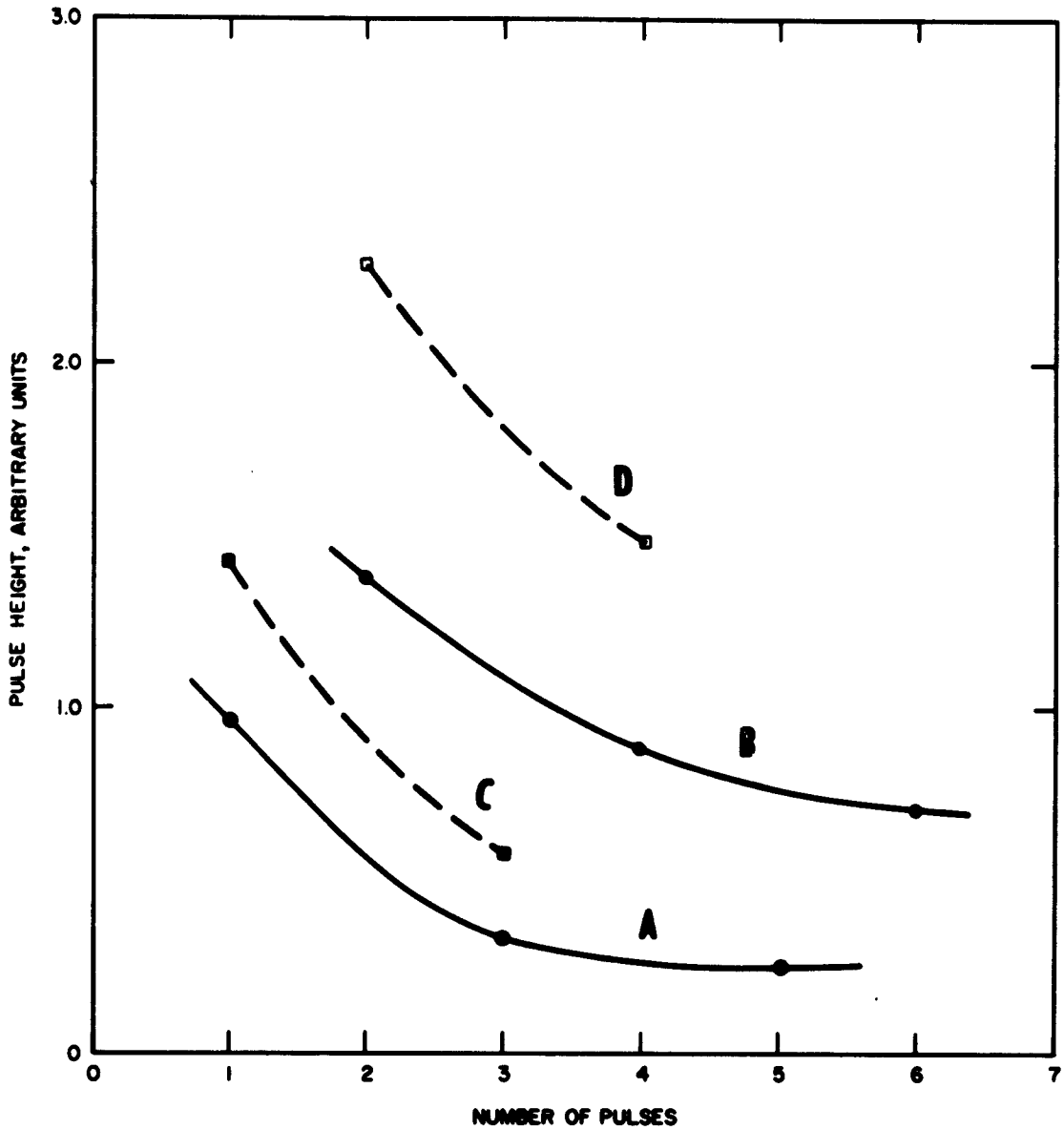

Fig. 28. Pulse height response as a function of the number of neutron pulses incident on a p-n junction detector. (a) bare detector operated at 10.5 volts junction potential; (b) bare detector operated at 60 volts junction potential; (c) p-n junction detector covered with 0.04 inch of cadmium and operated at a junction potential of 10.5 volts; (d) p-n junction detector covered with 0.04 inch of cadmium and operated at a junction potential of 60 volts.

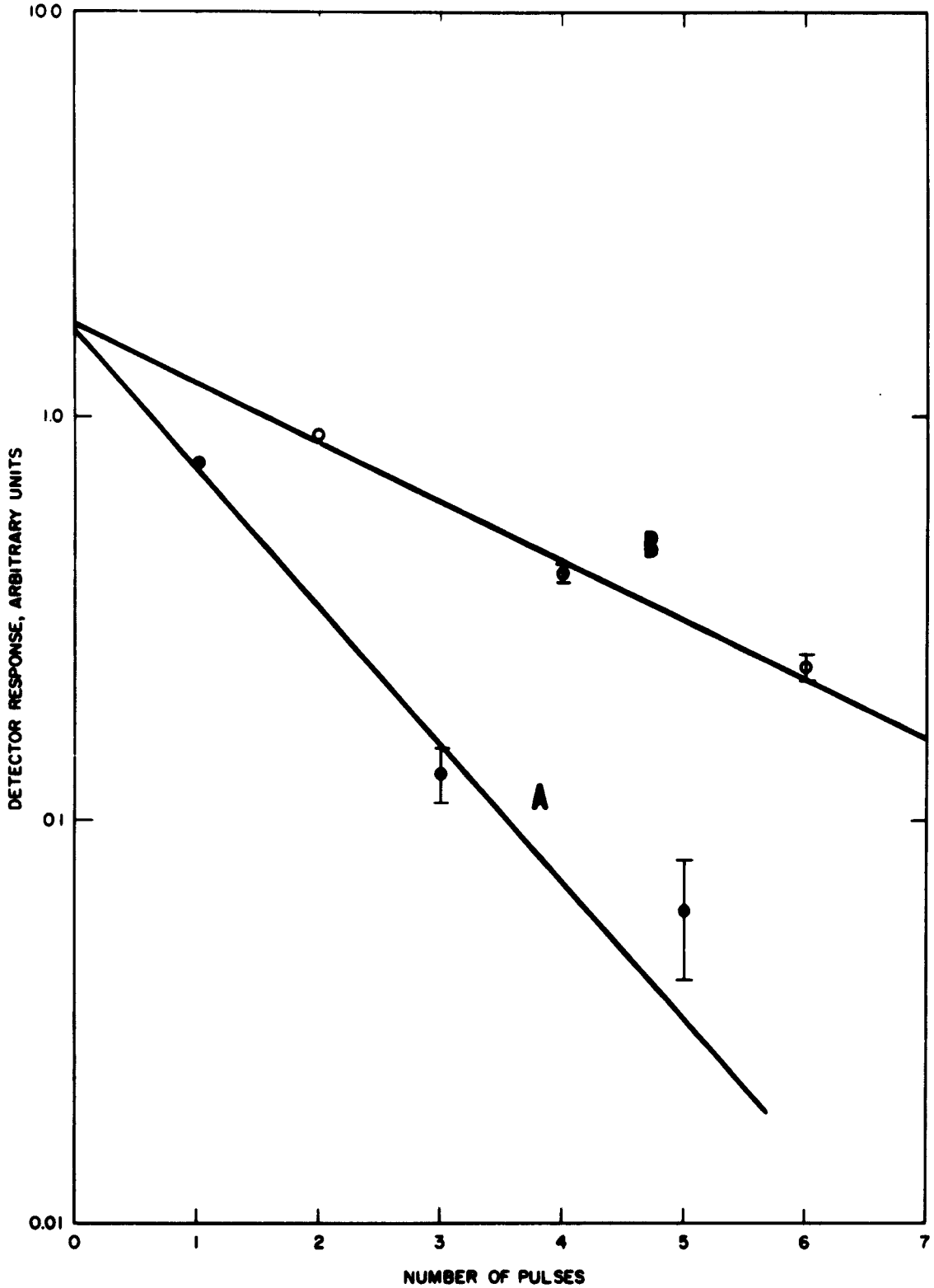

Fig. 29. Detector response (current/Mw/cm^2 at peak of pulse) as a function of the number of neutron pulses: (a) applied junction potential= 10.5 volts; (b) applied junction potential = 60 volts.

C. Permanent Effects

As shown above, the decrease in detector pulse height to successive reactor pulses is caused by radiation damage, which results from lattice defects due chiefly to fast neutrons. Considerable work has been done in determining the effects of neutron radiation on single silicon crystals.[11, 12] The principal effect observed when fast neutrons are incident on semiconductors is an increase in resistivity which results from carrier removal and a reduced carrier mobility, which is accompanied by a decreased carrier lifetime. These effects are attributed to the introduction of levels within the forbidden energy gap by the formation of vacancy-interstitial defects.[13]

In earlier studies on the effects of reactor irradiation on silicon junction diodes,[14] it was found that the forward and reverse currents approach each other as a regular function of radiation dose until the junction is destroyed. With the development of the p-n junction for use as a charged particle detector,[15] interest in radiation effects on silicon diodes was heightened. Recent experiments by Babcock[16] have shown that the detector's response to charged particles is affected by fast neutron irradiation.

Radiation damage affects both the depletion region and the diffusion region components of the current. In order to separate these two effects, we examined the following parameters as a function of both total radiation dose and as a function of dose rate.

1. Detector Response to Alpha Particles – In general, alpha particles will deposit their energy in the depletion region; by observing the resulting signals, we can obtain information on the effects which take place within the depletion region.

2. Short Circuit Photocurrent – The diffusion region component of the current is solely responsible for the short circuit photocurrent; therefore, by examining the effect of radiation on this parameter, we can obtain information on radiation damage which takes place in the region responsible for generating this component of the current.

The alpha particle produces hole electron pairs only over its range. When a high-resistivity material is selected and the unit is operated at a sufficiently high bias, the depletion region is greater than the range of the alpha particle. The collection of charge due to ionization initiated by the alpha particle is similar to that due to the reactor pulse, the only difference being the amount of ionization initiated per unit of time. Thus alpha particles provide a useful tool for examining the mechanism of decrease of the depletion region component of the photoresponse. This method is advantageous as it does not produce any further radiation damage. In the case of a reactor, damage is produced by the neutron flux during the pulse, and therefore it is impossible to separate damage from ionization effects.

Several detectors fabricated from 6000-ohm-cm silicon and having mesa dimensions of 2 x 2 mm were irradiated in the Triga reactor to total dosage levels ranging from 2×10^{11} nvt to 3.5×10^{14} nvt fast flux having rates (> 3 Mev) varying from 1.7×10^{9} nv to 3×10^{15} nv. The following results were observed:

a. Pulse height decreased as a function of neutron dose. The magnitude of this decrease is a function of applied voltage. This is in contrast to the behavior before irradiation, when pulse height was independent of applied bias. This behavior is illustrated in Figs. 30 and 31. The pulse height change at 100 volts bias ranged from 98 percent of the original pulse height for a total dose of 2×10^{11} nvt to 6 percent of the original pulse height after exposure to a total fast flux of 3.6×10^{14} nvt. A plot of these data is given in Fig. 32. The magnitude of the decrease was found to depend on total dose alone and does not appear to be a function of dose rate.

b. After irradiation, the rise time of the pulses increased greatly. The rise time of the detector before irradiation was on the order of 10^{-9} second. At a 25-volt bias, the time constant of the pulse rise τ_R was approximately 1 μsec for a dosage of 1.2×10^{13} nvt and increased to 6 μsec when the dose was increased to 3.4×10^{14} nvt. Increasing bias across the junction resulted in a faster rising pulse.

c. Detector resolution became extremely poor after irradiation. This is shown by the data plotted in Figs. 33 and 34. Both the 6- and 9-Mev peaks broadened as the irradiation proceeded, and after continued irradiations they could no longer be distinguished, finally merging into a single peak. After irradiation the resolution of all detectors tested fell within the band shown in Fig. 35. The resolution expressed in kiloelectron volts represents the full width at half maximum of the 9-Mev alpha peak. The linewidth approached 1 Mev for a total fast neutron flux of 4×10^{13} nvt.

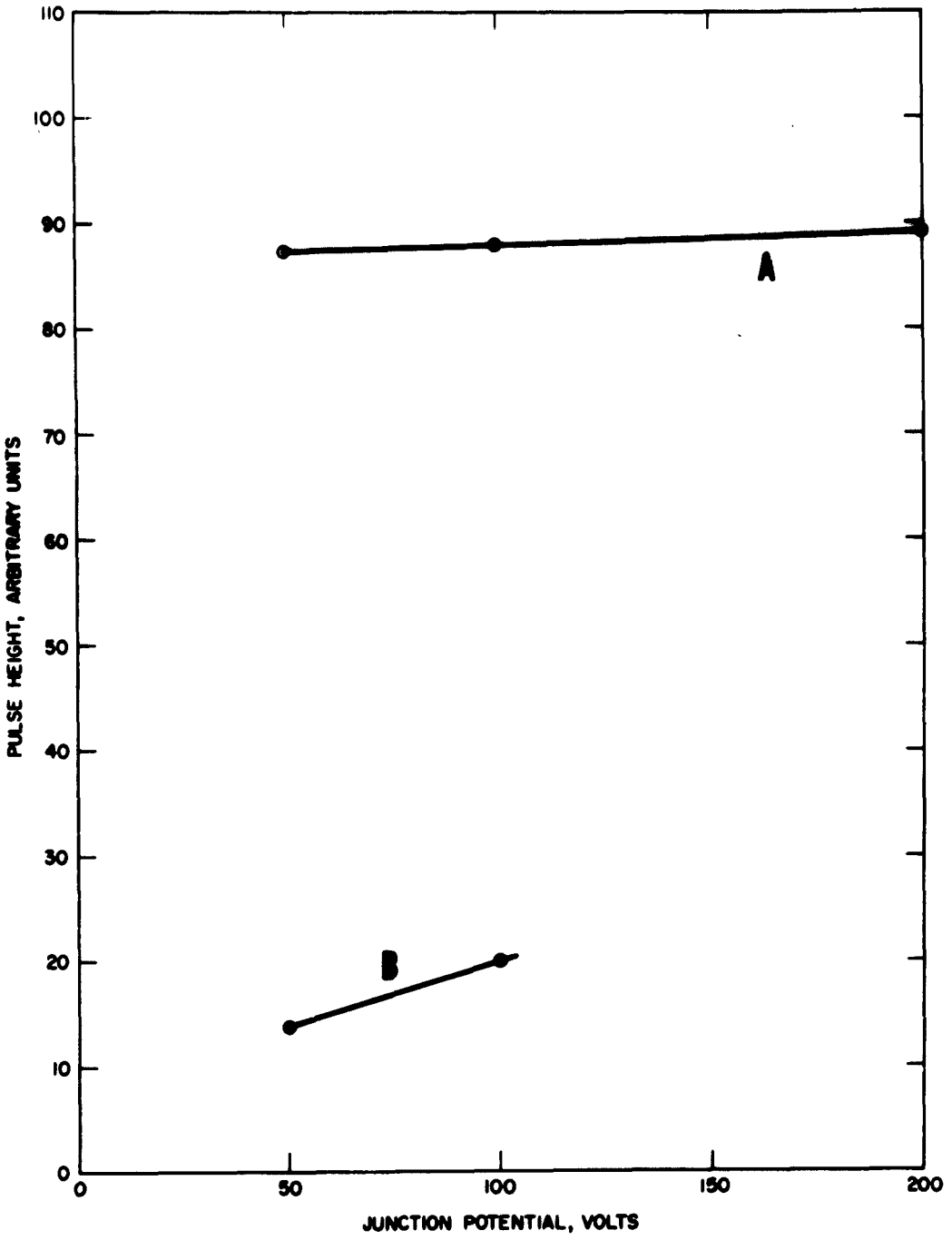

Fig. 30. Pulse height response of a p-n junction detector to alpha particles as a function of applied bias; (a) detector response before irradiation; (b) detector response after a total fast neutron dose of 5.3×10^{13} nvt.

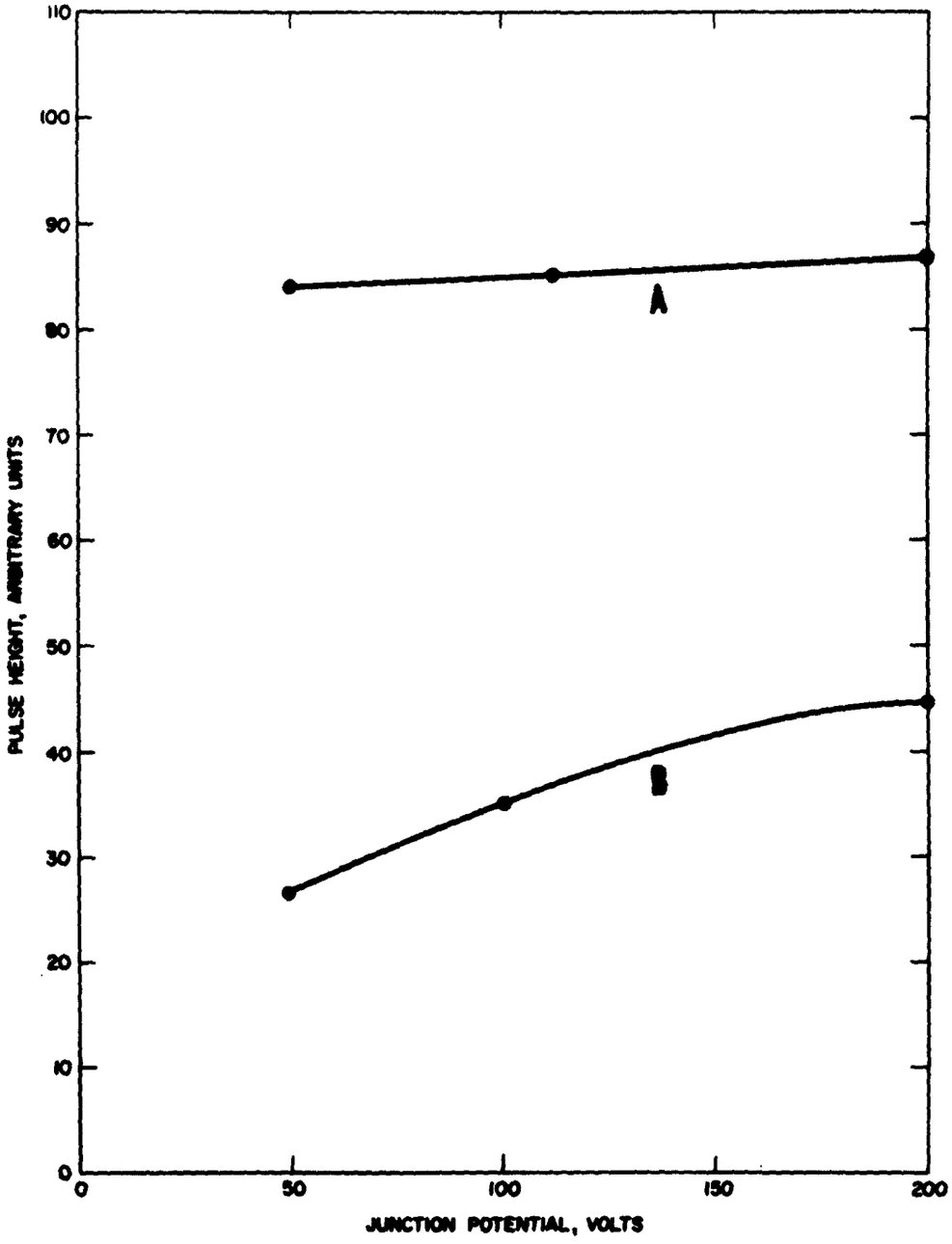

Fig. 31. Pulse height response of a p-n junction detector to alpha particles as a function of applied bias: (a) detector response before irradiation; (b) detector response after a total fast neutron dose of 8.8×10^{12} nvt.

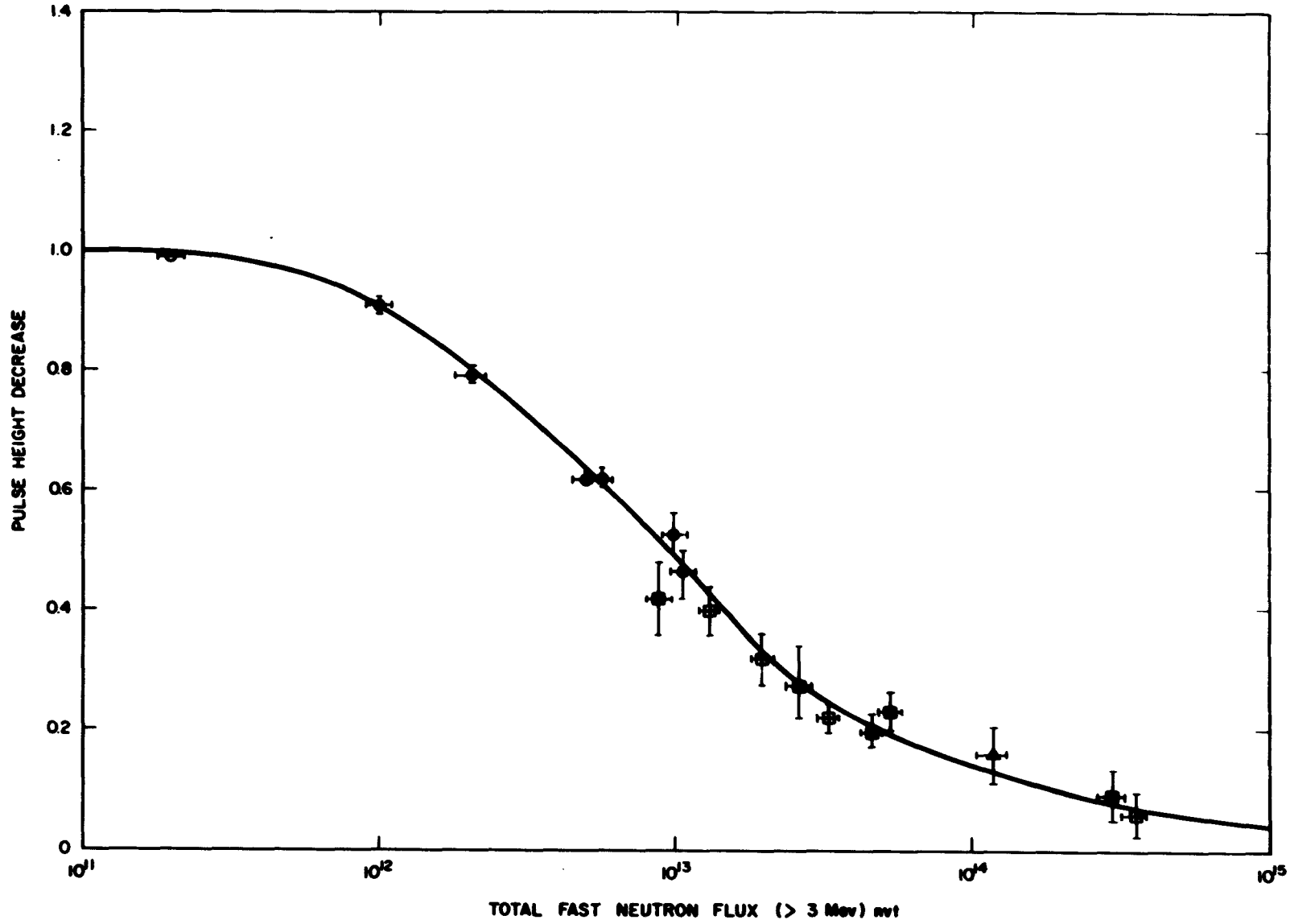

Fig. 32. Pulse height decrease as a function of total fast neutron dose. This curve represents an average of seven p-n junction detectors. These detectors were operated at an applied potential of 100 volts. The detectors had an area of 4 mm^2 and were fabricated from 6000 ohm-cm silicon.

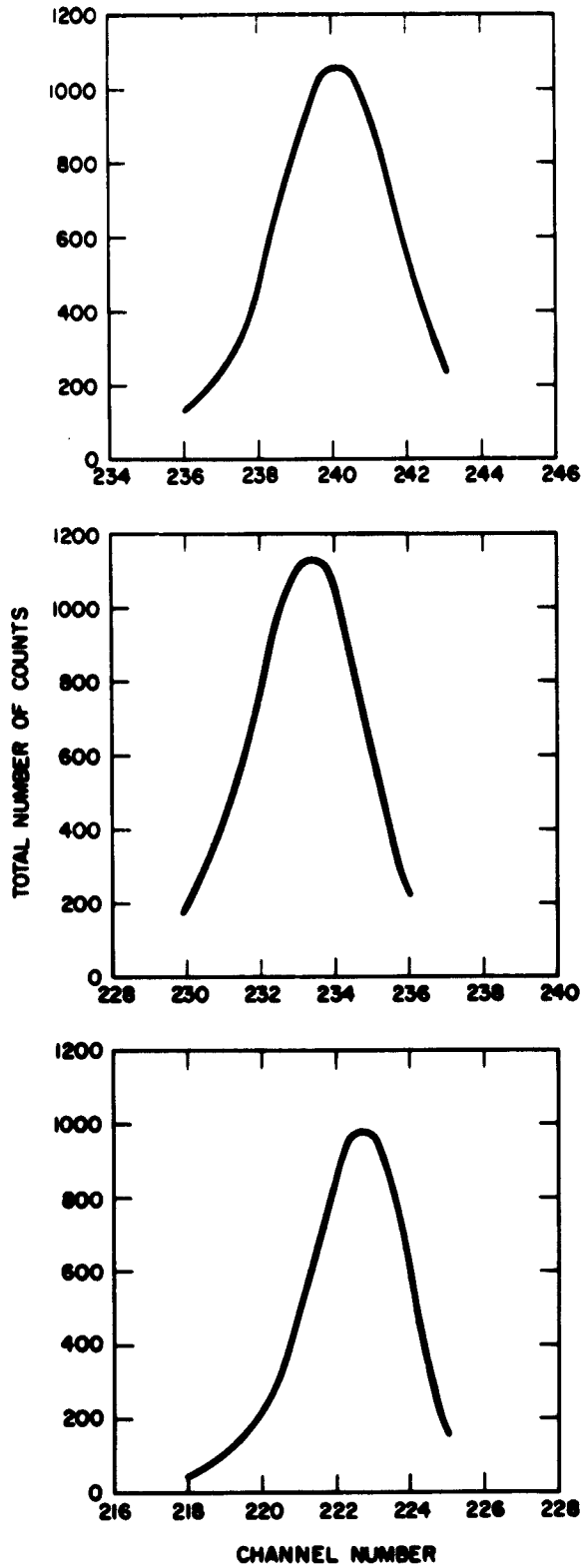

(a) bias = 200 volts, resolution = 1.7 percent

(b) bias = 100 volts, resolution = 1.6 percent

(c) bias = 50 volts, resolution = 1.4 percent

Fig. 33. Typical response of a p-n junction detector to 8.78 Mev alpha particles before radiation damage.

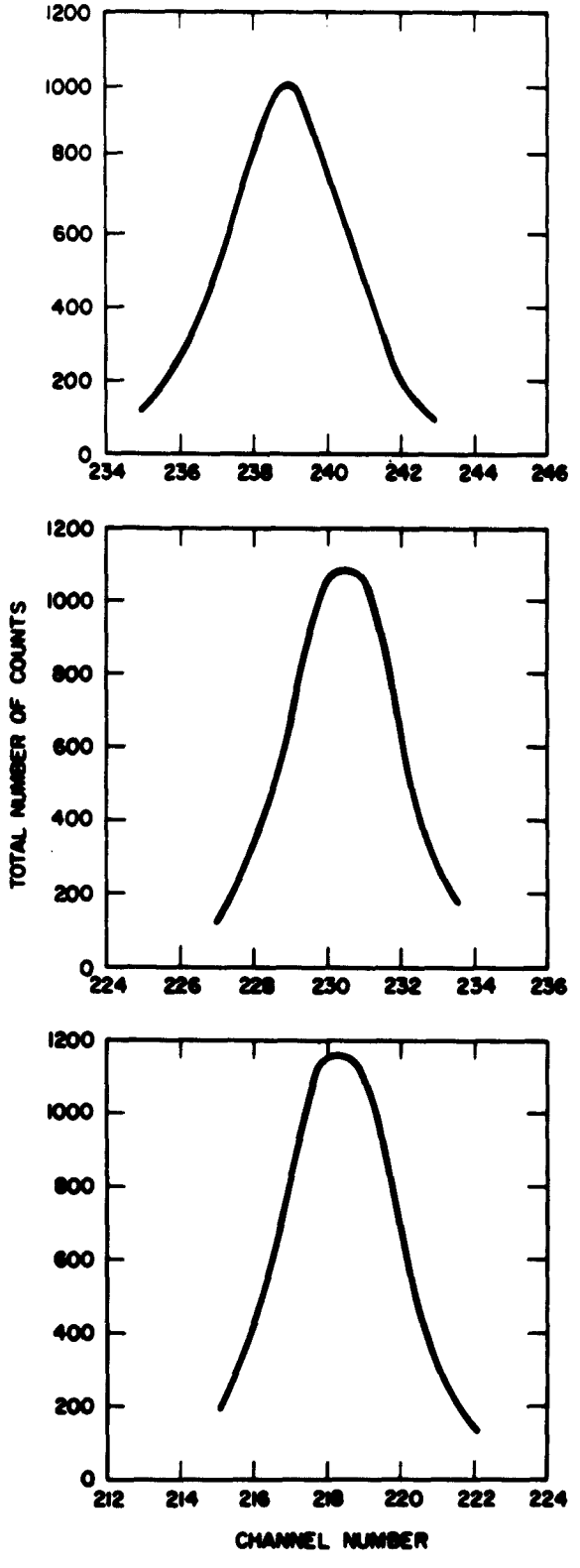

(a) applied bias = 200 volts, resolution = 1.7 percent

(b) applied bias = 100 volts, resolution = 1.6 percent

(c) applied bias = 50 volts, resolution = 1.7 percent

Fig. 34. Response of the detector shown in Fig. 33 after sufficient neutron irradiation has produced a moderate degree of damage.

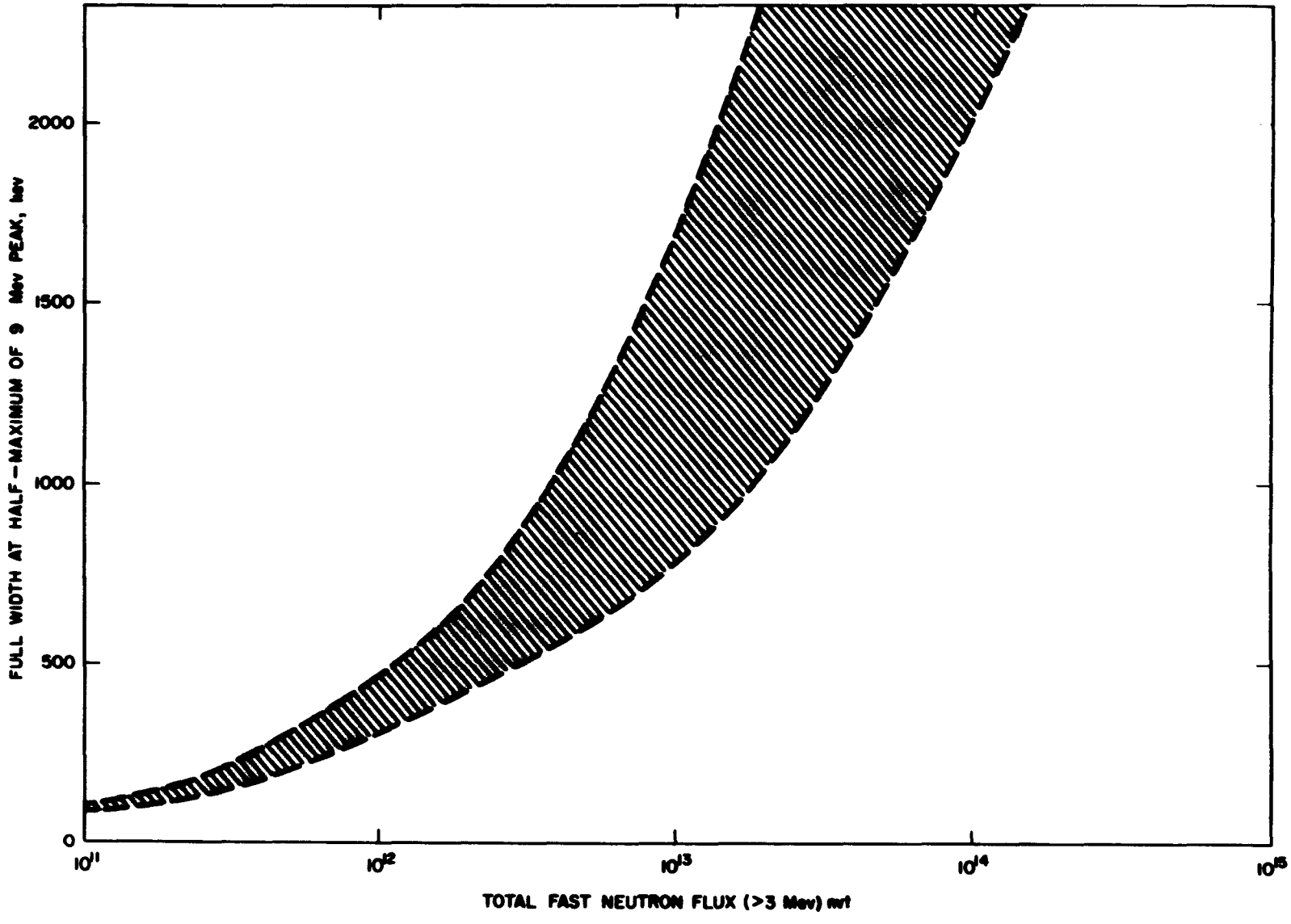

Fig. 35. The average value of a large number of p-n junction detectors is shown as a function of total neutron flux incident on the detector. The spread in the response peak to the 8.78 Mev alpha particles is plotted as a function of total fast neutron dose. The area between the two curves represents the spread in the values obtained when all irradiated detectors were considered.

d. The reverse current of the detectors increased after irradiation, while the forward current decreased. The magnitude of these changes is a function of total dose. Thus, both currents tend to approach each other as the junction is gradually destroyed. The results for a typical detector irradiated to a total dose of 5.3×10^{13} nvt is shown in Fig. 36. At a bias voltage of 2 volts, the reverse current increased from 8×10^{-8} ampere to 1.8×10^{-6} ampere. The forward current decrease was even more drastic, decreasing from 2×10^{-2} ampere before irradiation to 6×10^{-6} ampere after exposure to the neutron beam.

e. The capacitance of the detector junction increased after irradiation. Fig. 37 shows a typical shift in the C versus V curve after neutron irradiation. This would imply that the depletion region width had decreased,[17] or that the dielectric constant had changed: In a typical p-n junction the capacitance per unit area is given by

$$C = \frac{\epsilon}{4\pi X_p} ,$$

where

$\epsilon \equiv$ dielectric constant
$X_p \equiv$ depletion region width .

The capacitance of the detector shown in Fig. 37 increased from 75 $\mu\mu f/cm^2$ at 10 volts bias to 295 $\mu\mu f/cm^2$ at the same potential after a total dose of 5.3×10^{13} nvt. This corresponds to a decrease in depletion region width from 145 to 37 microns.

f. The short circuit photocurrent response of the detectors to a silicon-filtered light source was measured before and after the irradiations. It was observed to decrease sharply as a function of neutron dose. The short circuit photocurrent is the ionisation current produced when a very low resistance is placed in series with the junction. The resistance is adjusted so that the induced forward voltage is less than 0.025 volt. This current results chiefly from the diffusion of carriers to the junction. The magnitude of the current, therefore, is a measure of the diffusion length of minority carriers in the p-type base material and is related to the lifetime[7] by the relationship

$$L = \sqrt{D\tau}$$

where

$D \equiv$ diffusion constant
$\tau \equiv$ carrier lifetime .

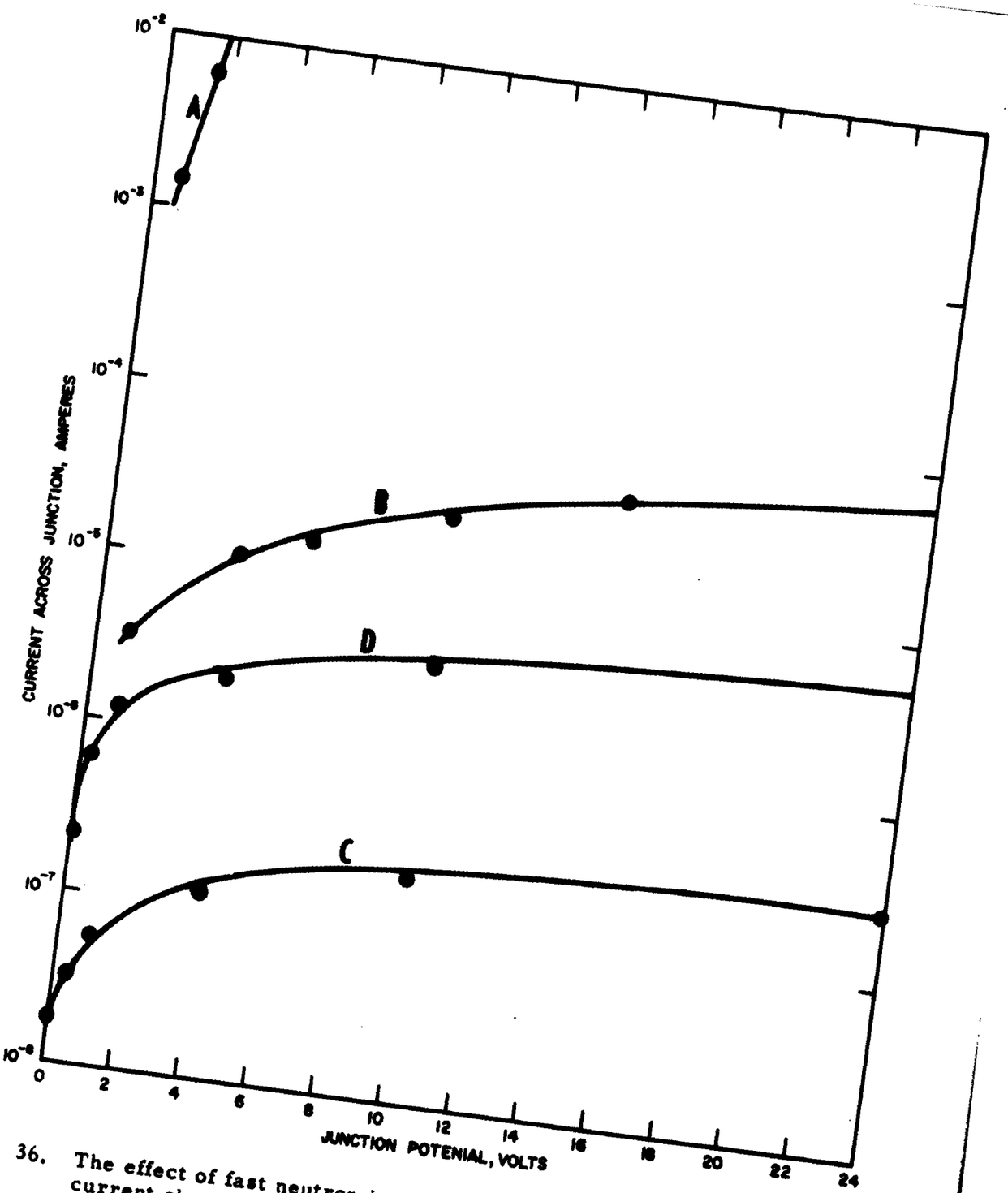

Fig. 36. The effect of fast neutron irradiation on both forward and reverse current characteristics of a p-n junction detector. The detector illustrated was irradiated to a total dose of 1.4×10^{15} nvt (greater than 3 Mev). (a) forward current characteristic before irradiation; (b) forward current characteristic after irradiation; (c) reverse current characteristic before irradiation; (d) reverse current characteristic after irradiation.

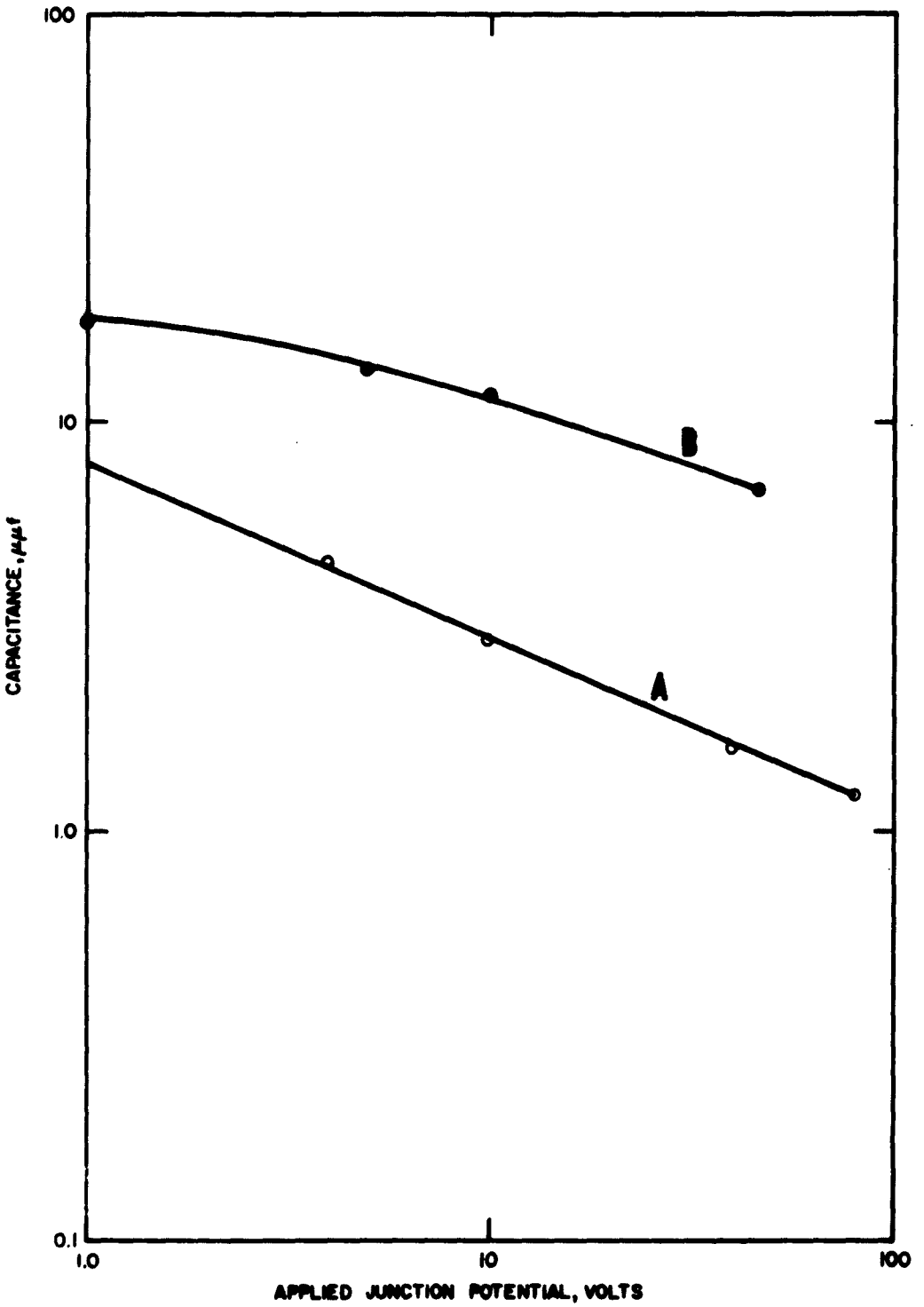

Fig. 37. Capacitance as a function of applied junction potential: (a) before irradiation; (b) after irradiation to a total fast neutron dose of 5.3×10^{13} nvt.

Referring to Fig. 38, one can see that the photocurrent decreases by three orders of magnitude after an exposure to 2.3×10^{13} nvt.

The average photocurrent of several other detectors as a function of dose rate is plotted in Fig. 39. The relationship is linear on a log-log plot with a slope of -1. Therefore, in the range of neutron dosage used,

Photocurrent x total fast neutron dose = constant.

The detectors used in all the above experiments were shallow, phosphorous-diffused silicon p-n junctions. The junction depth determined from lapping and staining techniques was less than 1 micron. The mesa dimensions ranged from 0.2 x 0.2 cm to 0.5 x 0.5 cm, on a wafer 0.062 cm thick. The dosimetry was performed with sulfur, phosphorous, uranium, and cobalt monitors, as referenced above.

Before irradiation, the detector capacities were measured using bridge techniques. After irradiation, the long RC time constants made it impossible to use the high-frequency (100-kc) signal of the bridge; the detector capacitance then was measured by comparing the pulse height of standard pulses transmitted through the detector with that transmitted through a series of standard capacitors. The circuit used is shown in Fig. 40. When a step function of voltage V is applied to the standard capacitor or detector, the pulse height observed at the amplifier output is given by

$$\frac{q}{C_A} = \frac{VC_D}{C_A + C_D}$$

where

$C_D \equiv$ detector capacitance
$C_A \equiv$ input capacitance of preamplifier.

In these measurements the amplifier must be operated with a sufficiently long time constant so that the output pulse will attain its maximum height. A comparison of this technique with the conventional bridge measurement is shown in Fig. 41 for an unirradiated detector.

The rise time of pulses was determined by observing the pulses on an oscilloscope trace with the amplifier operating with a relatively long time constant. Typical traces are shown in Fig. 42. The rise time was taken as the time for the pulse to reach a value of 1/e of its maximum.

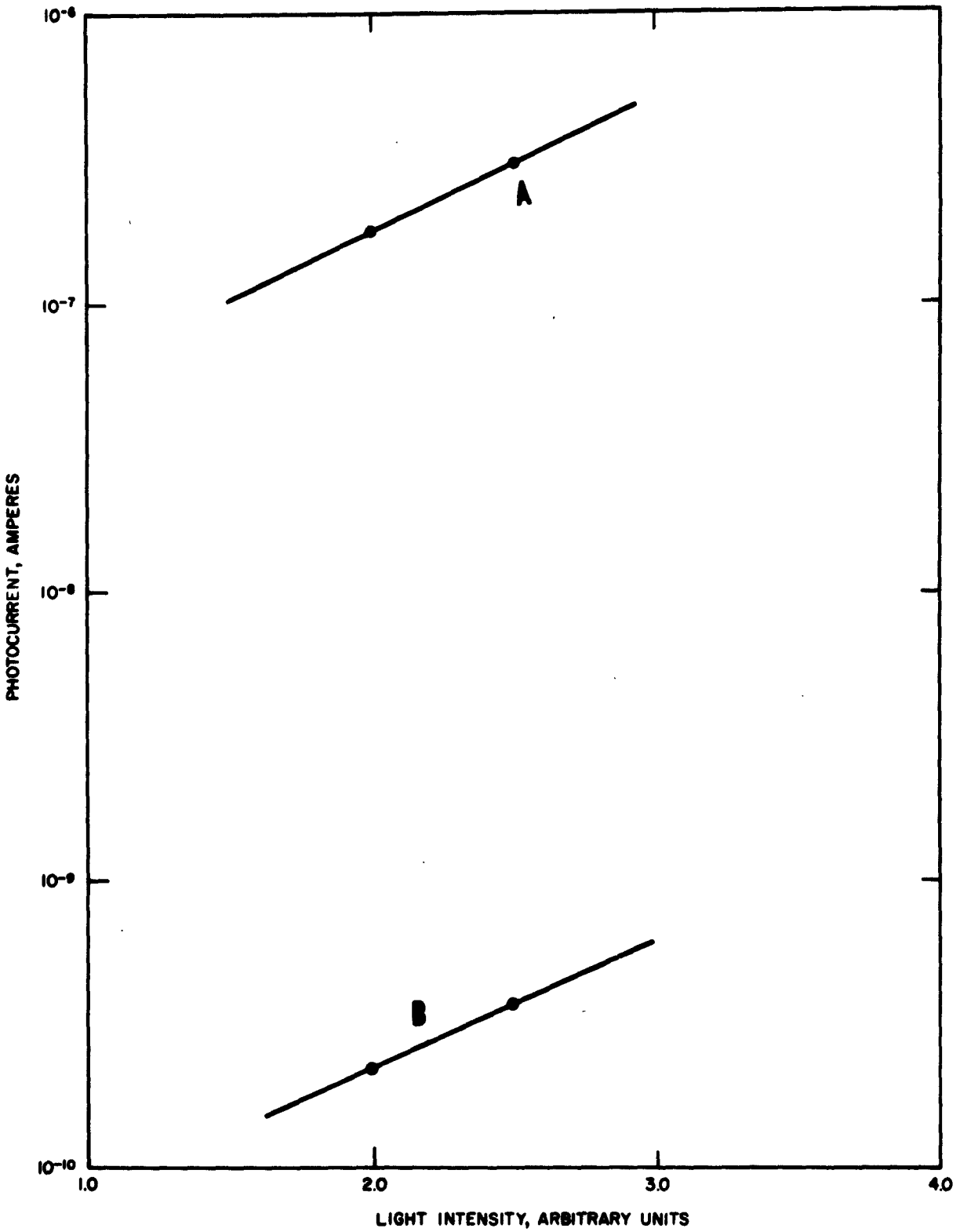

Fig. 38. Photocurrent induced by a silicon-filtered light as a function of light intensity: (a) before irradiation; (b) after irradiation to a total fast neutron dose of 5.3×10^{13} nvt.

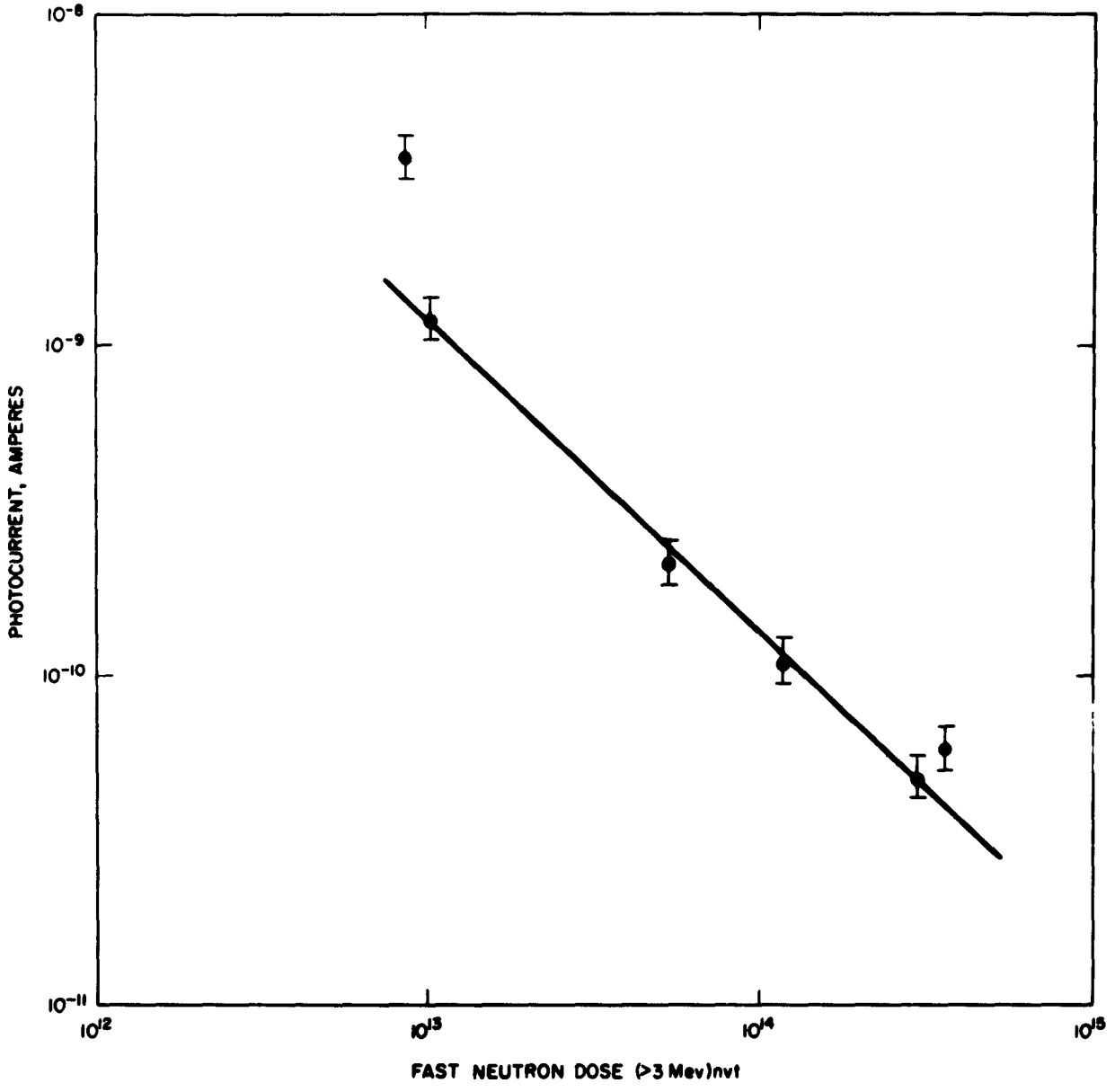

Fig. 39. Average photocurrent of irradiated diodes as a function of total fast neutron dose. The average photocurrent of this group of detectors before irradiation was 10^{-7} ampere.

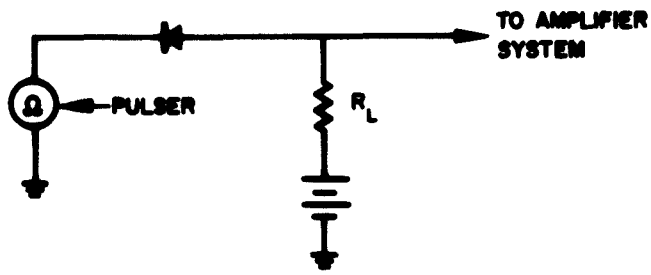

Fig. 40. Circuit used to determine capacitance values of p-n junction detectors after radiation damage had been induced.

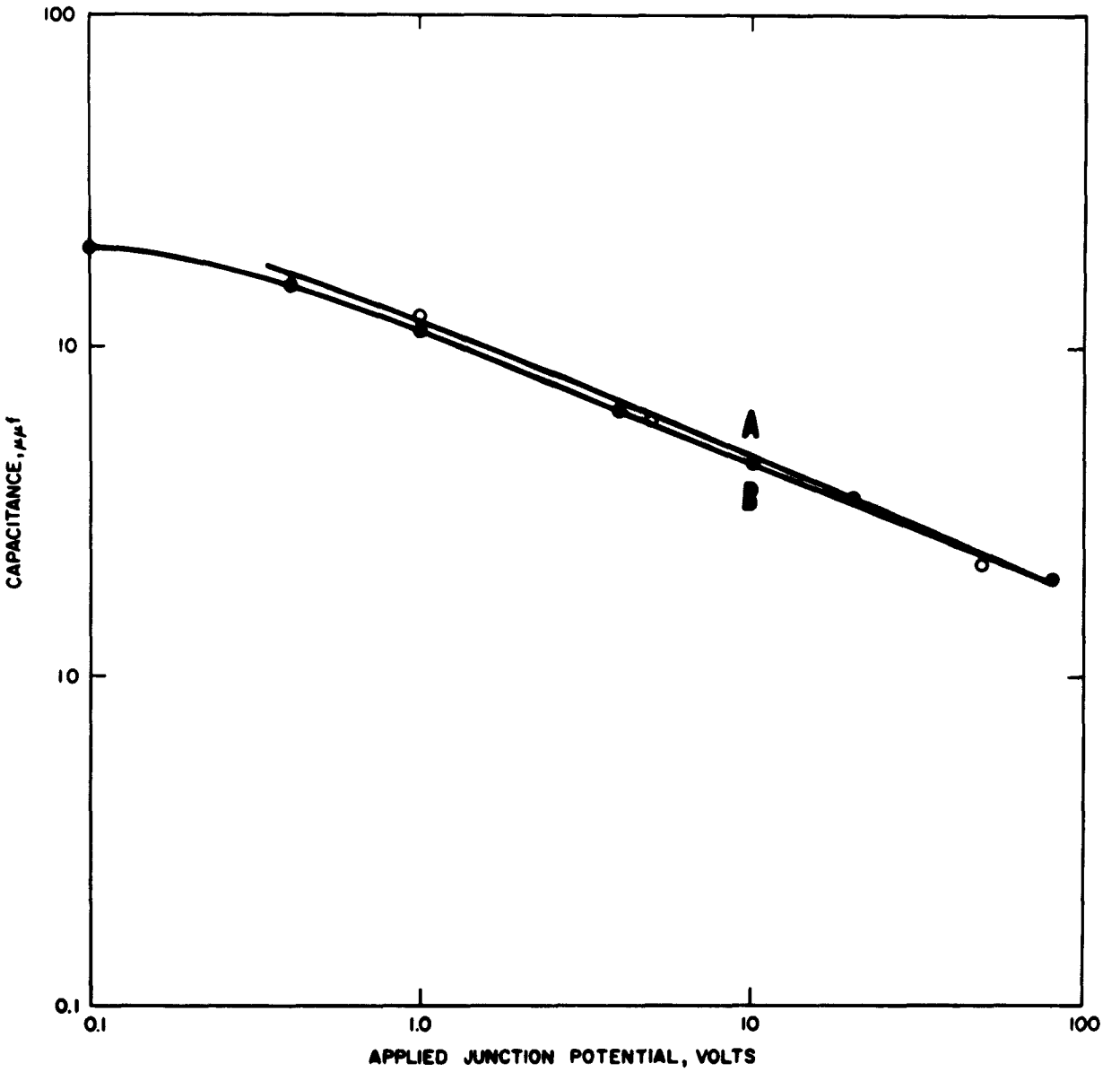

Fig. 41. Comparison of capacitance measurements made by using, as shown in Curve A, the circuit of Fig. 40, and those obtained in B by conventional bridge techniques.

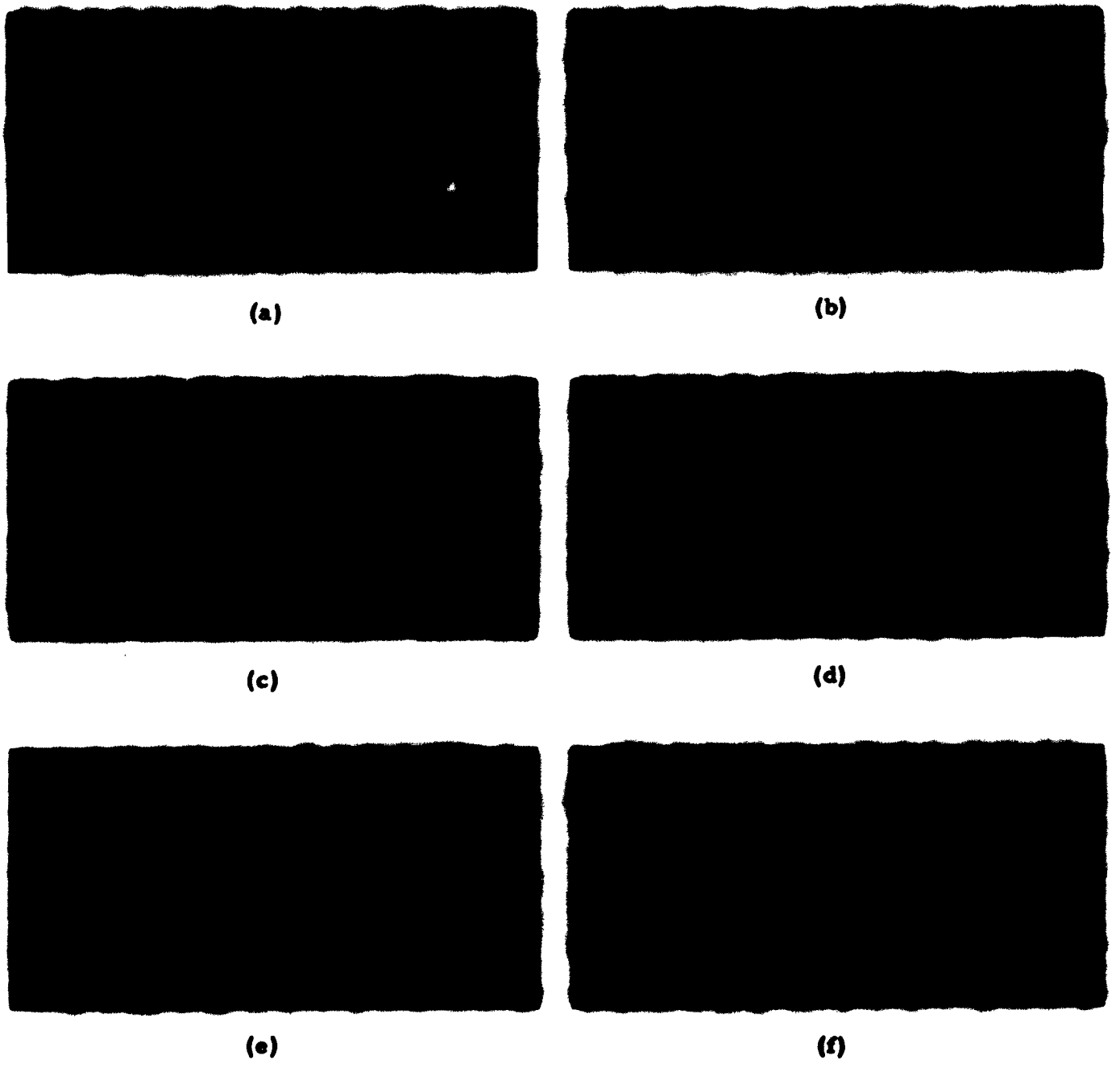

Fig. 42. Rise time and pulse height characteristics as a function of bias voltage before and after neutron irradiation to a total dose 8.8×10^{12} nvt of fast neutrons. Curve (a) shows the detector operated at bias voltages from 15 volts to 200 volts before irradiation. Curves (b) - (f) show detector operated at various junction potentials after irradiation. (b) 20 volts, (c) 30 volts, (d) 50 volts, (e) 100 volts, (f) 200 volts.

If the time constant for decay is comparable to that of the rise, then pulse clipping will not occur. In this case, if the decay time constant is known, then the rise time can be determined by measuring the time at which the pulse reaches its maximum. This will be treated more fully in the Appendix.

Pulse height and resolution measurements of the detector response to monoenergetic alpha particles were made from multichannel analyzer spectra. The circuit used is shown in Fig. 43. The alpha sources were made by depositing gaseous Pb^{212} on a small disc. Pb^{212} decays to Bi^{212}, which emits 6.05- and 6.09-Mev alpha particles, and in turn to Po^{212}, which emits 8.78-Mev alpha particles. All resolution values were determined from measurements of the full width at half maximum of the 8.78-Mev alpha line.

For the purposes of studying the influence of dose rate three 2- x 2-mm detectors were irradiated to the same total dose at different dose rates. These were 650 watts for 100 minutes, 6.5 kw for 10 minutes, and 65 kw for 1 minute. The dosimetry indicated that these runs corresponded to a total dose of approximately 10^{13} nvt ($E_n > 3$ Mev). The flux rates were 1.7×10^9 nv, 1.7×10^{10} nv, and 1.5×10^{11} nv, respectively. For evaluation of the detectors during the irradiations, the detector package was pulled out of the field of the reactor. The irradiation schedule is given in Table II.

The reactor pulses attained an average peak power of 800 Mw with the time spread of 15 msec at half maximum. The integrated power averaged 15.5 Mw-sec, which corresponds to an average integrated neutron dose of 5.3×10^{13} nvt delivered at an average peak rate of 2.7×10^{15} nvt.

The short circuit photocurrent was measured using white light filtered through a 0.020-inch-thick silicon filter. In each case the resistance was adjusted so that the forward bias developed across the detector was less than 10 mv. The current in the forward direction is given by[18]

$$I = I_s\left(\exp\frac{eV}{kT} - 1\right) ,$$

where

T = absolute temperature
I_s = saturation value of reverse current
e = electronic charge
k = Boltzmann constant

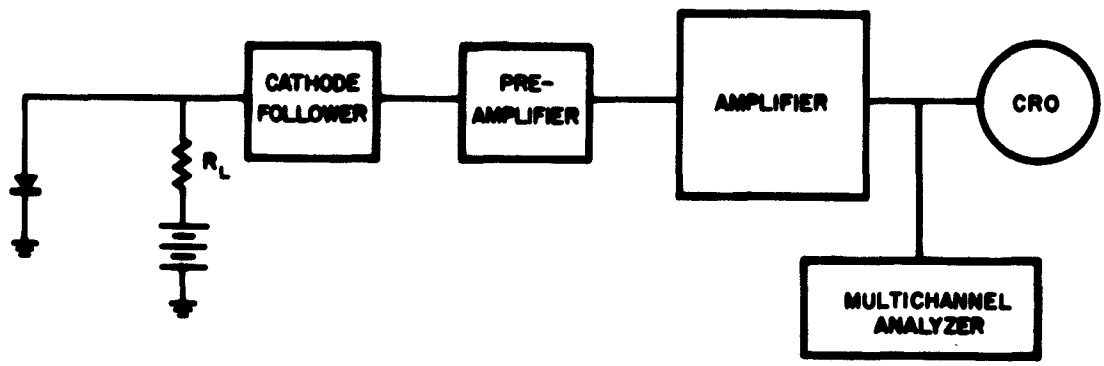

Fig. 43. Block diagram of circuit used for determinations of detector pulse height and resolution.

for

$$T_s \equiv 300^{\circ}K,\ V = 0.01 \text{ volts and } I = 0.49\ I_s.$$

TABLE II

Reactor Interaction Schedule

Run No.	Diode	Reactor Mode	Duration	Intervals between detector evaluation, minutes
1	2A1	650 watts steady state	100 minutes	0, 2, 10, 50, 100
2	2A8	6.5 kw steady state	10 minutes	0, 2, 5, 10
3 4 5	2A9 2B1 5A1	65 kw steady state	1 minute	0, 1
6	2A5	65 kw steady state	27.5 minutes	0, 1.0, 1.5, 2.0, 2.5, 3.5, 5.0, 10.0, 12.5, 27.5
7	5A2 2A2	800-Mw peak pulse	one pulse	—
8	2A3	800-Mw peak pulse	two pulses	—
9	2A4	800-Mw peak pulse	five pulses	—

Therefore, if the photocurrent is much less than I_s, contribution of the forward bias developed across the detector is negligible and a measurement of the short circuit photocurrent is then possible. The silicon filter removes all nonpenetrating wavelengths, which assures a uniform generation rate of carriers throughout the silicon.

Similarly, in the results of steady-state irradiations the pulse height response to alpha particles decreased with irradiation, and energy resolution was degraded. Some typical results are shown in Figs. 44 to 47. All detectors were able to count alpha particles after irradiation

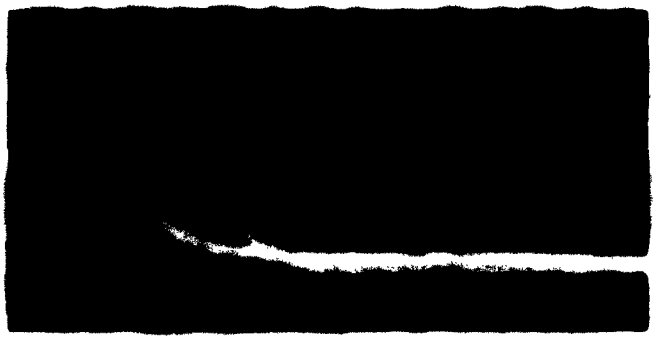

(a)

(b)

Fig. 44. Irradiated detector response to alpha particles showing degradation of pulse height as a function of radiation dose. Oscilloscope traces were photographed with the detector in the reactor.

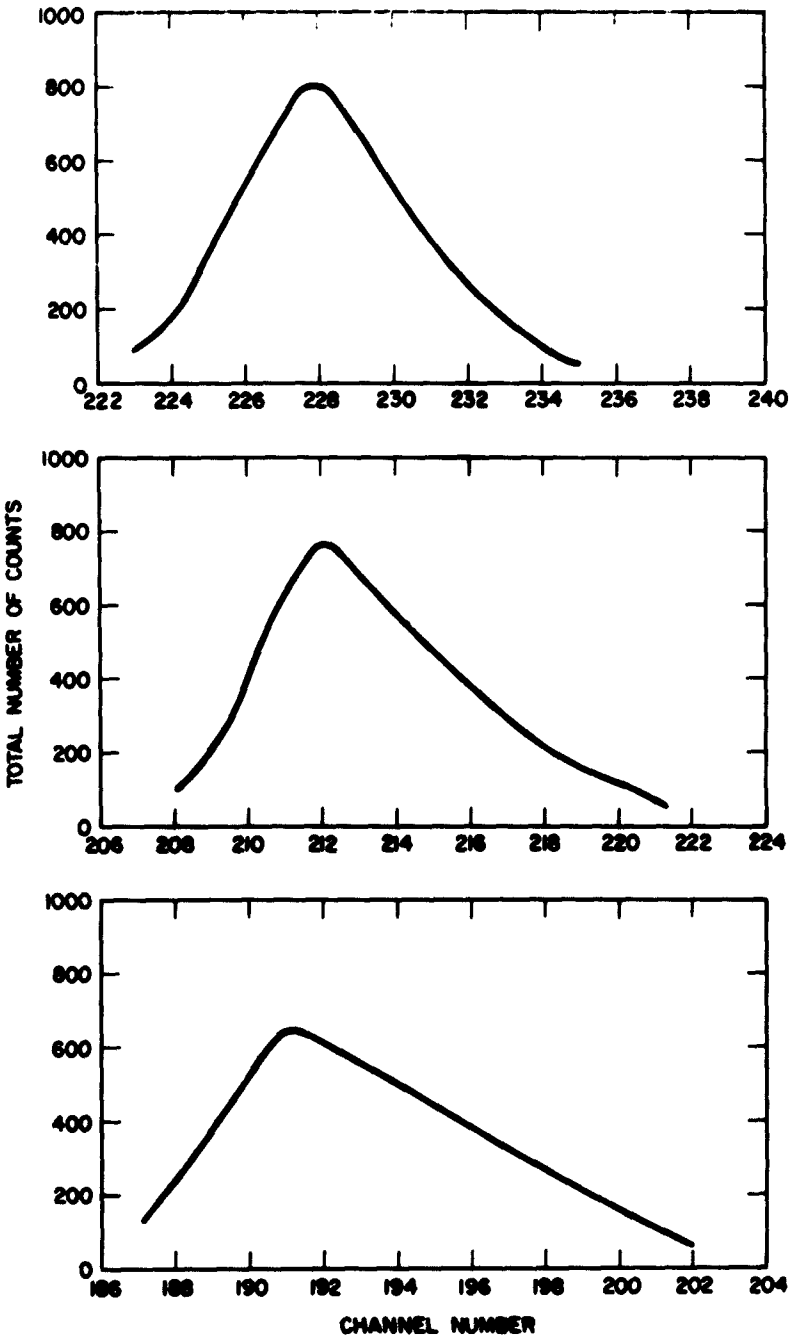

(a) operating potential = 200 volts, resolution = 2.5 percent

(b) operating potential = 100 volts, resolution = 2.9 percent

(c) operating potential = 50 volts, resolution = 4.4 percent

Fig. 45. Analysis of detector pulses due to 8.78 Mev alpha particles in an irradiated detector. This detector was exposed to the neutron beam of a pulsed reactor. Fast neutron dose = 9.9×10^{11} nvt.

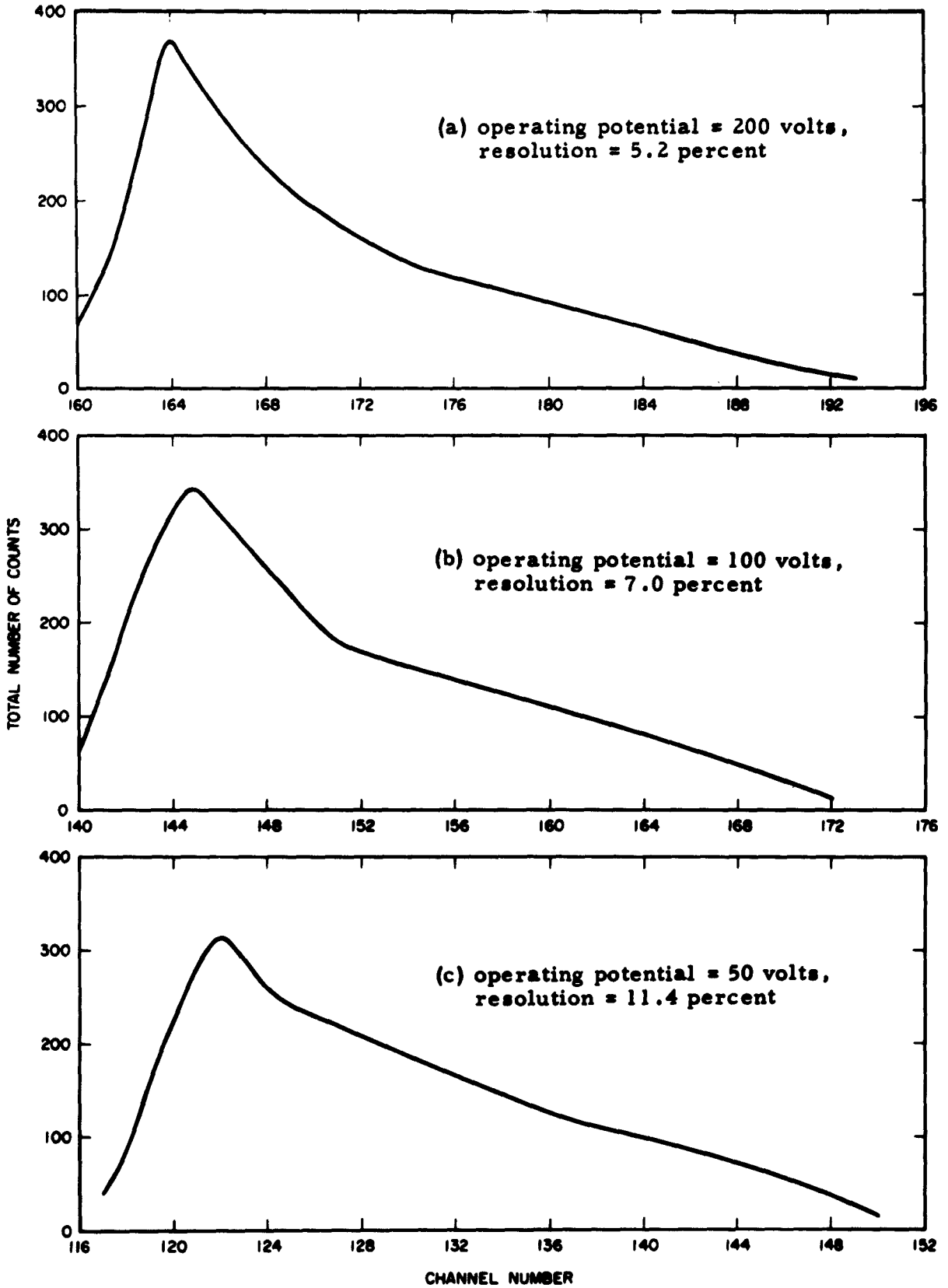

Fig. 46. Analysis of detector pulses due to 8.78 Mev alpha particles in an irradiated detector. This detector was exposed to the neutron beam of a pulsed reactor. This detector was exposed to five times the neutron flux to which the detector whose data is shown in Fig. 45 was exposed.

1.572

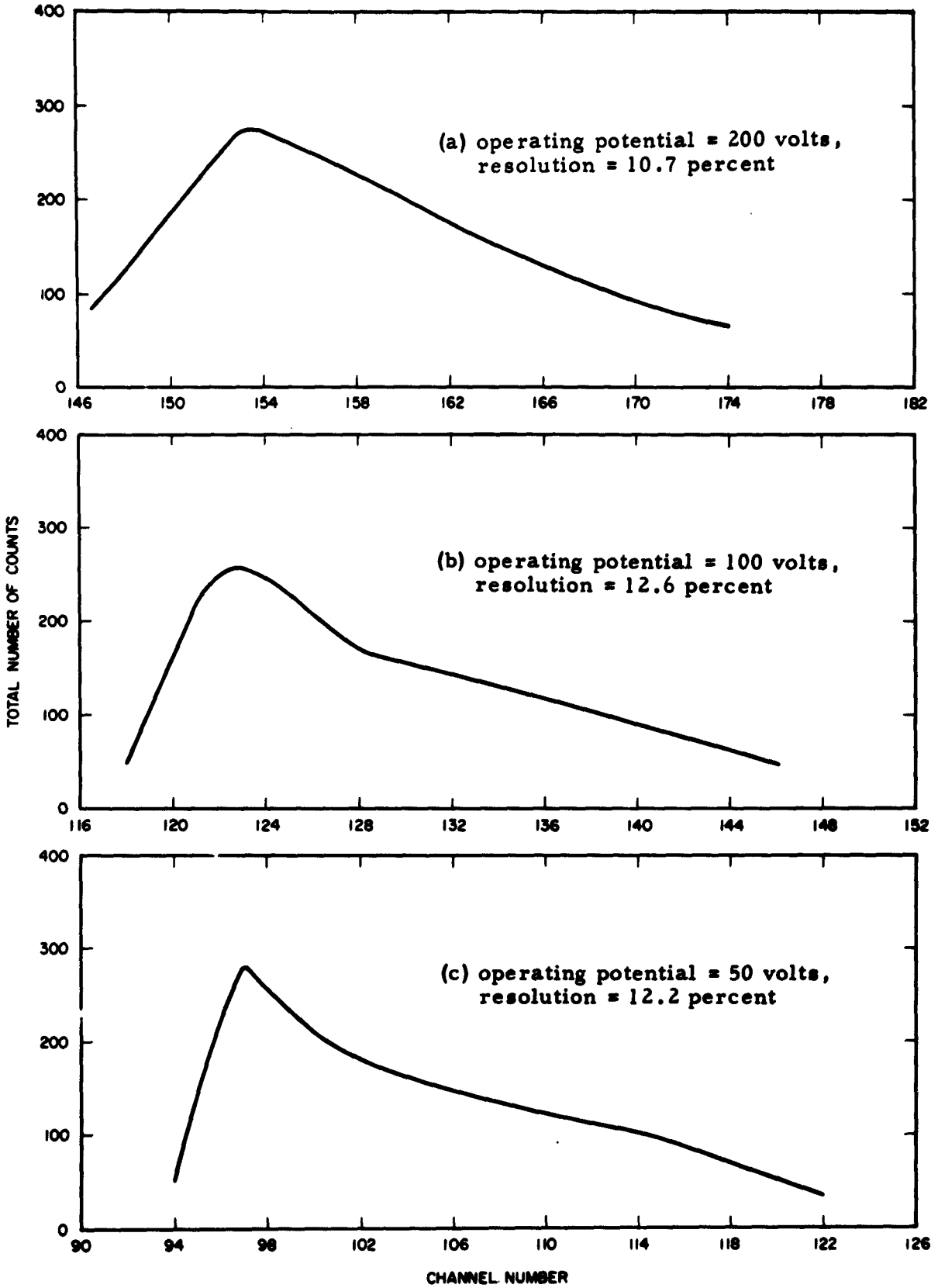

Fig. 47. Analysis of detector pulses due to 8.78 Mev alpha particles in an irradiated detector. This detector was exposed to the neutron beam of a pulsed reactor. The exposure was ten times that to which the detector whose data are shown in Fig. 45 was exposed.

with the maximum neutron dose (3.6×10^{14} nvt, 3 Mev). The pulse height began to approach the detector noise level of 100 kev when this dose level was used. The alpha peak recorded by the detector showed a spreading which was asymmetric, with a long tail on the high-energy side of the peak. This effect increased with increasing dose until finally the two peaks merged into one. The pulse height decrease recorded in these experiments was dependent only on the integrated fast neutron flux and showed no rate dependence.

The rise time of the pulses also showed an increase after irradiation. This is illustrated in Fig. 48. To determine whether this increase in rise time was a result of increases in either resistance or capacitance of the detector or whether it was a result of an increase in transit time of the carriers, the detectors were electrically pulsed. The long rise times were observed on the electrically transmitted pulses. Therefore, the increased rise times did not result from an increase in carrier transit time.

The increase was therefore a result of an increased time constant associated with the detector. The RC constant of the detector is determined both by the junction capacity and the resistance of the undepleted base region.

In this case the increase was caused in part by an increase in the junction capacity, but it was caused primarily by an increase in the resistivity of the base region. The resistance of the base region was determined by measuring the forward resistance of the detector. This increased by three orders of magnitude after irradiation by fast neutron totaling 5.3×10^{13} nvt. The resistance in series with the junction was determined by subtracting the resistance of the space-charge region from the resistance of the entire base region.

As the detector bias is increased, the capacitance decreases due to an increase in the width of the depletion region. This decreases the width of the undepleted base region and, therefore, the magnitude of the series resistance. A decrease in time constant results as the potential across the junction is increased. In Table III, the time constant is listed as a function of junction potential. A comparison is made between experimental and theoretical values. Good agreement for these two values was found.

A further decrease in pulse height resulted because a voltage-sensitive preamplifier was used. The pulse height output in this system due to a charge Q is

$$\text{Pulse height} = \frac{Q}{C_A + C_D} ,$$

where C_A is the amplifier capacitance and C_D is the detector capacitance.

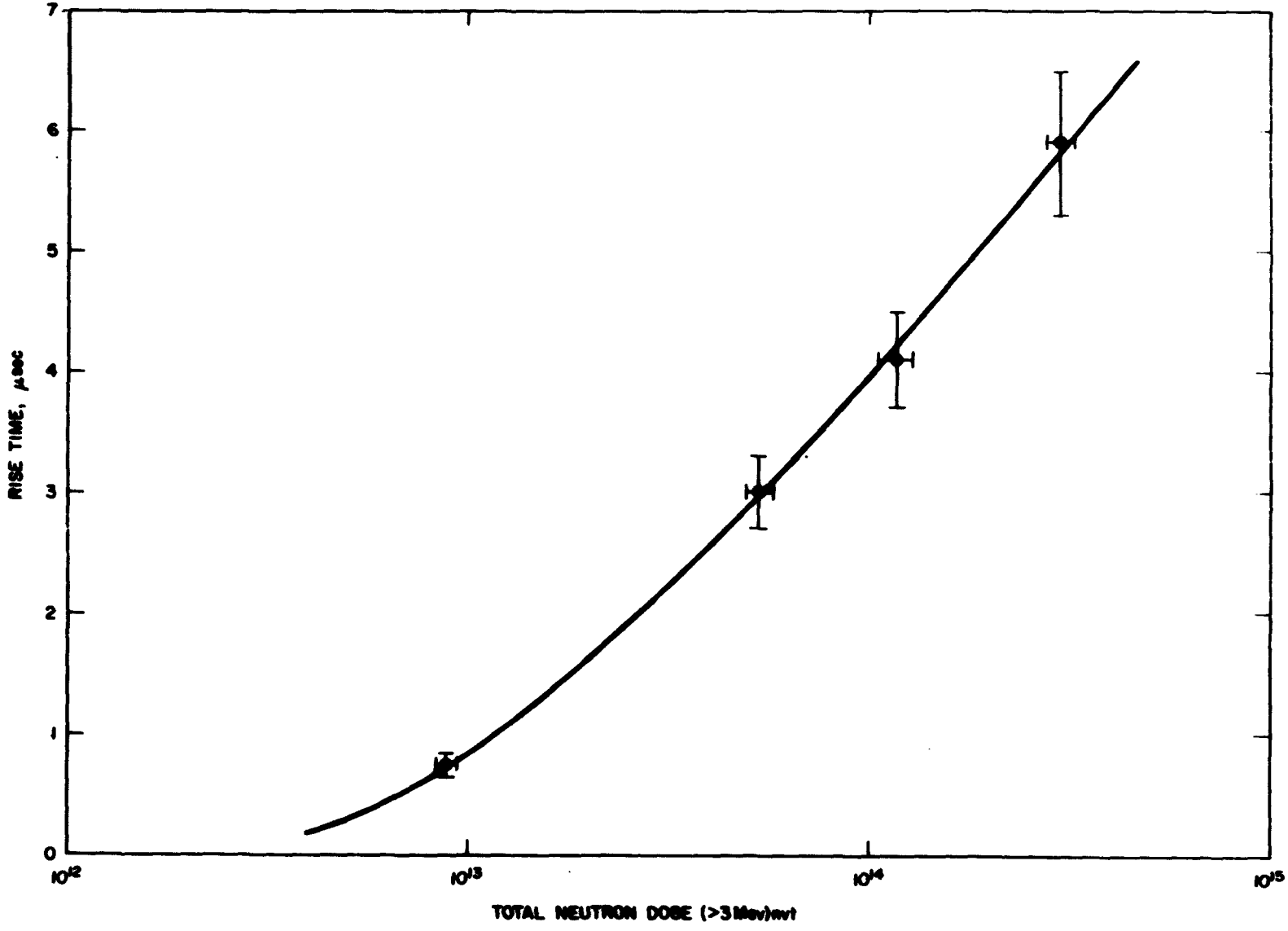

Fig. 48. Risetime of irradiated p-n junction detector as a function of total neutron dose. Exposure was affected through the continued operation of a pulsed neutron source.

TABLE III

Detector Rise Time;
Experimental and Theoretical Values of Indicated Detector Time Constants

Dosage = 5.3×10^{13} (> 3 Mev)

Bias, volts	C, μμf	X_p, microns	R_{series}, meg	Time Constant, Theoretical μsec	Time Constant, Experimental μsec
1	17.8	23.8	0.336	6.0	6.2
5	13.6	31.2	0.333	4.5	4.7
10	11.8	36.0	0.330	3.9	4.1
45	~6.8	62.5	0.314	2.1	2.4

The detector response was later examined with a charge sensitive system. This system employed a charge-sensitive preamplifier which gives a pulse height response that is insensitive to detector capacitance. The time constant of the amplifier in this system was 200 μsec.

This long clipping time assures us of no more than a 5-percent loss in pulse height due to clipping of the pulse which had a rise time of 3 μsec at 25 volts bias. The pulse-height-versus-bias relationship is plotted in reciprocal form in Fig. 49. The pulse height after irradiation is very much less than before irradiation when the detector is operated at low biases; as the voltage is increased, however, the pulse height of the irradiated detector approaches the pulse height of the unirradiated diode. By choosing a charge-sensitive, long time constant system, the pulse height will not depend on detector capacitance. The small depth of the space-charge region could account for a pulse height decrease when the applied junction potential is less than 30 volts. Increasing this potential does not restore the pulse height to the value obtained before irradiation. This remains true even when the depletion region depth is greater than the range of the alpha particles. This additional loss in pulse height is voltage dependent and tends to decrease with increased potential.

This field-dependent pulse-height decrease implies a charge loss within the space-charge region. This is a result of recombination of electrons and holes. Recombination within the space-charge region will occur when the lifetime of the carriers is reduced to a value which is of the same order of magnitude as the transit time of the carriers

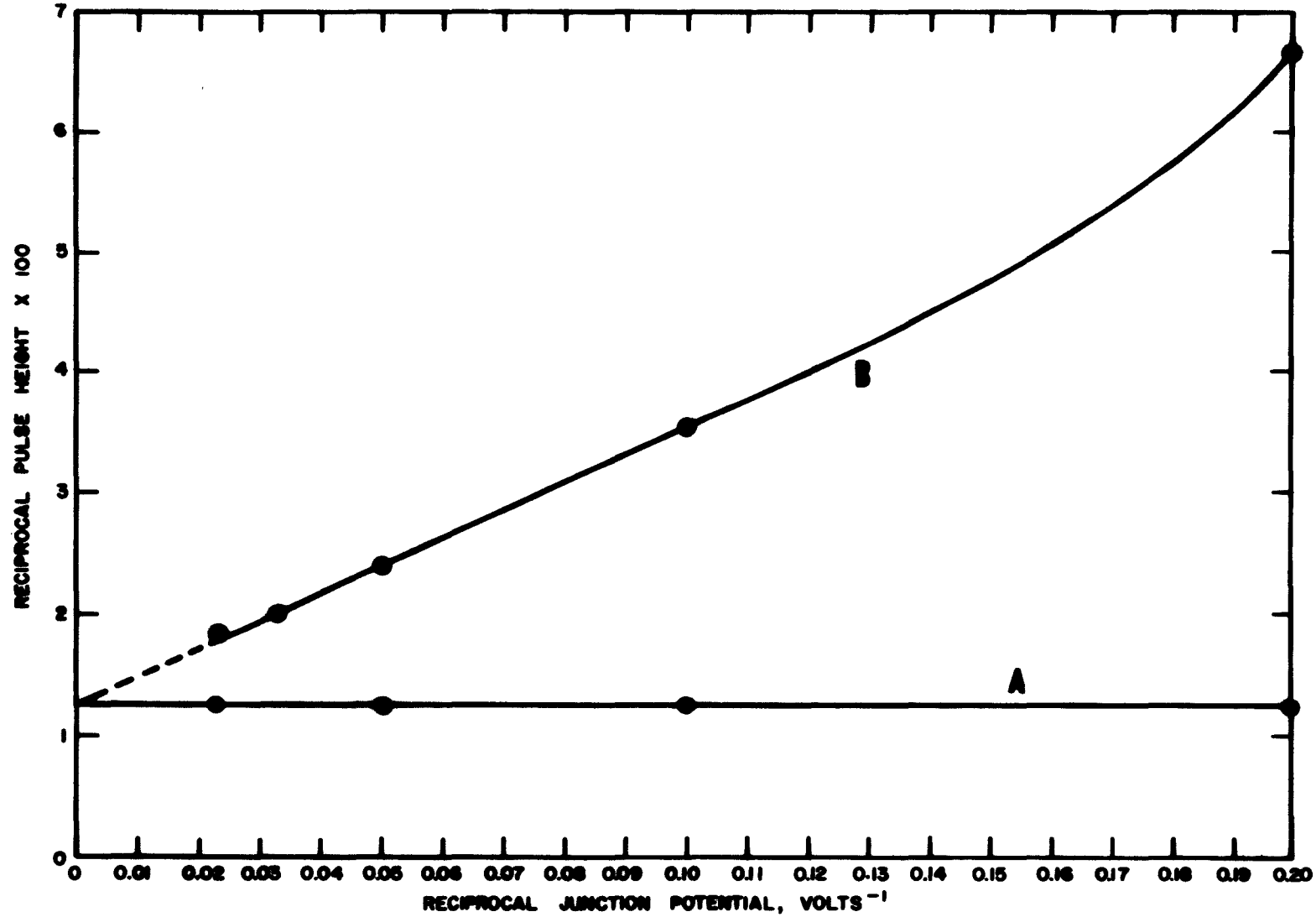

Fig. 49. Comparison of pulse height degradation of a p-n junction detector after exposure to 5.3×10^{13} nvt from a pulsed neutron source: (a) the pulse height as a function of junction potential before irradiation; (b) the pulse height response as a function of junction potential after irradiation. Pulses were induced by alpha particles and fed out from the detector to a charge-sensitive system.

across the space-charge region. The transit time t(x) for a carrier created at a position x to reach X_p in an abrupt p-n junction is given by

$$t(x) = T_R \ell n \, X_p/x;$$

where

$$T_R = \frac{\epsilon}{\mu N e},$$

and

N ≡ number of impurity atoms/cm^3
μ ≡ mobility of carrier
e ≡ electronic charge
ϵ ≡ dielectric constant .

The pulse height decrease which occurred during irradiation was a result of the following factors:

1. An increase in rise time due to physical changes in the detector.

2. Recombination of carriers within the space-charge region.

The decrease in carrier lifetime was confirmed by measurements of the short circuit photocurrent after irradiation. The current suffered a drastic decrease after irradiation. Since the photocurrent is a measure of the diffusion length, this implies a decrease in diffusion length and thus in carrier lifetime. The decrease in carrier lifetime after irradiation agrees with results obtained by other workers. Wertheim[11] gives the following equation for the lifetime of p-type silicon as a function of total neutron dose:

$$\tau \approx \frac{4.3 \times 10^5}{Q} \text{ seconds} .$$

Q is the total neutron flux incident on the detector and includes all neutrons having energies greater than 100 ev. This result was obtained using 2-ohm-cm silicon. Although our samples were of much higher resistivity, the calculated lifetimes for the integrated fluxes used in our experiment would predict the magnitude of recombination observed.

The observed changes and their associated causes can be summarized by the following:

	Effect	Cause
1.	Increased rise time pulses.	Increased junction capacity and increased bulk resistivity.
2.	Increased junction capacity.	Decreased depletion region and a possible change in dielectric constant.[19]
3.	Increased reverse current.	Lowered minority carrier lifetime.
4.	Decreased forward current.	Increased bulk resistivity.
5.	Decreased pulse height in response to charged particles.	Decreased width of space-charge region and recombination of carriers within the space-charge region.
6.	Decreased photocurrent.	Decreased diffusion length.

V. THERMAL EFFECTS

The experiments described compare the effects of temperature upon undamaged and neutron-damaged silicon-diffused p-n junction detectors. Quantities investigated were pulse height, resolution, signal-to-noise ratio, and pulse rise time.

Let us briefly review the characteristics of an undamaged detector as a function of temperature. It can be generally stated that thermally generated currents, probably both surface and bulk, give rise to detector noise, although not in quantitatively predictable amounts. Fig. 50 gives the behavior of the RMS noise as a function of temperature, while Fig. 51 shows those for both constant current and voltage. Resolution, which is governed by both system and device noise, shows significant improvement at lower temperatures. Conversely, resolution suffers considerable degradation at higher temperatures, usually degrading sharply when temperatures rise beyond 50°C. Alpha particle pulse heights exhibit no change over the temperature range of 125°C to - 200°C when operated at constant bias voltage if a voltage-sensitive preamplifier is used. This implies that the detector capacitance does not change, and consequently one can infer that the concentration of ionized impurity centers (number of donor minus number of acceptor atoms per unit volume) remains essentially constant over this temperature range. The signal-to-noise ratio tends to increase upon lowering the ambient temperature, at least until detector noise drops below the system noise. Pulse rise time which is governed by the product of depletion region capacitance and the undepleted region resistance will therefore be a function of the resistance change. More explicit details may be found in the report covering work done on this contract during 1960.

The need for understanding irradiated detector performance as a function of temperature has stemmed from the desire to determine optimum operating conditions for detector usage in a reactor field. The results presented here relate to post-irradiation behavior.

A re-examination of the basic effects of neutron irradiation upon matter will reveal that damage results from creation of interstitial atoms and vacancies in the lattice. Interstitial atoms give rise to donor levels, whereas lattice vacancies act as acceptors. Acceptor levels introduced below the Fermi level reduce the electron concentration in the conduction band for n-type semiconductors and increase the hole concentration in p-type semiconductors.[4] The opposite effects occur with the addition of donor levels above the Fermi level. However, donor levels below and acceptor levels above the Fermi level should have no effect upon carrier concentration. Deep defect levels are affected more by temperature changes than are the shallow impurity levels. Therefore one may expect radiation damage to reduce carrier concentration and therefore that concentrations will be relatively temperature sensitive.

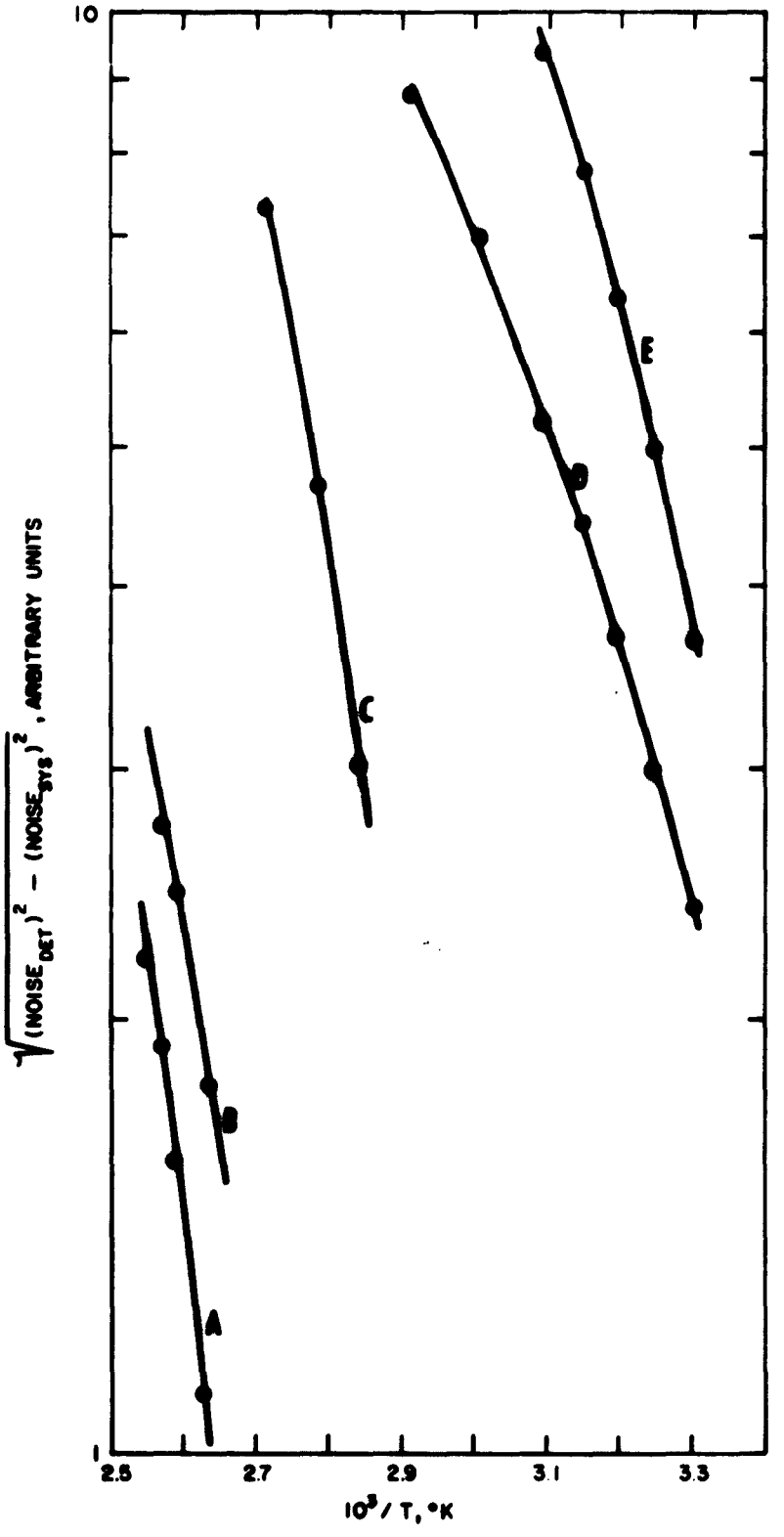

Fig. 50. RMS noise values recorded from an unirradiated p-n junction detector as a function of temperature: (a) junction potential = 2 volts; (b) junction potential = 6 volts; (c) junction potential = 24 volts; (d) junction potential = 30 volts; (e) junction potential = 40 volts.

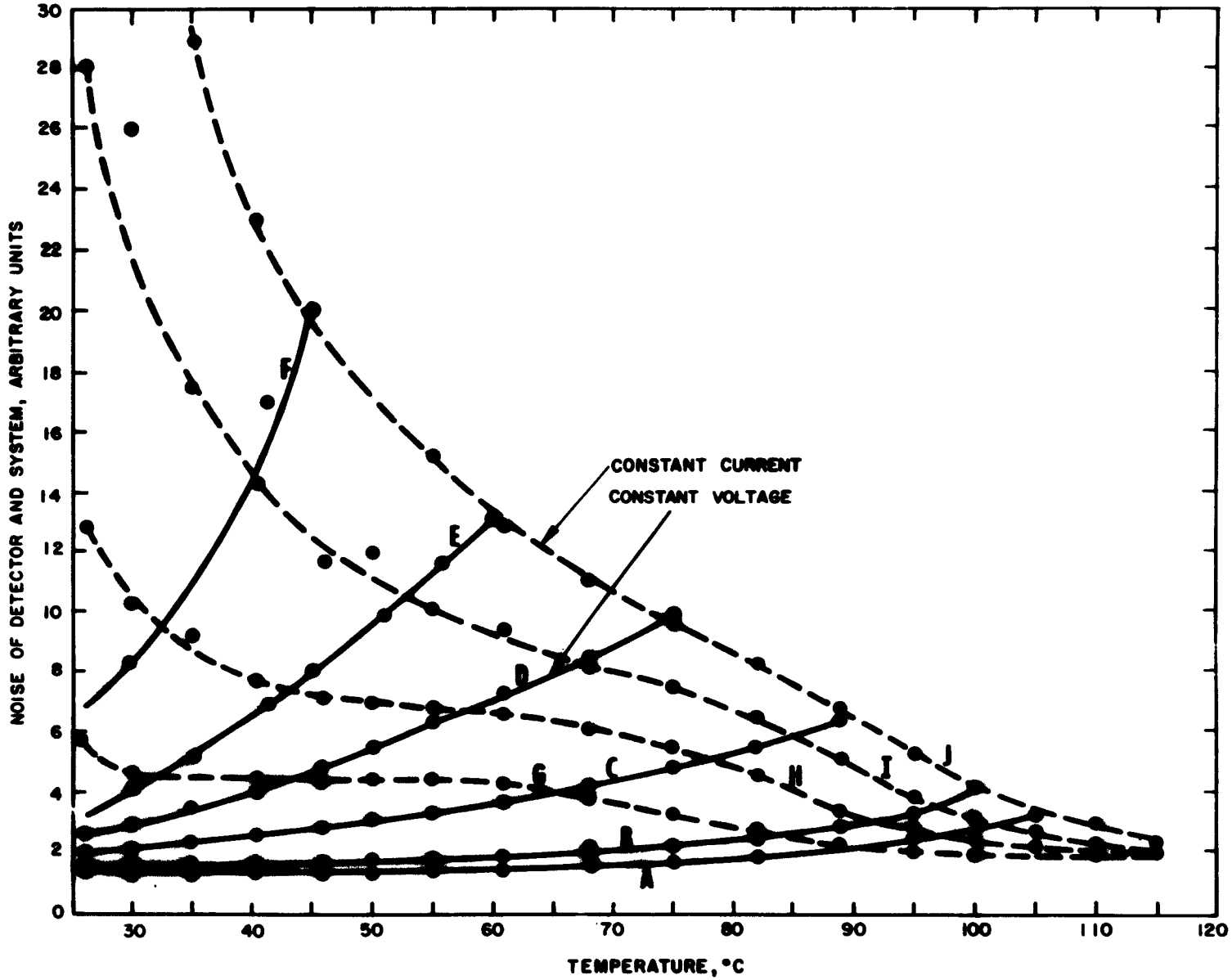

Fig. 51. Comparison of RMS noise values as a function of temperature under conditions of constant current and constant applied junction potential. Curves A through F represent operations at constant junction potentials. These are: (a) 5 volts; (b) 10 volts; (c) 20 volts; (d) 30 volts; (e) 40 volts; (f) 50 volts. Curves G through J show operation of the detector under constant current conditions. These are: (g) 30 μa; (h) 50 μa; (i) 70 μa; (j) 90 μa.

Since the distribution of ionized centers determines the electric field and depletion region width, any thermal perturbations in the concentration of ionized centers will be reflected in changes of these quantities. Accordingly, both capacitance and series bulk resistance should vary with temperature if the detector is held at constant applied voltage.

Several observations tend to verify that the depletion width changes with temperature. Indicative of such a change was the appearance of beta particle pulses near liquid-nitrogen temperature, though the detector remained at constant voltage. Such pulses were not observed at room temperature since the amount of energy deposited by beta particles in the detector's sensitive volume was insufficient to produce a pulse above the noise level. The appearance of the beta pulse suggests that higher beta energy deposition took place due to an enlarged sensitive volume.

A second source of supporting evidence for reduced concentration was the fact that breakdown voltage also decreased with decreasing temperature. The coincidence of a sudden onset of noise and a steep rise in current suggests that the effect being observed resulted from injection into a depletion region which extended to the back contact. The width W of this region obeys the relationship $W^2 \propto V/N$, where V is the applied voltage and N is the net impurity concentration. Since this relationship can be satisfied for different voltage values when W equals the device thickness, the conclusion reached is that N varies proportionally with breakdown voltage V_B. Plotting the log of V_B^{-1} versus T^{-1}, where T is the absolute temperature, should yield the value of the defect energy levels responsible for this charge.

The third indication of depletion width variation with temperature was manifested by the characteristic pulses obtained from 9-Mev alpha particles incident upon the back surface of an irradiated detector. Although undetectable at room temperature, even at 1000 volts bias, the pulses became quite prominent at low temperatures. The threshold for detection continued to decrease to lower voltages as the temperature was decreased. Pulses were clearly visible at an applied voltage of 70 volts when the detector temperature was reduced to 77°K. Response to alpha particles incident upon front and back may be compared by examining the spectra shown in Fig. 52. Both resolution and pulse height appear identical in the two cases. The detector was operated at 670 volts at 0°C. An anomaly that shows up when alpha particles were incident upon the back will be discussed below.

The effect of radiation damage upon pulse rise time will now be considered. Observations indicate that rise times become significantly longer after detectors have received large neutron dosages, as a result of gross resistivity increases. Since rise time is influenced primarily by the capacitance and resistance values of the detector, any temperature variation in resistivity can be expected to alter both the resistance and the capacitance.

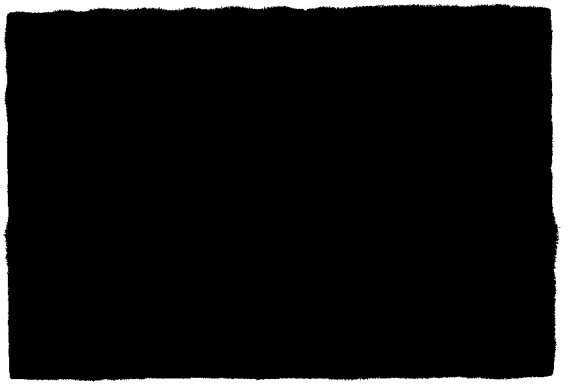

(a)

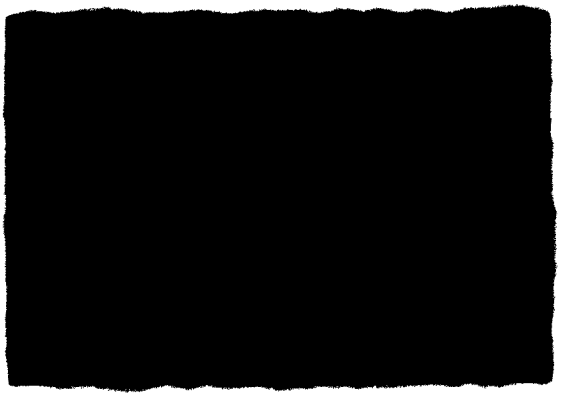

(b)

Fig. 52. Comparison of resolution and pulse height of an irradiated detector when alpha particles were incident (a) on the front surface and (b) at the rear surface.

The principal point to note is that the actual dimensions of the capacitive and resistive regions will vary with resistivity as a result of temperature changes even though operation is at a fixed bias voltage. Noting that $R \propto \rho L$, where L is the thickness of the series bulk region, and $C \propto \rho^{-1/2}$, it follows that $RC \propto (B - \rho^{1/2})\rho^{1/2}$, where B is a constant. According to this functional relationship, rise time should pass through a maximum as resistivity increases. Adopting a similar analysis, it is possible to show that rise time should become shorter with increasing applied voltage while a constant temperature and, hence, constant resistivity is maintained.

The above-mentioned functional relationship has not been verified because of the presence of an anomalous effect. Alpha particle pulses observed from the output of a charge-sensitive preamplifier were photographed with a polaroid oscilloscope camera. A series of photographs was obtained as a detector descended in temperature from 65°C to -196°C. At about 30°C pulses appeared with two discrete leading edge components. These exhibited a fast rise upon which was superimposed a more slowly rising component. The slow rise component disappeared near liquid-nitrogen temperature. This phenomenon might possibly be attributed to trapping. The fast rise then would correspond to the nearly instantaneous collection of hole-electron pairs and would have a value governed by the detector time constant. However, if some of the carriers, either holes or electrons, were trapped and subsequently released in a time greater than the value of the detector time constant, then one could expect the maximum pulse height to occur during a longer time interval. As the temperature is lowered, carriers remain longer in the trapping sites before being thermally released. This would account for the greater delay in the appearance of pulse maxima as the temperature decreases. Eventually trap release time becomes so long that the traps appear essentially filled to newly created hole-electron pairs. It might be argued that the absolute value of pulse height should increase under such circumstances.

Particularly noteworthy among the characteristics of neutron-damage junction detectors is the effect of temperature upon pulse height. During evaluation just below room temperature, pulse heights were observed to decrease. This effect was investigated from 85°C to -196°C using a voltage-sensitive preamplifier. Alpha particle pulse heights were recorded by a 100-channel analyzer. Nearly an order of magnitude decrease in pulse height occurred as the temperature was lowered from 85°C to -70°C. At an undetermined temperature close to that of liquid nitrogen, pulse heights suddenly began to increase. One detector showed a 70-percent recovery in pulse height upon reaching equilibrium at -196°C. A plot showing this reversal in pulse height is given in Fig. 53.

Analysis of this pulse height reversal was clouded by the fact that decreased detector capacitance could possibly account for the abrupt increase in pulse height since a voltage-sensitive preamplifier was being used. Also, the long rise time pulses were possibly being clipped by the amplifier

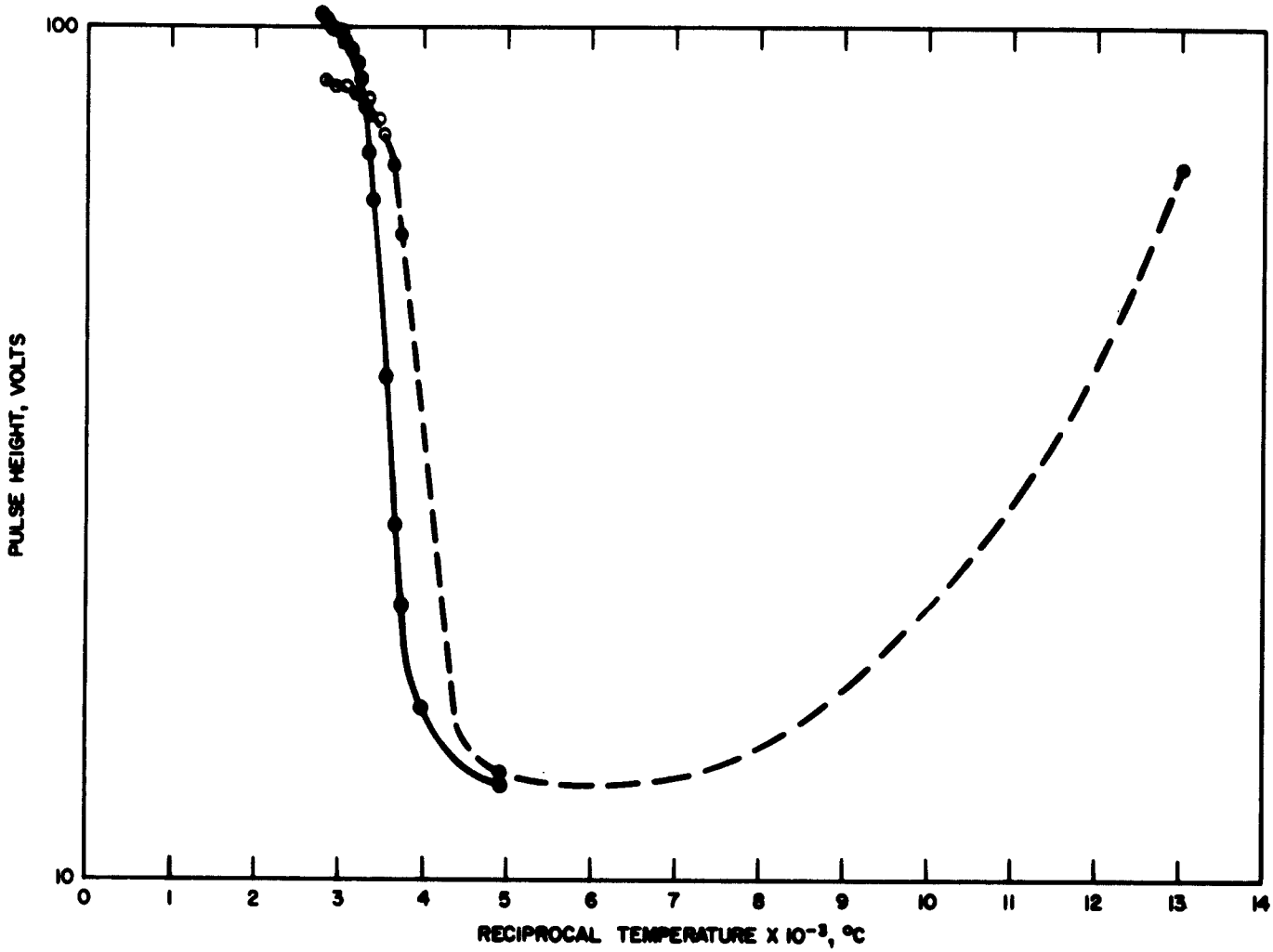

Fig. 55. Pulse height as a function of temperature in an irradiated detector illustrating the reversal in the pulse height function at low temperatures.

system and thus may not have been reaching their true height. For these reasons the experiments were repeated using a much faster system obtained by replacing the voltage-sensitive preamplifier by a charge-sensitive unit. Qualitative observations revealed that a similar reversal in pulse height occurred. However, it was apparent that the amplifier was causing some clipping. In order to avoid this complication, the amplifier was removed and output pulses from the preamplifier were displayed directly on the oscilloscope. Scope photographs confirming that a reversal occurs are shown in the sequence illustrated in Fig. 54.

In unirradiated detectors resolution improves at lower temperatures, but with neutron-damaged detectors it actually improves as the temperature increases. In fact, the best high-temperature (less than 70°C) performance yet noted during these studies has been achieved using an irradiated detector. The resolution obtained for 8.78-Mev alpha particles by an irradiated detector operating at temperatures between -7.5 and 85°C is illustrated by the data shown in Figs. 55 to 60. Since pulse height was found to vary with temperature, it was necessary to alter the gain settings of the amplifier at each temperature change. It should be noted that the symmetry about the peak improved as the temperature was increased. Poor resolution occurs for the dual rise component pulses mentioned earlier. Trapping is assumed to be the mechanism responsible for this effect. This mechanism of action is consistent with the observed changes in resolution. Fluctuations in the release of trapped carriers would also contribute to the spread in pulse heights. At higher temperatures, trapping is negligible and resolution would therefore improve.

Improved resolution at high temperatures suggested that perhaps an optimum operating temperature exists with regard to signal-to-noise ratio. It seemed reasonable to expect that a maximum value of signal-to-noise ratio could be found at some particular temperature. This was investigated in the temperature range of 24° to 88°C by computing signal-to-noise ratios from oscilloscope photographs. A plot of this ratio for 8.78 Mev alpha particles is presented in Fig. 61. The signal-to-noise ratio is higher at room temperature than above. This is similar to the behavior of unirradiated detectors. Therefore, the operating temperature of post-irradiated detectors should be governed by specific requirements, since high resolution and high signal-to-noise ratio are not compatible.

An investigation of the response of an irradiated detector to alpha particles incident upon the back surface was undertaken because of a lack of understanding of the aforementioned effects. It is possible that recombination within the space-charge region might differ for particles incident upon the back rather than upon the front. The chief difference in the two cases is that the former requires electrons to traverse the width of the depletion region, whereas the latter subjects holes to this transfer. Such traversals may expose the carriers to recombination and trapping centers. If the capture of one type of carrier dominates, then pulse heights should

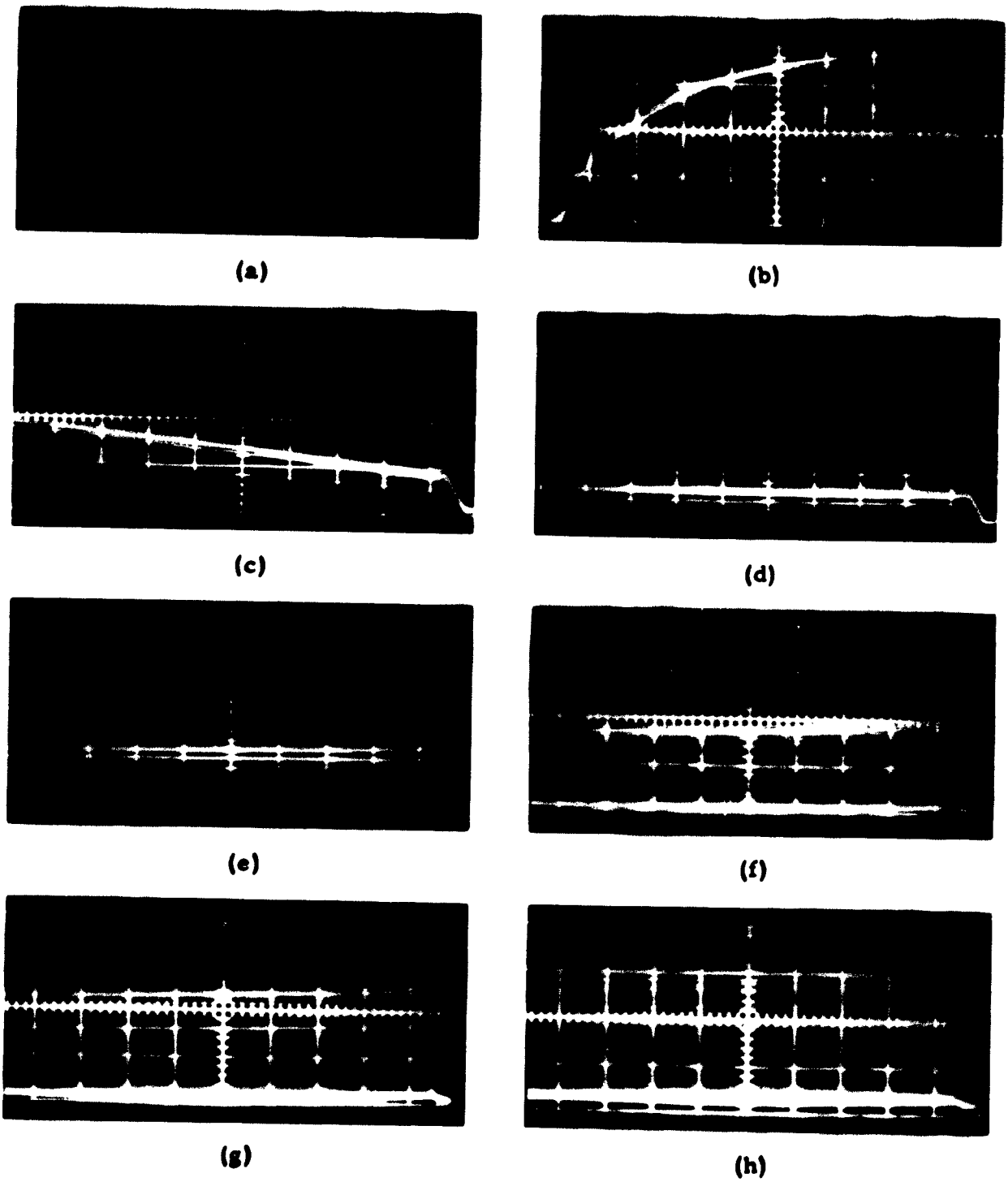

Fig. 54. Change in pulse characteristics (height and shape) as the temperature is lowered from room temperature through -196°C, where the return of original characteristics takes place.

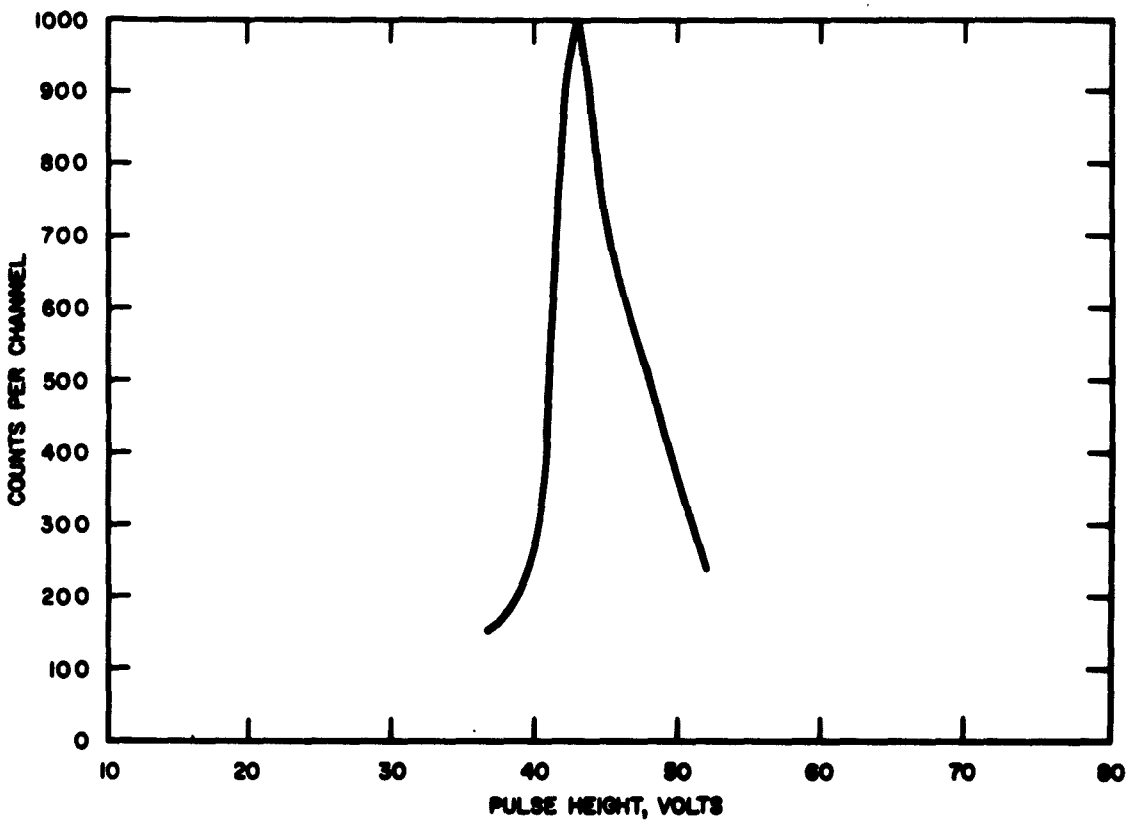

Fig. 55. Analysis of 8.78 Mev alpha pulses in an irradiated detector when operated at a junction potential of 50 volts and at a temperature of -7.5°C. The resolution in this case is 16 percent.

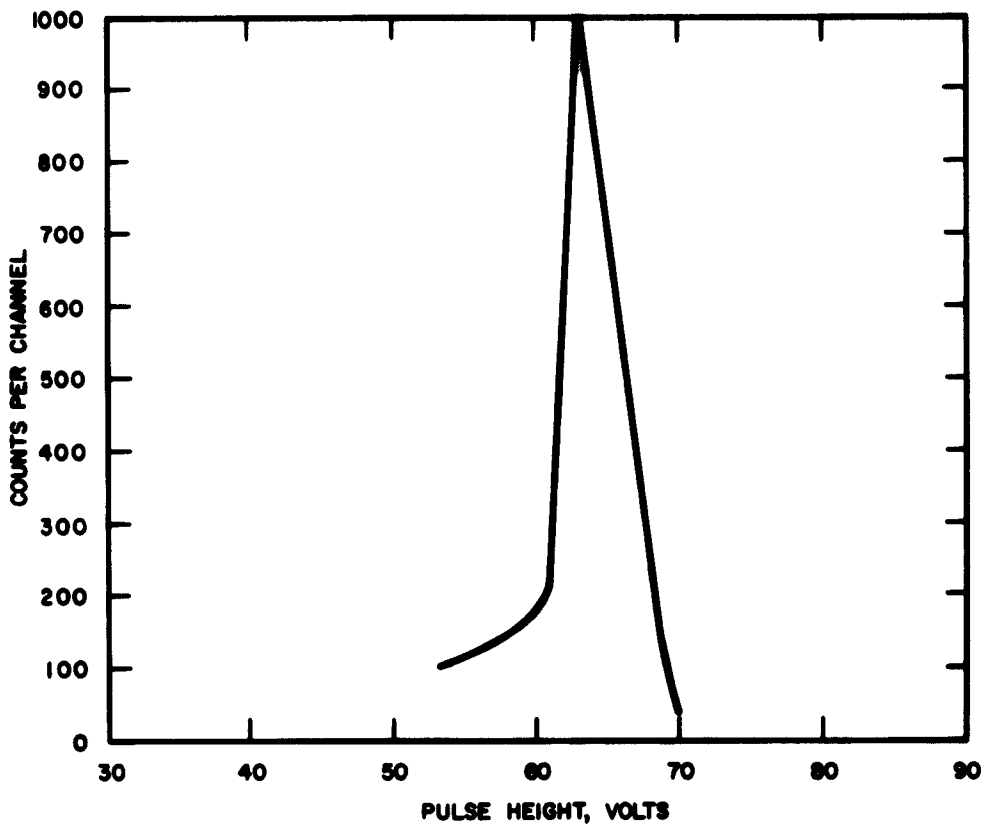

Fig. 56. Analysis of 8.78 Mev alpha pulses in an irradiated detector when operated at a junction potential of 50 volts and at a temperature of 22°C. The resolution in this case is 7.1 percent.

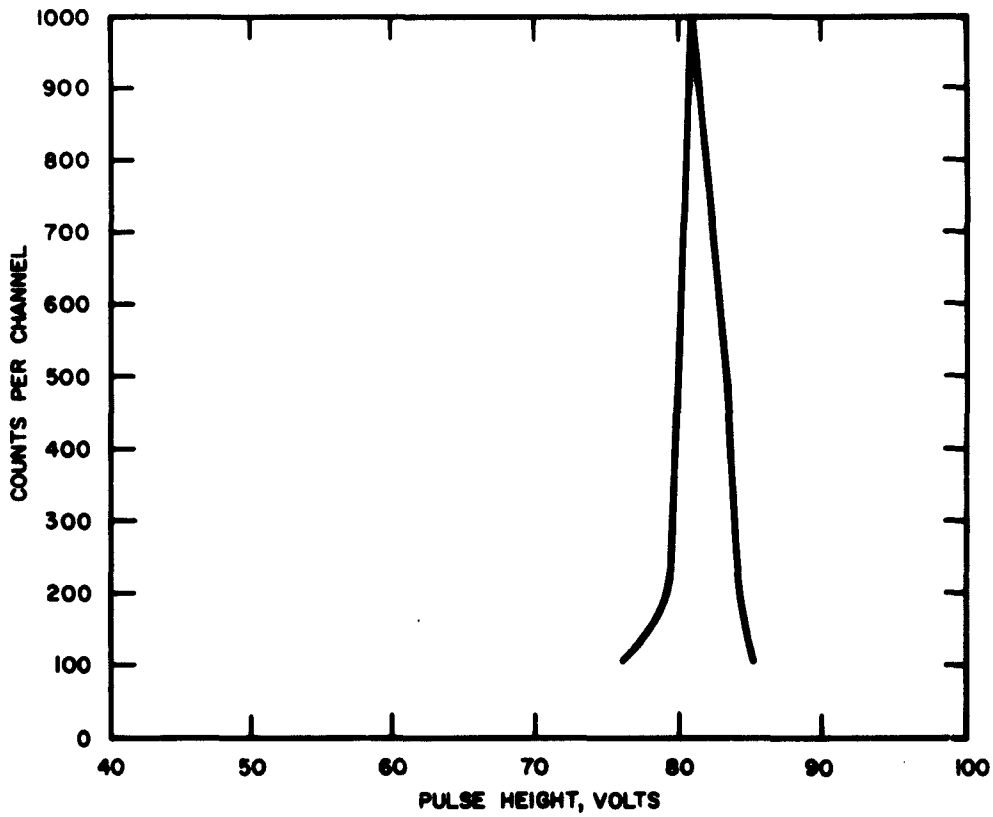

Fig. 57. Analysis of 8.78 Mev alpha pulses in an irradiated detector when operated at a junction potential of 50 volts and at a temperature of 33°C. The resolution in this case is 4.2 percent.

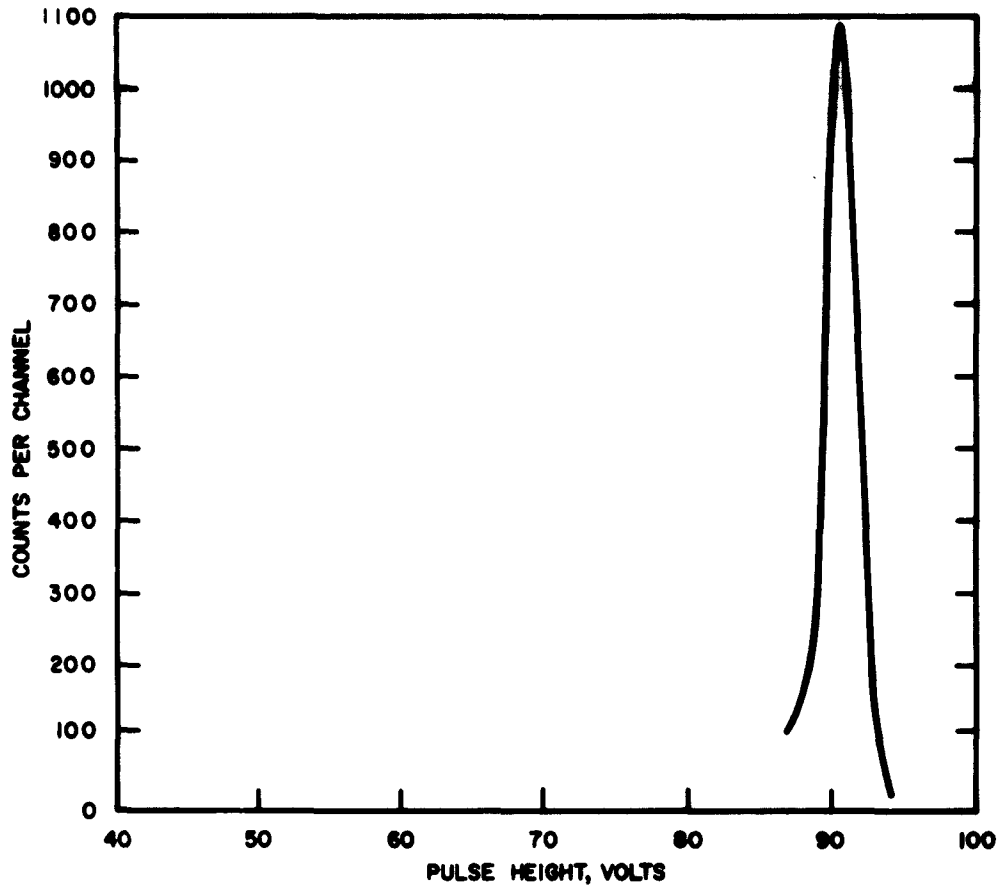

Fig. 58. Analysis of 8.78 Mev alpha pulses in an irradiated detector when operated at a junction potential of 50 volts and at a temperature of 41 °C. The resolution in this case is 2.8 percent.

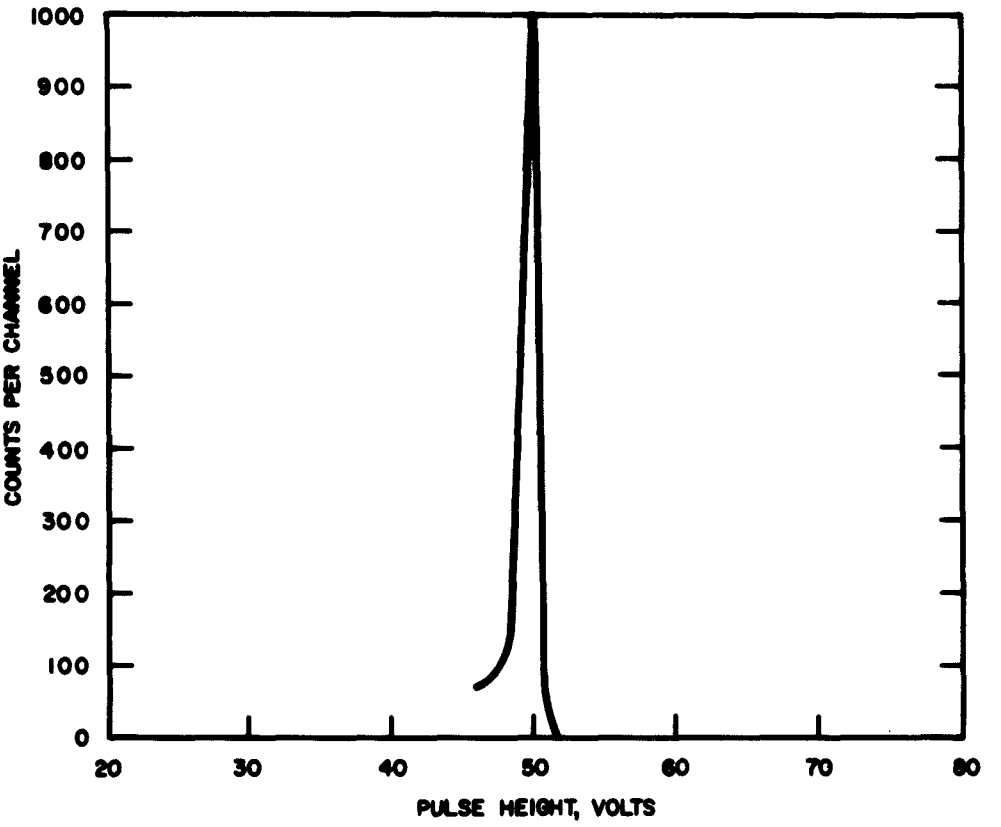

Fig. 59. Analysis of 8.78 Mev alpha pulses in an irradiated detector when operated at a junction potential of 50 volts and at a temperature of 62°C. The resolution in this case is 2.8 percent. Amplifier gain one-half value for Figs. 55-58.

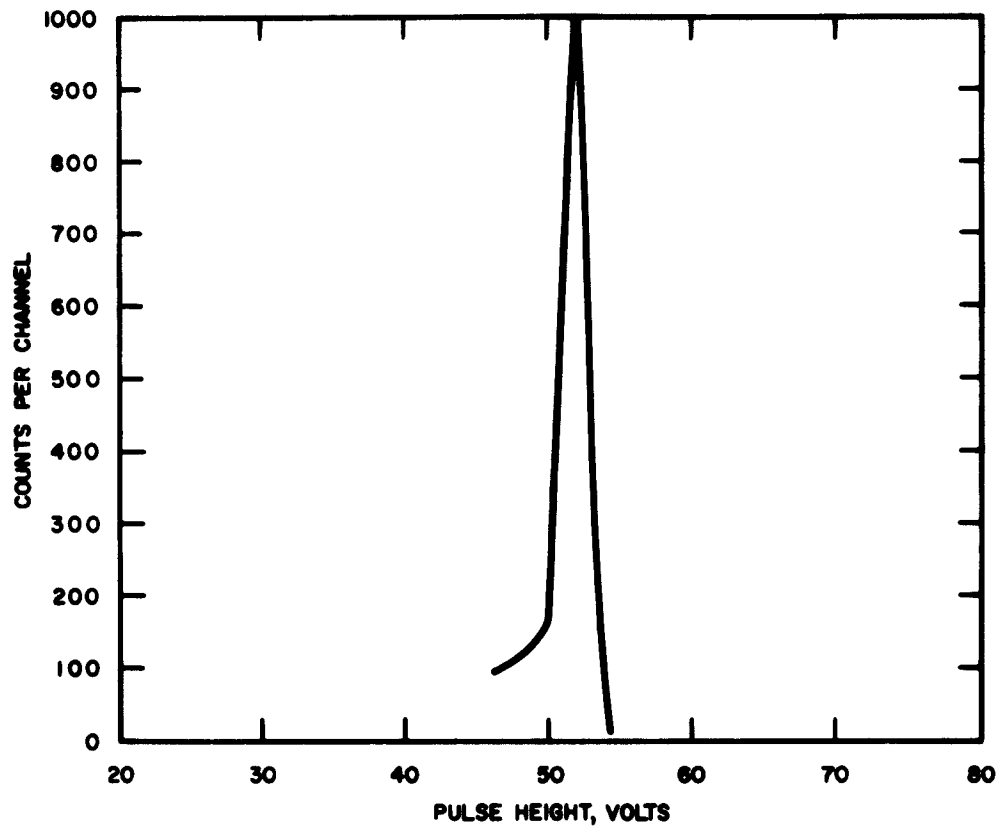

Fig. 60. Analysis of 8.78 Mev alpha pulses in an irradiated detector when operated at a junction potential of 50 volts and at a temperature of 85°C. The resolution in this case is 3.8 percent.

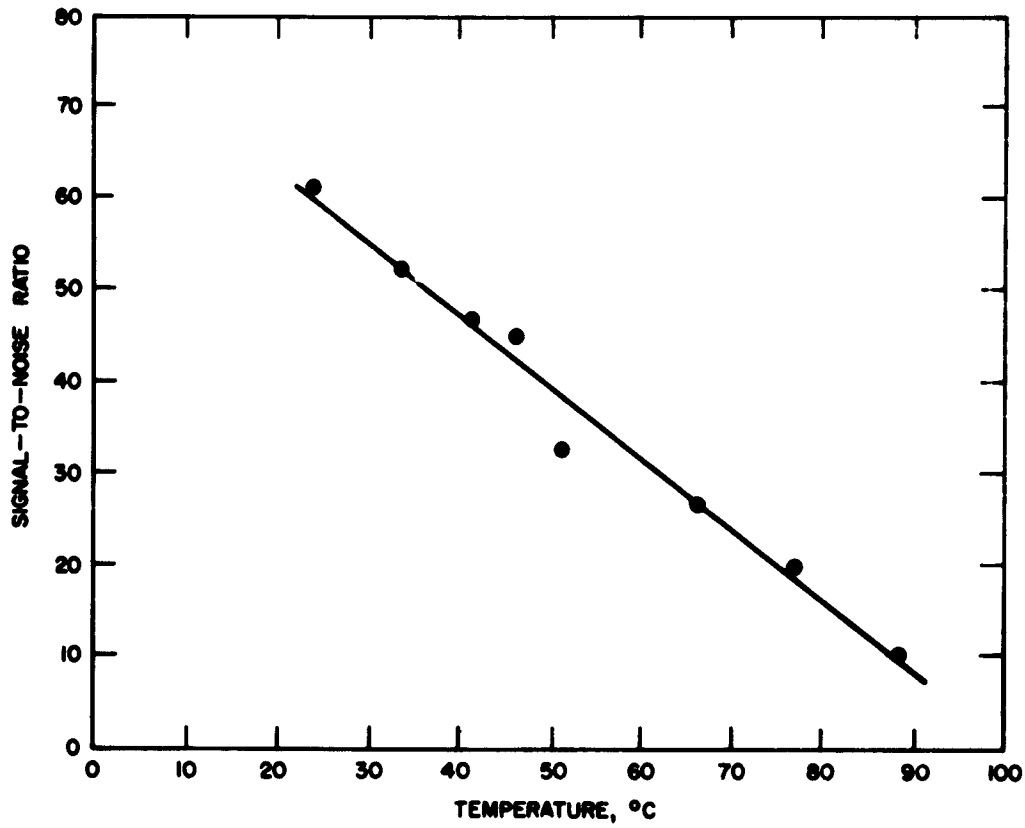

Fig. 61. Signal-to-noise ratio as a function of temperature in an irradiated detector operating at 50 volts applied potential. Total dose, 6.1×10^{13} nvt.

differ in the two cases. For proper comparison the depletion region must extend to the back contact so as to prevent energy loss by the alpha particles in bulk material. The experiment was performed in vacuum at $0^{\circ}C$ and at $-72^{\circ}C$ using bias voltages just beneath breakdown. Separate investigations were carried out for the two source geometries. Both resolution and peak positions were equivalent when the detector was operated at $0^{\circ}C$ and 670-volt applied potential. However, when the detector was operated at $-72^{\circ}C$ and 220 volts, the peaks of the pulses obtained from the alpha particles entering through the back aperture were actually appreciably higher (about 50 percent) than from those through the front face. The contribution of noise to the spectrum in the former case is much greater than in the latter because of a lower count rate. Similar results were obtained while operating at 150 volts and $-72^{\circ}C$, except that the peaks in both cases appear in lower channels. This may be seen from the data given in Fig. 62. Despite the fact that energy loss must be occurring in the bulk, the peaks were 10 percent higher for alpha particles through the back face.

The effect of electric field strength on pulse height when recombination and trapping are present will now be considered. Since the probability of hole or electron capture varies inversely with carrier velocity, it can be expected that less recombination and trapping will take place for higher values of the internal electric field. As temperature is lowered, two physical quantities change, resistivity and carrier lifetime. The resistivity increases and lifetime will generally decrease. Reciprocal pulse height versus reciprocal bias voltage is shown for two different operating temperatures ($0^{\circ}C$ and $-72^{\circ}C$) in Fig. 63. Since a charge-sensitive preamplifier was used, reciprocal pulse height is a measure of charge collected. The advantage of plotting V^{-1} is that the experimental curves should converge for infinite field strength, where no recombination should take place. If no recombination had occurred, a horizontal line would have been obtained. Precise analysis of data shown in Fig. 63 is difficult since it is impossible to separate the effects of reduced field strength and reduced lifetime.

A key property governing the observed phenomena is the lifetime of nonequilibrium carriers. The variation of this quantity with temperature is believed to be largely responsible for the observed temperature effects. The relaxation time constant τ' plotted as a function of the inverse of absolute temperature for n-type germanium which had been subjected to a series of successive gamma irradiations is shown[20] in Fig. 64. The most significant aspect of these data is the inversion of τ' with temperature in materials which have undergone radiation damage. In these samples, as temperature is lowered, lifetime values first decrease in a normal fashion but then increase sharply, the effect being more pronounced for those samples with high defect concentrations.[21,22] The explanation for this behavior may be seen from the theory. The theoretical behavior of

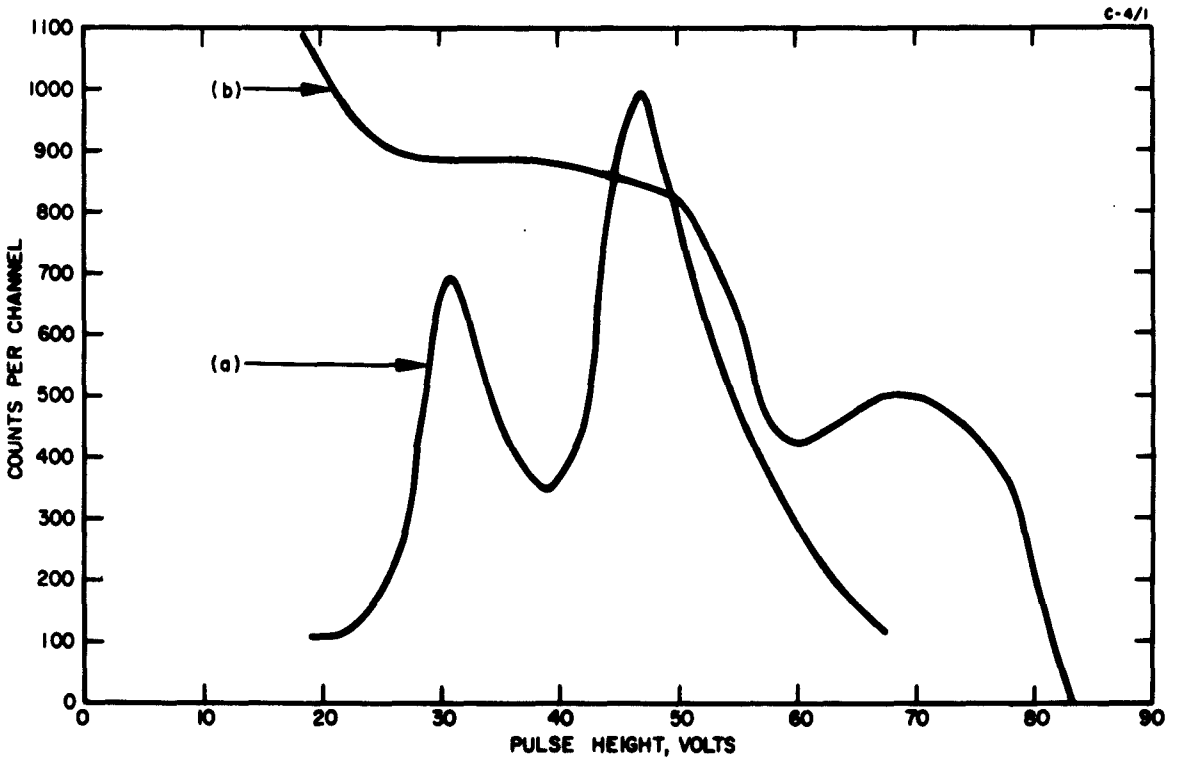

Fig. 62. Alpha spectra of Pb^{212} when the detector was operated at -72°C with an applied bias of 220 volts. Curve (a) shows alpha particles incident on the front face and Curve (b) shows alpha particles on the back face of the detector.

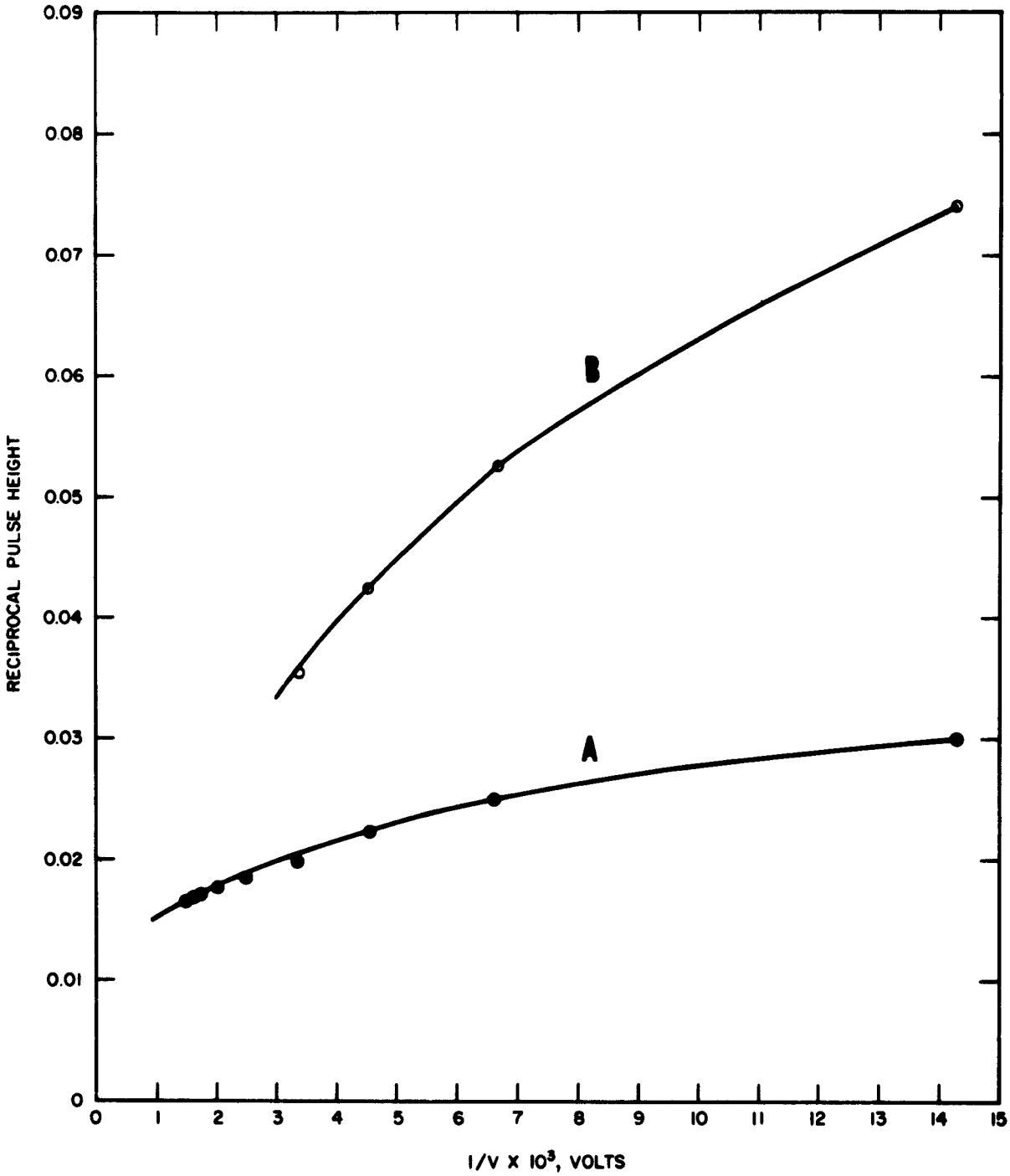

Fig. 63. Pulse height response to 8.78 Mev alpha particles as a function of bias voltage: (a) detector operated at 0°C; (b) detector operated at -72°C.

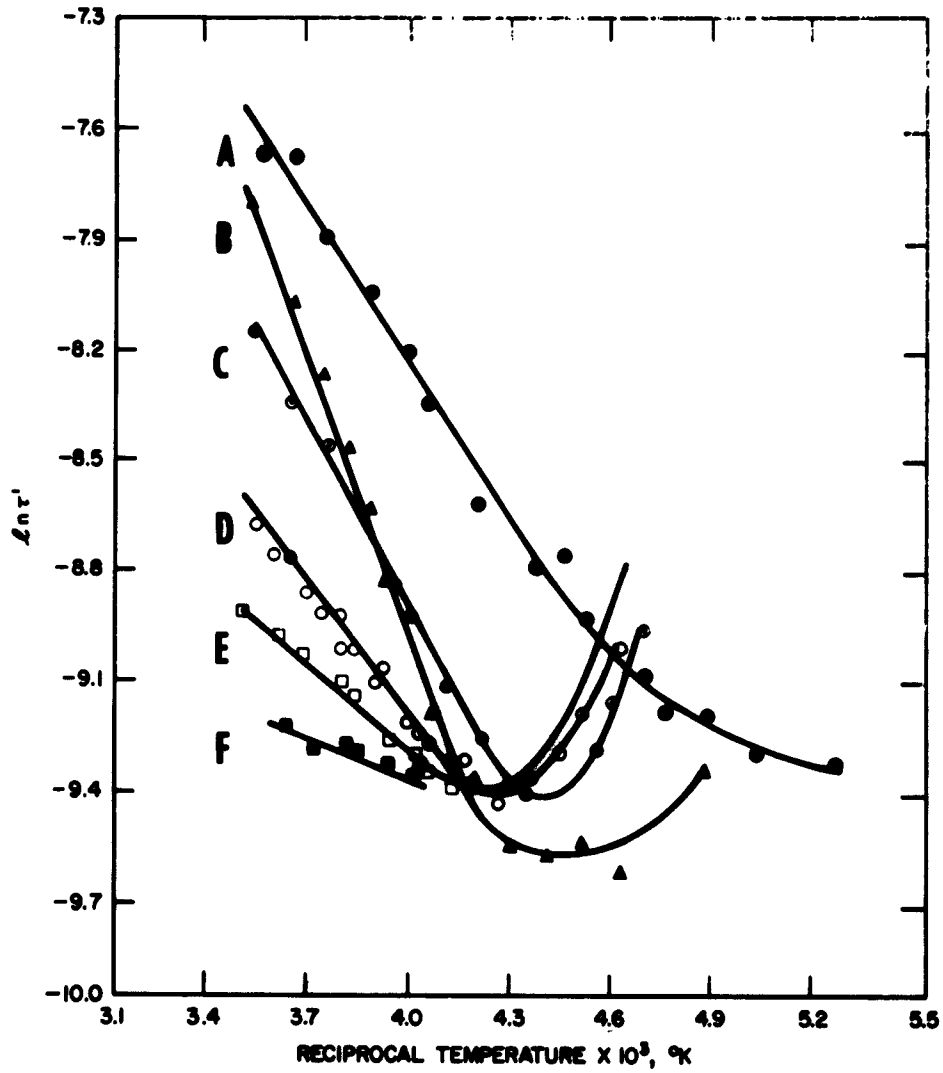

Fig. 64. Change in relaxation time constant as a function of temperature for radiation-damaged germanium: (a) unirradiated germanium; (b) defect concentration = 1.14×10^{12} cm^{-3}; (c) defect concentration = 2.76×10^{12} cm^{-3}; (d) defect concentration = 5.45×10^{12} cm^{-3}; (e) defect concentration = 8.1×10^{12} cm^{-3}; (f) defect concentration = 1.0×10^{13} cm^{-3}.

the relaxation time constant is shown in Fig. 65. First, it is assumed that there are recombination levels as well as trapping levels situated in the lower portion of the valence band. The latter may act as trap levels for holes under certain conditions. Section I of the theoretical curve is dominated by recombination due to the recombination levels. The slope of this curve then decreases as defect concentration increases where trapping begins to play a greater role. To properly interpret region II, we must consider the fact that the recombination rate is determined only by trapping of nonequilibrium holes on the recombination levels. As the temperature is lowered, the time that trapped holes spend on the trap levels becomes greater. Hence, the effective lifetime increases. Region III corresponds to recombination of conduction band electrons with trapped holes on the trapping levels. This recombination rate does not depend on temperature.

A definite similarity exists between the shape of the curves depicting the relaxation time constant as a function of $T(^{o}K)^{-1}$ and curves showing the relationship of pulse height as a function of $T(^{o}K)^{-1}$. This is reasonable since the amount of charge collected can be expected to depend on the lifetime of carriers within the depletion region. Measurements of both quantities as a function of temperature would be necessary in order to confirm this theory.

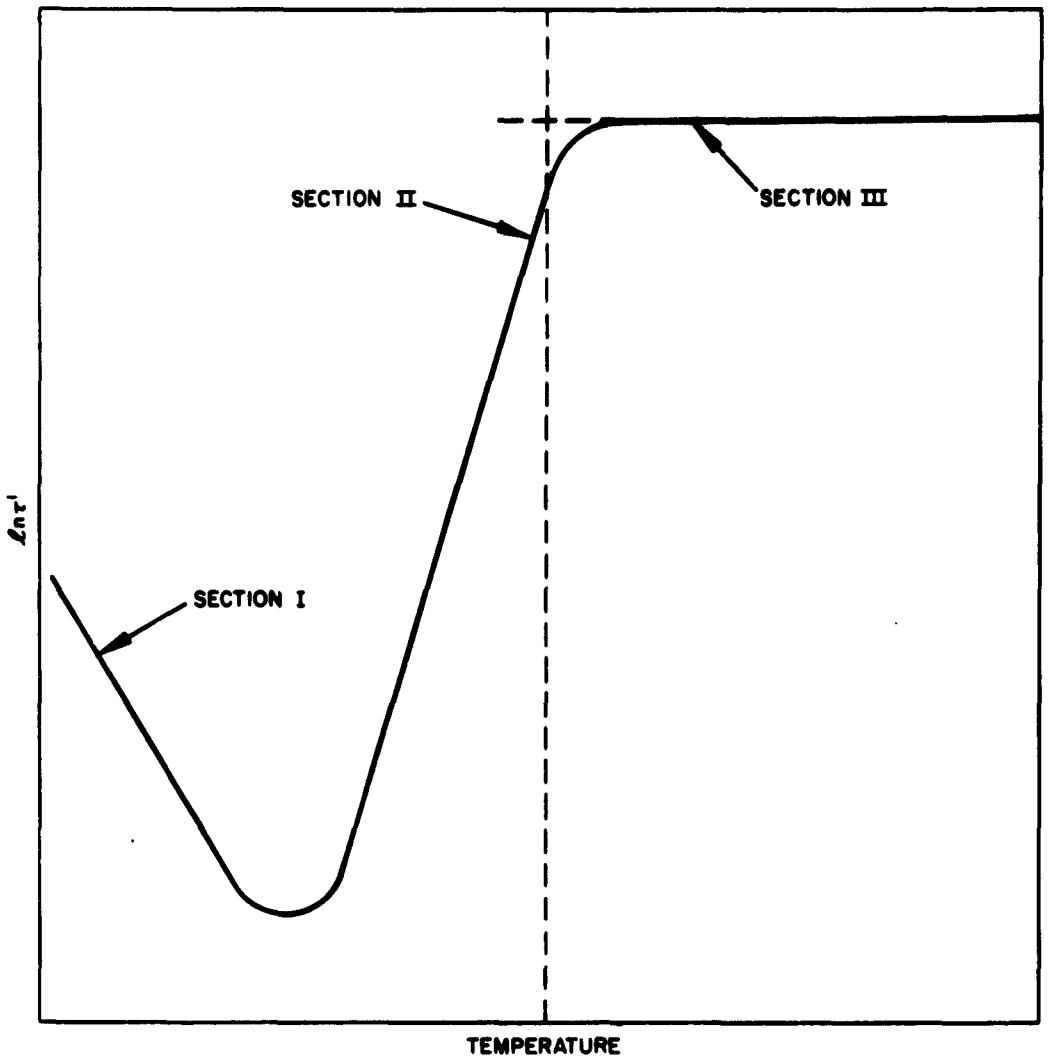

Fig. 65. Theoretical temperature dependence of the relaxation time constant.

VI. OPTIMIZATION OF DETECTORS

A. Operation of Detectors In Series Or Parallel

The compactness of the p-n junction detector strongly suggests the possibility of geometrical arrays of devices for beam profilometry, particle tracking, or possibly increased sensitivity. While ideally there are few problems associated with arrays, practical limitations often become severe. For instance, the problem of a preamplifier attached to each detector may limit the proximity of neighboring detectors. The economics of the situation may also limit the amount of electronics to be used. It is therefore of interest to investigate the possibility of series and parallel arrangements of detectors, which involve the use of single rather than multiple preamplifiers or amplifiers.

We shall first discuss the predicted effect of the addition of detectors in series or parallel on the pulse height and rise time. This will be followed by a description of an experiment with a series array of detectors.

Consider the schematic diagrams of series and parallel detectors shown in Fig. 66. R and C are, respectively, the internal resistance and capacitance of each detector, which, for the purposes of this analysis, are assumed to be the same in all detectors. C_A is the input capacity of the electronic system and includes lead capacitances. Assume a pulse in any one detector and consider the distribution of charge over the capacitances of the other detectors and the amplifier. For the series arrangement, the process may be seen as a stepwise one where the charge is transferred from the right-hand plate of one condenser to the neighboring plate of the next condenser. The end result must be equal charges on each condenser. For the parallel case, the process might be pictured such that there is a transfer of charge to every succeeding condenser, which results in equal voltages on all condensers.

Since the charge is the important parameter for the series arrangement, a comparatively large voltage will appear on C_A when $C_A \ll C$. Conversely, since voltage is the important parameter for the parallel array, it will be superior to the series arrangement if $C_A \gg C$. The latter is analogous to the case of the charge-sensitive amplifier.

The parallel array has the advantage of reducing the effective resistance.

A quantitative treatment for the series case involves the equation

$$n\left(\frac{q}{C} + R\,\frac{dq}{dt}\right) + \frac{q}{C_A} = \frac{Q}{C},$$

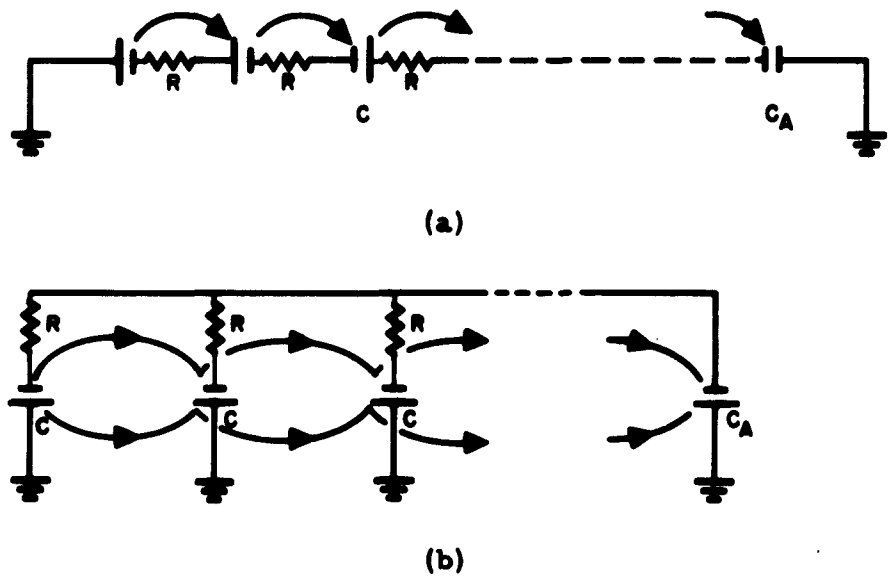

Fig. 66. Equivalent circuits for detectors used (a) in series array (b) in parallel array.

where Q is the charge originally injected at time t, q is the final charge on each capacitor, and n is the number of like detectors. As $t \to \infty$,

$$n \frac{q}{C} + \frac{q}{C_A} = \frac{Q}{C} ,$$

and the voltage appearing on the amplifier capacitance is therefore

$$\frac{q}{C_A} = \frac{Q}{nC_A + C} \left[1 - \exp - \left(\frac{nC_A + C}{nRCC_A} \, t \right) \right] .$$

For the parallel case, we have the set of equations

$$\frac{q_i}{C} + R \frac{dq_i}{dt} = \frac{q_A}{C_A} , \qquad i \neq k$$

$$= \frac{q_A}{C_A} + \frac{Q}{C} , \qquad i = k ,$$

where k signifies the detector on which the initial charge Q is developed. Since

$$\sum_{i=1}^{n} q_i + q_A = Q ,$$

we obtain

$$\frac{q_A}{C_A} = \frac{Q}{nC + C_A} \left[1 - \exp - \left(\frac{nC + C_A}{RCC_A} \, t \right) \right] .$$

Pulse heights and rise times for the two types of arrays are summarized in Table IV.

TABLE IV

Comparison of Pulse Height and Rise Time Characteristics for Series and Parallel Detector Arrays

	Series	Parallel
Pulse Height	$\frac{Q}{nC_A + C}$	$\frac{Q}{nC + C_A}$
Rise Time	$\frac{nC_A + C}{nRC\,C_A}$	$\frac{nC + C_A}{RC\,C_A}$

For maximum pulse height, the series array is preferred when $C_A < C$ and the parallel array when $C_A > C$. Fig. 67 shows the ratio of pulse height for these arrays as a function of C_A/C. If rise time is the only consideration, the parallel array is always superior, but the values in each case approach each other as $nC \ll C_A$.

The experiment performed to confirm this analysis utilized a series array of detectors each having different capacitances C_i. The expected pulse height will not vary with the particular detector on which the radiation deposits a charge Q.

B. Experimental Results

1. Counting Rate – Four p-n junction detectors were used in a series arrangement, each with individual sources. These sources were made from the decay products of Pb^{212} which emit two alpha particles, one at 8.78 Mev and the other at 6.26 Mev. The count rate of each detector was determined singly and in combination with the other detectors. A schematic diagram of the arrangement is shown in Fig. 68. In order to eliminate noise and other extraneous pulses, the discriminator level on the scaler was set to give minimal background when both the sources and their shields were in place. Under these conditions the background count rate was approximately 0.07 percent of the lowest counting rate used. The results based on six separate determinations of each quantity are shown in Table V. In every case the expected count rates agree with those obtained experimentally to better than 0.5 percent.

2. Pulse Height – In order to determine the influence of this arrangement on pulse height, the circuit was modified so that a constant bias would be maintained independently across each detector. Since the resultant pulse height is a function of the junction capacitance which in turn

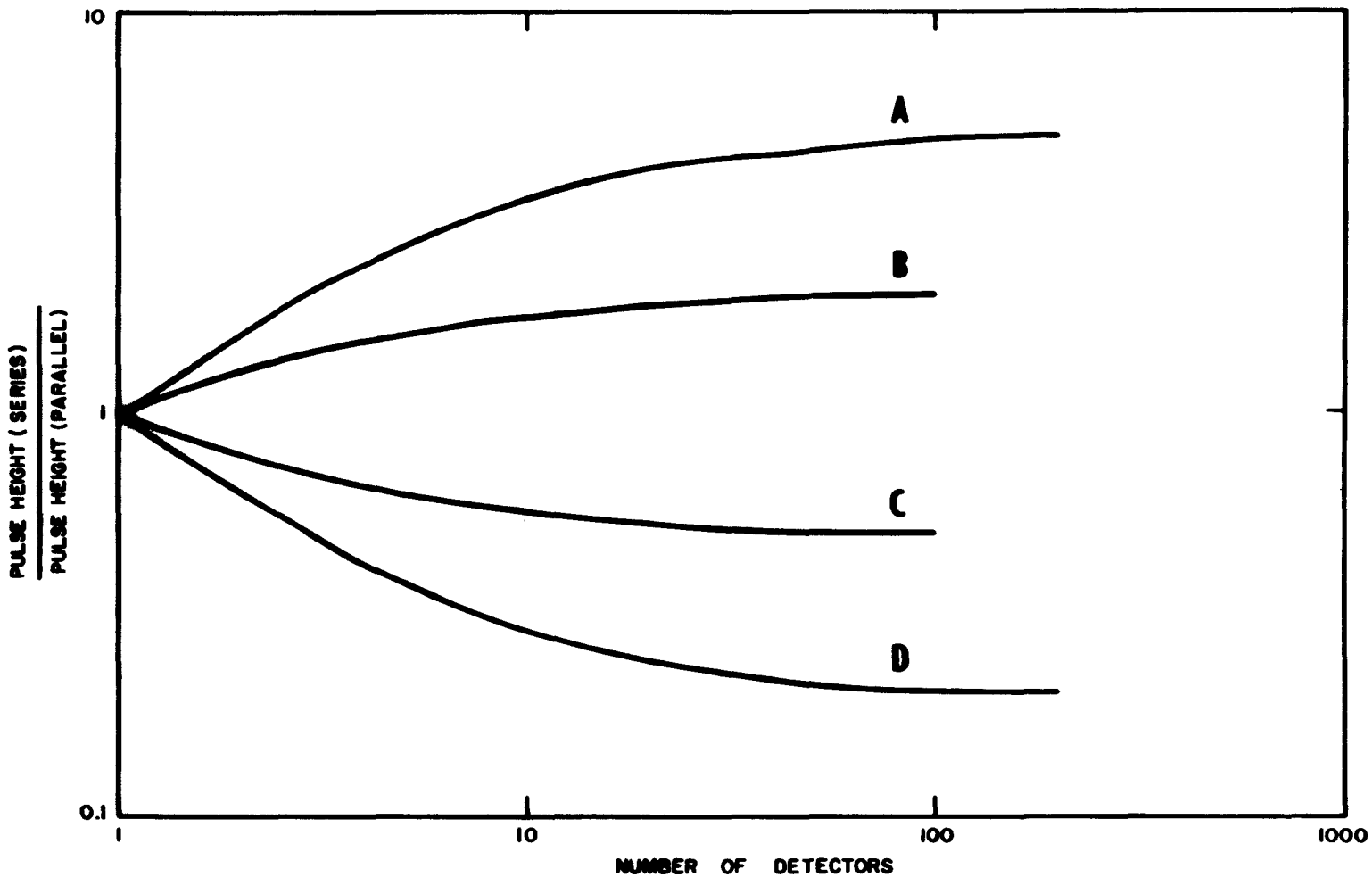

Fig. 67. Ratio of pulse heights obtained when a series array of detectors is used to that obtained when a parallel array of detectors is used plotted as a function of the number of detectors in the array. (a) Relationship for the ratio of input capacity of the amplifier to that of an individual detector of 0.2. (b) Ratio of input capacity of the amplifier to that of an individual detector is 0.5. (c) Ratio of input capacity of the amplifier to that of an individual detector is 2. (d) Ratio of input capacity of the amplifier to that of an individual detector is 5.

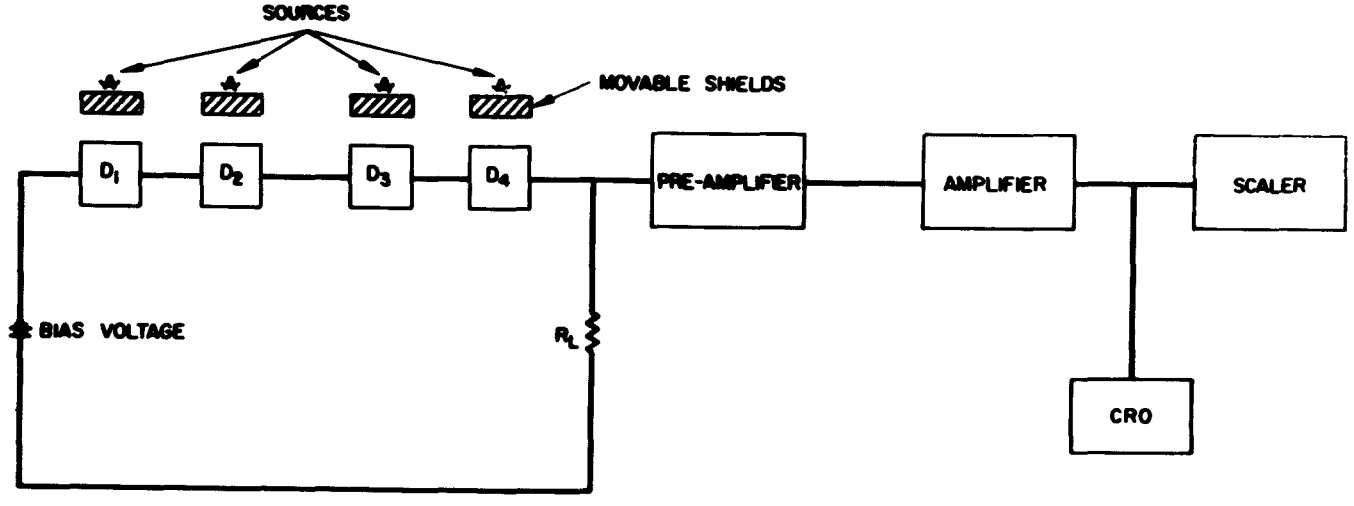

Fig. 68. Experimental setup for measuring response of a series array of detectors to individual and multiple sources.

is a function of the applied voltage, one must keep this quantity constant as circuit elements are added and subtracted. If the applied voltage is not adjusted as series elements are added, junction capacitance will be increased. A true comparison of the effects of series operation depends upon all parameters being held constant. Since we were dealing with high impedance devices, an electrometer circuit was used to measure the voltage drop across the junctions after each circuit change was effected.

TABLE V

Counting Rates for Various Combinations of Series-Operated p-n Junction Detectors[a]

Detector	Counts per minute (actual)	Counts per minute (expected)
1	81,400 ± 350	----------
2	88,760 ± 660	----------
3	59,730 ± 190	----------
4	41,490 ± 170	----------
1 + 2	169,400 ± 100	170,200 ± 150
1 + 2 + 3	228,800 ± 180	229,900 ± 900
1 + 2 + 3 + 4	270,900 ± 140	170,400 ± 1,070

[a]Background corrections are not included since they are negligible.

P-n junction and amplifier input capacitances were measured using an a-c bridge technique. Pulse heights examined were generated by an 8.78 Mev alpha line emitted by the decay of Po^{212}. These were examined and separated with a 100-channel pulse height analyzer. Amplifier gains were held constant throughout each run by calibration with a pulse generator. The height of these pulses was measured using only the first detector. Initially all other units were shorted out. After the initial measurement, detectors 2, 3, and 4 were unshorted successively, repeating the initial measurements each time another unit was added to the circuit. The decrease in pulse amplitude is clearly seen as detectors are added to the array.

TABLE VI

Circuit Parameters and Measured Pulse Heights for Series Operation of Four p-n Junction Radiation Detectors. The Input Capacitance of the Preamplifier was Equal to 19 μμf.

Detectors in Circuit	Potential Across Junction, volts	Pulse Height, volts	Junction Capacity, μμf	Total Capacity, C_T, μμf
1	30.0	77	6.8	4.2
1	30.0	52	6.8	2.8
2	40.0		8.4	
1	30.0	50	6.8	2.7
2	40.0		8.4	
3	7.0		61.7	
1	30.0	49	6.8	2.6
2	40.0		8.4	
3	7.0		61.7	
4	2.6		79.3	

Table VI shows the resulting pulse heights and also the various circuit parameters which were used. All values shown in the table are measured ones except C_T, the total circuit capacitance as seen by the charge cloud. A comparison of the theoretical and experimental results is shown in Table VII. The close correlation between theory and experiment makes it possible to select detectors for optimum series operation.

TABLE VII

Comparison of Measured and Computed Pulse Heights for Series Operation of Four p-n Junction Radiation Detectors. The Value Obtained when Only One Detector was Operating in the Circuit is Taken as 100 Percent.

Detectors in Circuit	Theoretical Pulse Height, percent	Measured Pulse Height percent
1	100	100
1 2	66.6	67.5
1 2 3	63.7	65.0
1 2 3 4	61.6	63.6

VII. CONCLUSIONS

The feasibility of utilizing p-n junction, phosphorous-diffused detectors to map radiation fields of a pulsed reactor or linear accelerator has been established. Such detectors have been found to produce large signals without amplification when exposed to the high-intensity fields due to such machines. The output may be monitored or even measured after calibration of the detectors by operating the detector as a current device and recording changes in dark current. The ability to distinguish between intensity changes over small spatial dimensions is extremely good. Since the detector pulse shape is a faithful reproduction of electron beam intensity in a LINAC and since the response to gamma-ray pulses produced by a pulsed reactor has been shown to be a faithful reproduction of the neutron flux, these detectors can be used to give faithful dosimetric information on the operation of these machines. Under conditions where detectors may be expected to suffer neutron irradiation damage, operation at low temperatures would make such application feasible.

VIII. SUMMARY

Phosphorous-diffused p-n junction semiconductor detectors have been successfully used in high-intensity, pulsed neutron and gamma-ray fields. The resultant signals have been large enough so that they may be directly displayed on standard laboratory oscilloscopes.

Such detectors have been found not to suffer permanent damage from gamma rays or electrons for total dosages of less than 10^5 r. However, such detectors have been observed to undergo permanent damage due to neutron irradiations. The permanent effects observed after the detector has been removed from the neutron field are: (1) increased resistivity, (2) a decrease in carrier lifetime. These permanent damages, in turn, reduce the photocurrent response to radiation.

Such detectors have been used as monitors for x- or gamma-radiation flux through measurements of the change in dark current which is found to occur under irradiation. This increase in dark current has been studied and found to be a linear function of dose rate. The ability of such detectors to map beam intensity as a function of various geometrical parameters has been found to be excellent since abrupt changes in beam intensity may be plotted with extreme accuracy due to the small size of the detectors and the close proximity within which these may be placed to each other.

The response to an 8-microsecond pulse of x rays produced by a high-current linear accelerator operating at 10 Mev produced pulses having a magnitude of 0.2 to 0.4 ampere depending on the operating bias when exposed to peak dose rates of 2.5×10^7 r/second. The shape of the output pulse from the detector was found to be a faithful reproduction of the electron beam intensity. The optimum detector characteristics for such an application would be that the detector be made from high-resistivity material and from very thin slices and then operated at a high bias so that the depletion region essentially becomes the entire wafer thickness. Under these conditions, the detector response is independent of the potential across the junction.

The p-n junction detector, when exposed to pulses from the TRIGA reactor, gave responses which were primarily due to the gamma rays; that is, the reaction or the response to the neutron flux produced less than 1 percent contribution to the total pulse height. The current associated with the peak value of these pulses was approximately one ampere. Due to radiation damage, the observed pulse height is reduced by each successive TRIGA pulse. The damage threshold for this effect is of the order of 10^{11} nvt of fast neutrons. No rate dependence for this total dose threshold was observed, at least for fluxes as high as 10^{15} nv. The damage induced by the neutron irradiation also caused an increase in the pulse rise time of the detector when exposed to alpha pulses, an increase in detector capacity, and a decrease in the forward current.

Operation at low temperatures was found to produce some recovery of the pulse height which had been lowered because of neutron damage. At -196°C, detectors were noted to achieve 70 percent of the original output pulse height. However, the resolution of such radiation-damaged detectors was found to improve when temperature increased. Since the thermal noise generated within the detector also increases with temperature, these two conditions do not make for compatible operation and, therefore, a compromise must be worked out to achieve optimum operating conditions.

When more than one of these detectors are to be used in the same associated circuitry, it was found that operation of the detectors in series would produce maximum pulse height. However, if risetime is the main consideration, then arrays of such detectors should be used under parallel operation.

APPENDIX

The effect of RC clipping on the pulse height of an exponentially rising pulse may be seen by considering a voltage pulse which enters a system and decays with an exponential decay whose time constant is τ_D and whose rise time is given by τ_R.

$$q_{IN} = Q\left(1 - e^{-t/\tau_R}\right) \tag{A-1}$$

Differentiating (A-1),

$$\left(\frac{dq}{dt}\right)_{IN} = \frac{Q}{\tau_R} e^{-t/\tau_R} . \tag{A-2}$$

(A-2) is therefore the rate at which charge enters the system. The rate at which charge decays from the system is governed by τ_D.

$$\left(\frac{dq}{dt}\right)_{OUT} = q/\tau_D \tag{A-3}$$

Thus the rate of change of charge in the system is

$$\frac{dq}{dt} = \left(\frac{dq}{dt}\right)_{IN} - \left(\frac{dq}{dt}\right)_{OUT} = \frac{Q}{\tau_R} e^{-t/\tau_R} - \frac{q}{\tau_D} . \tag{A-4}$$

The general solution is

$$q = \frac{Q}{1 - \tau_R/\tau_D} e^{-t/\tau_D} - \frac{Q}{1 - \tau_R/\tau_D} e^{-t/\tau_R} . \tag{A-5}$$

Differentiating this expression to determine the time t_{max} at which q is a maximum and substituting back in (A-5) to find q_{max}, we obtain

$$t_{max} = \frac{\tau_R}{\theta - 1} \ln \theta \tag{A-6}$$

where

$$\theta = \tau_r / \tau_D \ ,$$

and

$$q_{max} = \frac{Q}{1 - \theta} \left\{ \theta^{\theta/1-\theta} - \theta^{1/1-\theta} \right\} . \qquad \text{(A-7)}$$

These relationships are shown in Fig. 69.

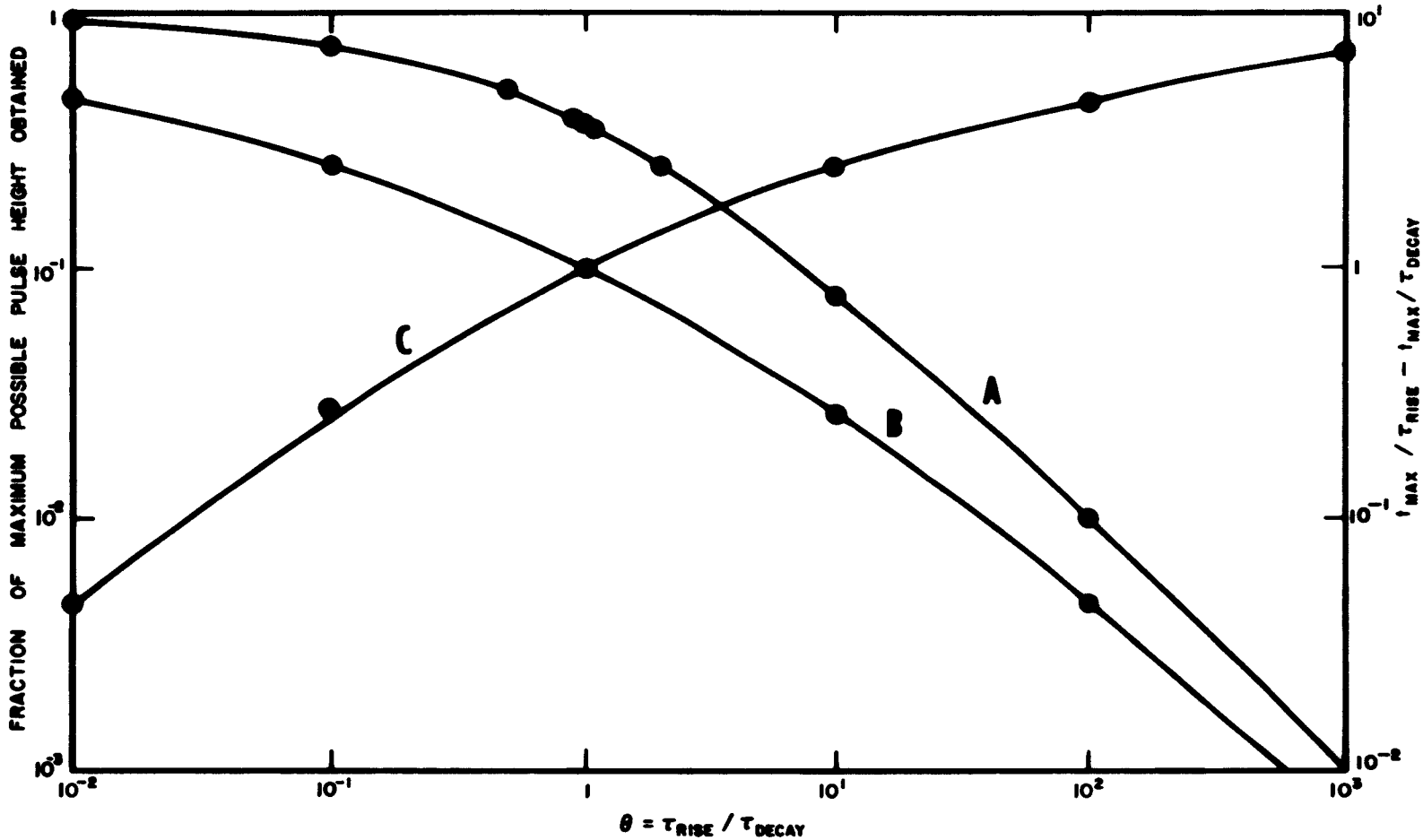

Fig. 69. The above curves show the relationship of various circuit parameters to charge and time constants of detector configurations. Curve A shows the fraction of the total charge which appears at the pulse maximum as a function of the ratio of rise to decay time constants. Curve B shows the ratio of the time necessary to reach maximum pulse height to the rise time constant as a function of the rise to decay time constants. Curve C shows the relationship between the time necessary to reach maximum pulse height and the decay time constant as a function of the rise to decay time constants.

REFERENCES

1. R. D. Evans, The Atomic Nucleus, McGraw-Hill Book Company, Inc., New York (1955), p. 715.

2. K. G. McKay and K. B. McAfee, Phys. Rev. 91, 1079 (1953).

3. R. L. Cammeron, Phys. Rev. 95, 16 (July 1, 1954).

4. R. D. Middlebrook, An Introduction to Junction Transistor Theory (John Wiley and Sons, Inc., New York, 1947), pp. 160-170.

5. Harwood, Hausner, Morse, and Rauch, The Effects of Radiation on Materials (Reinhold Publishing Corporation, New York, 1958), p. 166.

6. F. J. Morin and J. P. Maita, Phys. Rev. 96, 28 (October 1, 1954).

7. R. Gremmelmaker, "Irradiation of P-N junctions with gamma rays – A method for measuring diffusion lengths," Proc. IRE 46, 1045 (June 1958).

8. D. J. Hughes and R. B. Schwartz, Neutron X Sections, BNL 325, 2nd edition, 1958.

9. G. S. Hurst, J. A. Hurter, P. N. Hensley, W.A. Mills, M. Slater, and P. Reinhardt, Rev. Sci. Instr. 27, 153 (1956).

10. G. West, private communications.

11. G. K. Wertheim, Phys. Rev. 3, 6 (1958).

12. O. S. Billington and J. H. Crawford, Radiation Damage on Solids (Princeton University Press, Princeton, 1961) pp. 312-365.

13. H. M. James and K. Lark-Horowitz, Z. Physik Chime 198, 107 (1951).

14. Pigg and Robinson, ORNL, Progress Report 2128, 1956.

15. S. S. Friedland, J. W. Mayer, J. M. Denney, and F. Keywell, Rev. Sci. Instr. 31, 74-75 (January 1960).

16. R. V. Babcock, IRE Trans. on Nuclear Science NS-8, 98 (January 1, 1961).

17. Eberhard Spenke, Electronic Semiconductors (McGraw-Hill Book Company, Inc., New York, 1958), p. 109.

18. W. Shockley, Electrons and Holes in Semiconductors (D. Van Nostrand Co., New York, 1950), p. 314.

19. J. C. Pigg, ORNL, private communication.

20. S. M. Ryvkin and I. D. Yaroshetskii, Soviet Phys. – Solid State 2, 1773 (1961).

21. O. L. Curtis, Jr., and J. H. Crawford, Jr., ORNL-3108, UC-34 – Physics, p.

22. G. K. Wertheim, Phys. Rev. 109, 1090 (1958).

DISTRIBUTION LIST

1. Headquarters, Defense Atomic Support Agency, ATTN: Major Verser (2 copies), Washington 25, D.C.
2. Director, Armed Forces Radiobiology Research Institute, National Naval Medical Center, ATTN: CDR Chapman, Bethesda 14, Maryland.
3. Commanding Officer, Diamond Ordnance Fuse Laboratories, Connecticut Ave. and Van Ness Street, N.W., ATTN: Mr. Paul Caldwell, Washington 25, D.C.
4. Commanding Officer, U.S. Army Chemical Corps Nuclear Defense Laboratory, ATTN: Mr. John Kinch, Army Chemical Center, Maryland.
5. Director, U.S. Army Ordnance, Ballistic Research Laboratories, ATTN: Dr. Minor, Aberdeen Proving Ground, Maryland.
6. Director, National Bureau of Standards, Washington 25, D.C., ATTN: Dr. R. Caswell.
7. Los Alamos Scientific Laboratory, P.O. Box 1663, Los Alamos, New Mexico, ATTN: Dr. Biggers.
8. Director, U.S. Naval Research Laboratory, ATTN: Dr. Pearse, Washington 25, D.C.
9. AFSWC, ATTN: Lt. Col. Gross, Kirtland AFB, New Mexico.
10. Director, Oak Ridge National Laboratory, P.O. Box X, Oak Ridge, Tennessee, ATTN: Dr. Auzier.
11. Director, National Naval Medical Center, ATTN: Capt. Chambers, Bethesda 14, Maryland.
12. Commanding General, Walter Reed Army Hospital, Washington 25, D.C.
13. SAM, ATTN: Lt. Col. Pickering, Brooks AFB, Texas.
14. Commanding Officer, U.S. Army Signal Research & Development Laboratory, ATTN: Mr. W. Lonnie, Fort Monmouth, N.J.
15. Chief of Research and Development, Department of the Army, ATTN: Lt. Col. Conarty, Washington 25, D.C.
16. Chief of Naval Operations, Navy Department, ATTN: CDR Eaton, OP-75, Washington 25, D.C.
17. HQ USAF (AFRDR/NU) ATTN: Major Lowry, Washington 25, D.C.
18. OAR, Bldg. T-D, ATTN: Lt. Col. Ivan C. Atkinson, RROSP, Washington 25, D.C.
19. Commanding Officer and Director, U.S. Naval Radiological Defense Laboratory, ATTN: Dr. Cook; Dr. Kreger; Dr. Alpen, San Francisco 24, California.

20. ASD, Wright-Patterson AFB, Ohio.

21. President, Sandia Corporation, Sandia Base, Albuquerque, New Mexico, ATTN: Dr. Mehl.

22. AFSWC, ATTN: Major Alderman, Kirtland AFB, New Mexico.

23. Headquarters, Defense Atomic Support Agency, ATTN: Document Library (5 copies), Washington 25, D.C.

24. Commander and Director, Armed Services Technical Information Agency, Arlington Hall Station, Arlington 12, Virginia (20 copies).